Ecological Interactions Among Nitrate-, Perchlorate-, and Sulfate-Reducing Bacteria in Hydrogen-Fed Biofilm Reactors

by

Aura Ontiveros-Valencia

A Dissertation Presented in Partial Fulfillment
of the Requirements for the Degree
Doctor of Philosophy

Approved March 2014 by the
Graduate Supervisory Committee:

Bruce Rittmann, Co-chair
Rosa Krajmalnik-Brown, Co-chair
César I. Torres

ARIZONA STATE UNIVERSITY

May 2014

ABSTRACT

Water contamination with nitrate (NO_3^-) (from fertilizers) and perchlorate (ClO_4^-) (from rocket fuel and explosives) is a widespread environmental problem. I employed the Membrane Biofilm Reactor (MBfR), a novel bioremediation technology, to treat NO_3^- and ClO_4^- in the presence of naturally occurring sulfate (SO_4^{2-}). In the MBfR, bacteria reduce oxidized pollutants that act as electron acceptors, and they grow as a biofilm on the outer surface of gas-transfer membranes that deliver the electron donor (hydrogen gas, (H_2)). The overarching objective of my research was to achieve a comprehensive understanding of ecological interactions among key microbial members in the MBfR when treating polluted water with NO_3^- and ClO_4^- in the presence of SO_4^{2-}. First, I characterized competition and co-existence between denitrifying bacteria (DB) and sulfate-reducing bacteria (SRB) when the loading of either the electron donor or electron acceptor was varied. Then, I assessed the microbial community structure of biofilms mostly populated by DB and SRB, linking structure with function based on the electron-donor bioavailability and electron-acceptor loading. Next, I introduced ClO_4^- as a second oxidized contaminant and discovered that SRB harm the performance of perchlorate-reducing bacteria (PRB) when the aim is complete ClO_4^- destruction from a highly contaminated groundwater. SRB competed too successfully for H_2 and space in the biofilm, forcing the PRB to unfavorable zones in the biofilm. To better control SRB, I tested a two-stage MBfR for total ClO_4^- removal from a groundwater highly contaminated with ClO_4^-. I document successful remediation of ClO_4^- after controlling SO_4^{2-} reduction by restricting electron-donor availability and increasing the acceptor loading to the second stage reactor. Finally, I evaluated the performance of a two-stage

pilot MBfR treating water polluted with NO_3^- and ClO_4^-, and I provided a holistic understanding of the microbial community structure and diversity. In summary, the microbial community structure in the MBfR contributes to and can be used to explain/predict successful or failed water bioremediation. Based on this understanding, I developed means to manage the microbial community to achieve desired water-decontamination results. This research shows the benefits of looking "inside the box" for "improving the box".

TO MY FATHER

To whom hard work was his passion and giving up didn't exist in his mind and now neither in mine.

Thanks for teaching me with exemplary strength how to face tough times.

ACKNOWLEDGMENTS

I am deeply thankful to several people who contribute to my research and motivate me during adversity in my PhD program. The mentoring from my co-advisors, Dr. Bruce Rittmann and Dr. Rosa Krajmalnik-Brown, is the building block of my research. Because of their complementary feedback, I was able to blend Engineering, Chemistry, and Microbial Ecology into a concrete and fascinating research project. I'm profoundly honored by being a member of their teams. I can't thank enough Dr. Rittmann for all his grammar and writing lessons, his focus on the "take-home messages" within my wordy writing, and for encouraging me to become a team leader. I will never forget how much he trusted my work and was confident that "I can". Dr. Krajmalnik-Brown always led me to critically think about my research results and communicate better with visuals. Coming from the same country as Dr. Rosy, I was eagerly inspired by her example to develop my passion for Science. I'm also grateful to both of them for understanding my personal difficulties, and offering me their support beyond academic responsibilities.

I thank Dr. César Torres for serving in my Doctoral Committee and giving me invaluable input on my work. His feedback after my research proposal was critical to not forget the big picture. I would also thank Diane Hagner for her incessant crusades to keep the lab organized and neat. Through my PhD, I had a tremendous opportunity to work with Environmental Engineers Dr. Patrick Evans and David Friese, whose perspective from the field made my research holistic.

I give credit to my lab mentors and team partners. Dr. Michal Ziv-El, a PhD student when I started my program, trained me on the Membrane Biofilm Reactor

(MBfR) and taught me to navigate the lab. Dr. Youneng Tang, Dr. HePing Zhao, Chen Zhou, and Bi-o Kim were my MBfR team partners, and their expertise made the project a great success. My PhD fellow Esra Zehra Ilhan and Dr. Dae-wook Kang taught me pyrosequencing. A great team member was graphic designer Rosa Romero-Benitez, who always was willing to help and make science more understandable, creative, and fun.

I have grown and continue to grow as a researcher thanks to mentoring younger researchers Joshua Steele, Mackenzie Hagan, and Michael Alder, and visiting scientists Dr. Eri Nakahihara, Dr. Liang Feng, Sumaira Aslam, Louis de Saint Cyr, Alisson Theuillon, Luis Ordaz Diaz, and Xiaoyin Xu.

I could not make it to this point without my friend and PhD fellow Michelle Young, who is definitely my biggest support at school. I also would like to thank my fellow PhD student and friend Diana Calvo for always cheering me up.

Last, much of my success in graduate school is because of my family. I am grateful to my parents for embracing with happiness and enthusiasm my dreams and goals. I thank my brother for remaining positive and easing harsh times for all the family. I thank my second mother, my grandma auntie Esperanza, for her dedication to raise me. Many words of thanks go to my boyfriend and forever partner: Jesus, thank you so much for understanding my work, and for helping me to balance my life.

My research was funded by the Consejo Nacional de Ciencia y Tecnologia (CONACyT) as a scholarship to study at ASU, by the Environmental Security Technology Certification Project (ESTCP) grant ER200541, and by the Swette Center for Environmental Biotechnology. I am greatly thankful to Private Association “Alberto and Dolores Andrade” for funding me from elementary school until today.

TABLE OF CONTENTS

Page

LIST OF TABLES

Table Page

Table Page

LIST OF FIGURES

Figure Page

Figure Page

Chapter 1

INTRODUCTION

1.1 Water: a constrained non-renewable resource

Continuous population growth and demand for clean water have made water availability one of the biggest problems worldwide (Vorosmarty et al., 2000). The United Nations (UN) estimates that one in six people lack access to clean water (UNEP, 2010). The Millennium Development Goals (UN, 2012) established a target in this regard: "halve by 2015, the proportion of the population without sustainable access to safe drinking water." While progress has been made -- according to UN (2012), 89 percent of the world population by 2010 had access to safe drinking water -- statistics report an aggregated "big picture" that may mask severe problems in specific parts of the world. In fact, severe water shortage problems worldwide are due to water pollution as result of improper disposal of industrial, agricultural, and municipal waste. For instance, 70% of the industrial waste at developing countries is discharged untreated into water bodies (UNEP, 2010). Anthropogenic activities (e.g., agricultural production, chemical manufacturing, and nuclear weapon testing) have led to water pollution and reduced the amount of safe drinking water sources.

The release of billions of pounds of toxic waste to water sources affects human health and ecosystem equilibrium. On the health side, some of these chemicals are considered carcinogens (e.g., vinyl choride, arsenic, trichloroethene (TCE)); others affect the thyroid (e.g., perchlorate (ClO_4^-)), cause kidney problems (e.g., heavy metals and uranium (UVI)), disrupt the nervous system (e.g., lead), and impair language, attention, and memory in children (e.g., mercury). The consequences are biggest among sensitive

populations (e.g., pregnant women, children, and the poor). For example, the UNEP (2010) estimated that about 90% of deaths connected to water-related diseases are children under 5 years old. Water pollution also destroys ecosystems and alters the cycle of ecosystem services, those on which human health, biodiversity, and food production rely (UNEP, 2010). For example, agricultural, fisheries, and livestock activities, which rely on sufficient water quantity and quality, are harmed if water quality is compromised.

While preventive actions have been promoted by stronger regulations and awareness campaigns (UNEP, 2010), remediation technologies are needed to enhance water quality. My research focuses on understanding a novel form of biological treatment that offers the possibility of being more effective than conventional water treatment for some of the most harmful water contaminants that have emerged in the past few years.

Physico-chemical water treatment

Polluted waters are often treated using separation units that apply physico-chemical principles such as adsorption, ionic attraction, and filtration. While effective in some cases, treatment technologies such as activated carbon, ion exchange, and reverse osmosis are expensive, require considerable energy inputs, and only concentrate the pollutants (Cha et al., 1999). In particular, ion exchange is the most commonly used water treatment technology to remediate ClO_4^- pollution (US EPA, 2005). However, it generates brine that contains such high salinity that it can be disposed of only in the ocean or in isolated deep wells, both options are expensive and not always logistically feasible. The generation of brine during ion exchange exemplifies how conventional

technologies generally do not destroy water pollutants; instead, these technologies only isolate or concentrate the pollutants into a new medium.

1.2 Microbial reduction of oxidized compounds in water

In contrast to conventional water treatment, biological technologies can transform a broad spectrum of hazardous chemicals and convert them into safer substances. In my research, I utilized the intrinsic capacity that microorganisms have to reduce or oxidize chemical compounds while obtaining energy for growth. The reduction of an oxidized contaminant (electron acceptor) occurs at the expense of the oxidation of an electron donor, such as an organic compound, hydrogen (H_2), or sulfide. The coupling of the reduction and oxidation reactions of these chemicals is also known as redox. Due to the relevance of microbial driven redox reactions for water reclamation, in my research I sought to understand the microorganisms capable of reducing three oxyanions: two of them are water pollutants (nitrate (NO_3^-) and ClO_4^-), while the third one is a common natural water constituent (sulfate (SO_4^{2-})). In the next sections, I describe the metabolic pathways through which key microorganisms reduce these three oxyanions.

NO_3^- reduction. Denitrifying bacteria (DB) are able to use NO_3^- as a terminal electron acceptor and capture energy as ATP by generating a proton motive force. In the case of NO_3^- reduction (called denitrification), these DB utilize a set of enzymes called reductases to produce nitrogen gas (N_2) through a series of intermediates. The denitrification process uses 5 electron equivalents from the donor (H_2) and yields -112 kJ/e^- eq (Nerenberg and Rittmann, 2004). Figure 1.1 shows the particular reductases used by microorganisms at each step of the denitrification process. Because the DB are

phylogenetically diverse, the genes that codify for the reductase enzymes have been used as molecular markers to quantify DB. Braker et al. (2000) proposed using the copper-containing nitrite reductase and the cytochrome nitrite reductase genes, *nirK* and *nirS,* as a proxy to measure the abundance of DB (Kandeler et al., 2006; Yoshida et al., 2009; Bàrta et al., 2010).

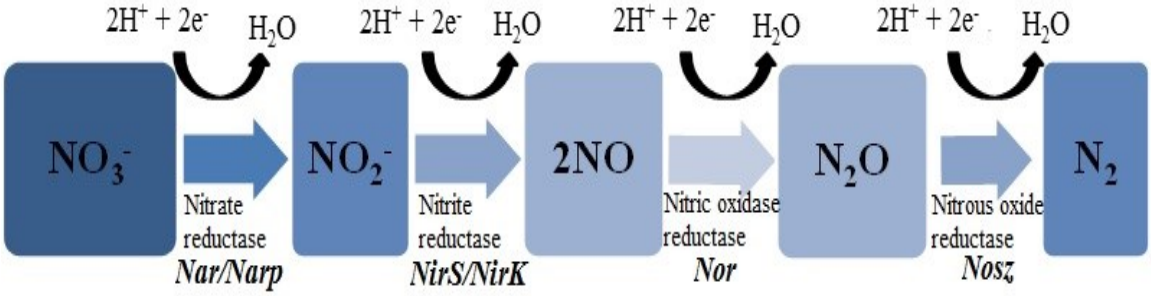

Figure 1.1 NO_3^- reduction metabolic pathway and involved reductases.

ClO_4^- reduction. For ClO_4^-, a different set of reductases is involved on the stepwise reduction from the most oxidized form to the reduced final product: chloride (Cl^-) ion. This process uses 8 electron equivalents from the donor (H_2) and yields -118 kJ/e eq (Nerenberg and Rittmann, 2004) that the perchlorate-reducing bacteria (PRB) capture as ATP via ClO_4^- respiration. PRB possess specific enzymes to reduce ClO_4^- step by step as illustrated in Figure 1.2. Similar to DB, PRB are phylogenetically diverse, and the perchlorate-reductase gene, or *pcrA,* often is used to identify PRB because of its specificity to this microbial group (Nozawa-Inoue et al., 2008).

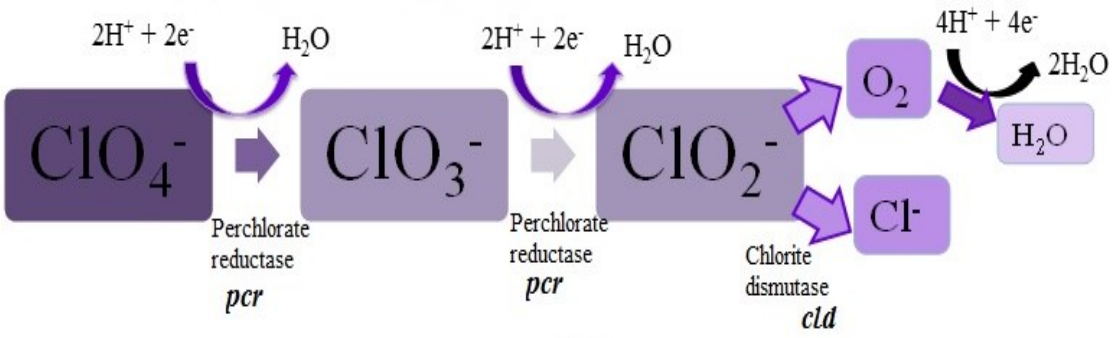

Figure 1.2 ClO_4^- reduction methabolic pathway and involved reductases.

SO_4^{2-} reduction. Sulfate-reducing bacteria (SRB) are microorganisms that use SO_4^{2-} as their terminal electron acceptor. SO_4^{2-} is reduced to hydrogen sulfide (H_2S), which requires 8 electron equivalents from the electron donor (e.g., H_2). As seen in Figure 1.3, a SO_4^{2-} molecule is first activated by a molecule of ATP, producing adenosine phosphosulfate (APS), which is further reduced into sulfite (SO_3^{2-}). SO_3^{2-} is reduced by the dissimilatory sulfite reductase enzyme (*dsr*) to produce H_2S (Peck, 1959). SO_4^{2-} reduction yields a much lower amount of energy for microbial growth, -18.3 kJ/e eq when H_2 is the electron donor, in comparison to denitrification and ClO_4^- reduction (Madigan et al., 2009). However, SRB are able to capture energy from SO_4^{2-} respiration via the proton motive force. Many SRB are metabolically versatile and can survive in the absence of SO_4^{2-}. They also are phylogenetically diverse, and the *dsr* gene is frequently used to detect them (Kondo et al., 2004, 2008; Pereyra et al., 2010).

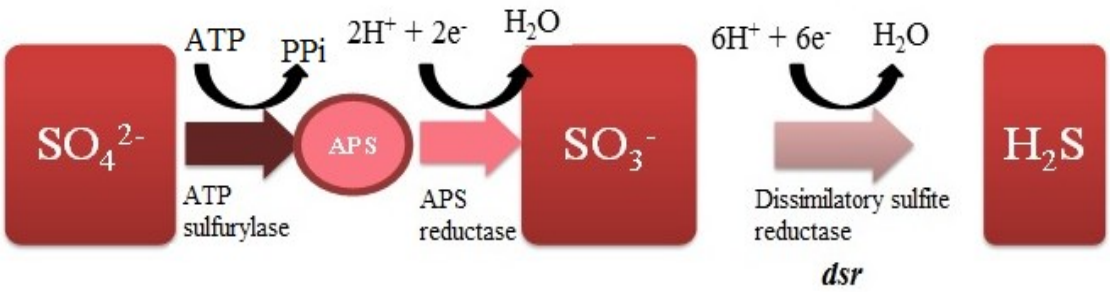

Figure 1.3 SO_4^{2-} reduction methabolic pathway and involved reductases.

Whereas NO_3^- and ClO_4^- are water pollutants for which reduction is desired, SO_4^{2-} is not considered a water pollutant and its reduction is usually undesired. One reason for this is that SO_4^{2-} reduction generates odorous and toxic H_2S. Additionally, SRB compete with DB and PRB for common resources, such as the electron donor or space in a biofilm. Therefore and as explained later in this chapter, it is imperative to manage the ecological relations among microorganisms when relying on a microbial reduction process. Usually, the growth of DB and PRB should be encouraged while SRB are suppressed.

What is known about ecological interactions among DB, PRB, and SRB? The literature reports that based on the energy yield achieved by each microbial group, DB ought to outcompete SRB (e.g., if the electron donor is not sufficient to reduce both) (Madigan et al., 2009; Tang et al., 2012a). DB can grow at much faster rates than SRB, which allows them to outcompete slow-growing SRB. While this is a generally well-accepted statement among the scientific community, it also is true that SRB and DB co-exist in some circumstances such as after suppressing SO_4^{2-} reduction activity by addition of NO_3^- (Mohanakrishnan et al., 2011).

Ecological interactions between DB and PRB are harder to elucidate, because a clear competition or collaboration has not been established yet. Some studies report that DB reduce ClO_4^- in the presence of NO_3^- (Van Ginkel et al., 2010), while others show that ClO_4^- reduction stops when NO_3^- is introduced as additional electron acceptor (Herman and Frankenberger, 1999; Choi and Silverstein, 2008).

The literature is inconclusive about detrimental effects from SO_4^{2-} reduction on ClO_4^- reduction (Waller, 2002); depending on the microbial community, both processes might occur in parallel. Moreover, the relationships among DB, PRB, and SRB are hardly understood at all. Clearly, gaining a thorough understanding of relationships among DB, PRB, and SRB is a significant need for reliable control of the reductions of NO_3^-, ClO_4^-, and SO_4^{2-}. My research focuses on understanding the ecological interactions among DB, PRB, and SRB when the goal is NO_3^- and ClO_4^- reduction, but not SO_4^{2-} reduction.

1.3 The MBfR: coupling engineering with microbial ecology

Microbial redox reactions are naturally occurring processes that can be promoted and managed in a biological reactor. I employed the Membrane Biofilm Reactor (MBfR), an *ex situ* bioremediation-based technology for water reclamation (Rittmann, 2007), to reduce NO_3^- and ClO_4^- in the presence of significant concentrations of SO_4^{2-}. In this section, I describe the principles on which the MBfR is based and what has to be done to advance this novel technology for my goal.

Figure 1.4 shows the setup of a typical bench-scale MBfR. In the MBfR, H_2 gas diffuses through the membrane walls and is used as an electron donor by microorganisms

growing as a biofilm on the outside of the membrane walls. The contaminant(s) are dissolved in the bulk liquid, which is pumped through the tubing and connecting valves and are used as electron acceptor(s) by the microorganisms growing in the biofilm. The structure of the biofilm is counter-diffusional: the electron donor (H_2) travels from the inner core of the membranes to the biofilm layer, while the electron acceptor is transported in the opposite direction, from the bulk liquid to the biofilm layer. The biofilm community carries on a series of redox reactions in which the contaminants are reduced into innocuous or into immobilized forms. Besides the reductions already presented for NO_3^- and ClO_4^-, other oxidized compounds have also been successfully reduced in the MBfR, some examples include: soluble selenate (SeO_4^{2-}) (Chung et al., 2006b) and trichloroethene (TCE) (Chung et al., 2008; Ziv-El et al., 2012). Under anaerobic conditions, the right microorganisms can convert SeO_4^{2-} into selenite (SeO_3^{2-}) and elemental selenium (Se^0), a precipitate, and a different set of microorganisms can reductively dechlorinate TCE to ethene.

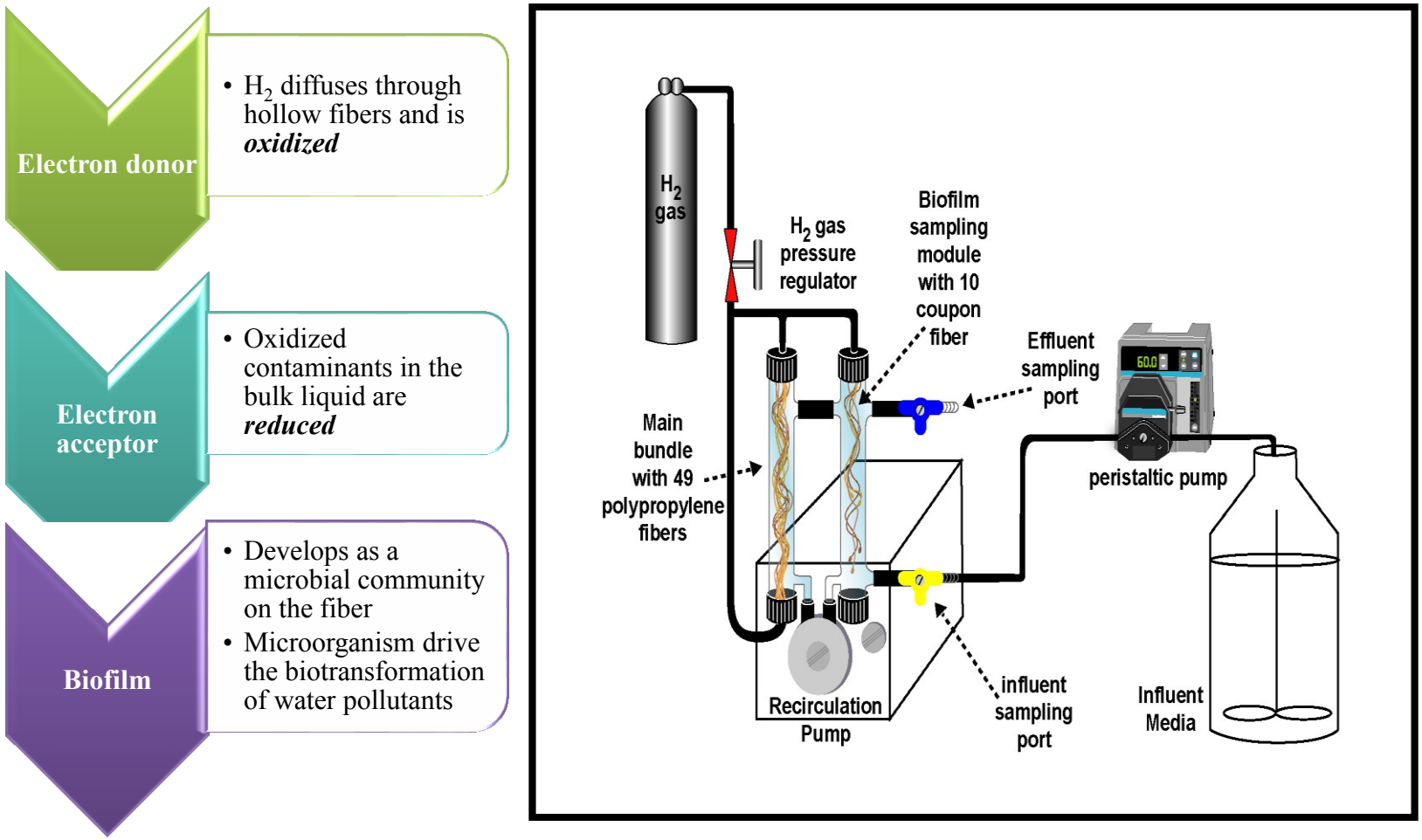

Figure 1.4 The MBfR, a bioremediation-based water reclamation technology. The diagram at the left explains in short the redox principle of the MBfR, while the schematic at the right shows the bench-scale configuration of the MBfR.

What do we know and not know about the MBfR?

Past research about the MBfR is extensive and shows progress and promise, including successful results at the pilot scale (Adham et al., 2003; Tang et al., 2010; Evans et al., 2013) and full industrial-scale application (APTWater Technologies®, 2013). In chronological order, Lee and Rittmann (2000, 2002) developed the original MBfR to reduce NO_3^-, and their efforts were followed by Nerenberg and Rittmann (2002) for ClO_4^- reduction. Nerenberg and Rittmann (2004) also developed a series of screening tests to demonstrate the capacity of the MBfR to reduce several other oxidized contaminants. Since then, studies have focused on characterizing the key operational parameters (e.g., H_2 pressure, acceptor loadings) that govern the reduction of several contaminants: arsenate (AsO_4^{3-}) (Chung et al., 2006a), SeO_4^{2-} (Chung et al., 2006b), chromate (CrO_4^{2-}) (Chung et al., 2006c), and chlorinated solvents (Chung and Rittmann, 2007; Chung et al., 2008; Ziv-El et al., 2012). Often, the reductions occurred with several electron acceptors simultaneously (e.g., Chung et al., 2007b; Ziv-El et al., 2009). Even ion exchange brines containing $NO_3^-$and ClO_4^- were successfully treated in MBfRs (Chung et al., 2007a; Van Ginkel et al., 2008).

An important milestone accomplished in MBfR research was the modeling work developed by Tang et al. (2012a, b, c; 2013). They developed mathematical models to predict the behavior of the MBfR biofilms during simultaneous reduction of NO_3^- and SO_4^{2-}, NO_3^- and ClO_4^-, or NO_3^- and TCE. These modeling works provide a framework for my research.

Another important step was characterizing the MBfR's "performance surface". Ziv-El and Rittmann (2009) illustrated how the combination of H_2 availability and

electron-acceptor loading rate control the contaminant's reduction. In brief, a higher H_2 pressure promotes a higher rate of contaminant reduction at a constant electron acceptor loading, while an increase to the electron acceptor loading decreases the contaminant's reduction at a constant H_2 delivery.

Only modest attention has been paid to the role of microbial interactions and microbial ecology in the biofilm. While some studies took the initiative to study the biofilm's community structure when aiming for specific water-reclamation goals with the MBfR (Chung et al., 2006d; Nerenberg et al., 2008; Van Ginkel et al., 2010; Zhang et al., 2010), those studies were not performed in a systematic way; they just gave a "snapshot" of the biofilm community. Nevertheless, those studies pointed to the value of a thorough understanding of the microbial ecology for the MBfR. More recently, Zhao et al. (2011) implemented a more comprehensive program to understand the interactions between DB and PRB. Likewise, Ziv-Et al. (2012) demonstrated systematically the significance of understanding important microbial interactions in order to efficiently manage and achieve an optimal microbial community of a mixed consortium to achieve complete dechlorination of TCE. Ziv-El et al. (2012) employed a management strategy that emphasized suppressing the activity of non-desired methanogens and to certain degree restricting the electrons flow for homoacetogenesis.

The insights gained in the above-listed studies inspired me to investigate the microbial ecology of the biofilm with multiple electron acceptors. I wanted to understand the principles needed to manage the co-reduction of several acceptors. These principles involve, competition between microbial groups and synergistic relationships among the members in the microbial community. To achieve the desired contaminant destruction

and understanding of the developed microbial communities, I crafted ways to attain the desired reductions without enhancing undesired reductions. For instance, H_2 delivery and electron acceptor loading are the two key parameters that affect the MBfR's performance (Ziv-El and Rittmann, 2009) and thus determine developing interactions and frame the microbial ecology of the biofilm. An over-supply of electron donor (H_2) can favor SO_4^{2-} reduction and enhance the growth of SRB, which reduce SO_4^{2-} into toxic and corrosive H_2S (US EPA, 2012c). Despite the fact that SRB are slow-growing microorganisms (Rittmann and McCarty, 2001), under conditions favorable to them, they can outcompete fast growing desirable bacteria such as PRB (Sorokin et al., 2003). Hence, suppressing SO_4^{2-} reduction is important given its possible competition with other important microbial processes such as ClO_4^- reduction.

It is clear that to advance the emerging MBfR technology, efforts must be oriented toward managing the microbial community in the biofilm to attain desired water treatment goals. Thus, my research focus was on controlling the interactions in the biofilms of the MBfR so that two commonly found together oxidized contaminants (i.e., NO_3^- and ClO_4^-) are reduced in the presence of a natural water constituent (i.e., SO_4^{2-}) that I did not want to reduce. I sought to manage the ecological interactions among microorganisms in the biofilm by promoting favorable NO_3^- and ClO_4^- reduction while minimizing undesirable SO_4^{2-} reduction.

My strategy involved balancing the MBfRs critical parameters that ought to control the microbial interactions and reactor performance. Specifically, H_2 pressure and electron acceptor loading were the levers that I employed. If I balance them properly, I should grow the "right bacteria" to do the "proper job." I also aimed to know that I have

achieved the desired biofilm community. For that, I opened up the "black box" of the biofilm's microbial ecology and looked at the microorganisms present and what they were doing.

1.4 Opening the black box by defining the microbial ecology

In an opinion article, Ward (2004) stated that bioremediation can be viewed as a "black box" that hides the features of the community that performs the detoxification service. In fact, bioremediation is carried out by microbial communities rather than a single strain. Communities are advantageous because they can have high metabolic diversity and redundancy. To fully exploit the potential of the community, the microbial ecologist needs to know what microorganisms are present in the community, what these microorganisms are doing, and how they interact with other members in the microbial community. This assessment correlates the microbial community's structure and function. It opens the black box, making it possible to understand how the community works.

In this assessment, genomics -- analysis of nucleic acids (i.e., DNA) -- determine the abundance of different types of microorganisms, along with the presence of specific genes involved in degradation pathways. Continual advances in genomics (Liu and Suflita, 1993; Iwamoto and Nasu, 2001; DeLong, 2002; Rittmann, 2006) accelerate our understanding of microbial communities and means to manage them towards delivering a service to society, such as water remediation.

In my research, I rely heavily on two microbial ecology techniques to understand what microorganisms are present: quantitative Polymerase Chain Reaction (qPCR) and

pyrosequencing, as has been advocated by others (Zhang et al., 2011; Ziv-el et al., 2012). Both methods are based on the polymerase chain reaction. On the one hand, qPCR amplifies a specific DNA section in such a manner that the number of gene copies per volume can be computed based on fluorescent emission (Smith and Osborn, 2009). On the other hand, pyrosequencing is high-throughput sequencing technique that provides a high level of resolution for the diversity within the community (Ronaghi, 2001). The two methods are complementary.

Figure 1.5 illustrates how, by applying these two techniques together, the structure within the "black box" can be elucidated. The two analyses work in concert to assess the microbial community structure of the biofilm to relate it with the microbial community function at a critical reactor's performance period. On one side, qPCR allows the quantification of known microbial groups by targeting specific genes (e.g., reductase enzymes involved in the reduction pathway of an oxidized contaminant). On the other side, pyrosequencing is a high-throughput sequencing analysis that permits to assess the relative abundances of microbial phylotypes (classification given by evolutionary relationships among microorganisms), thus revealing the microbial diversity and the community structure within the community.

The two tools are well tuned to provide different, but complementary information. While qPCR is a semi-quantitative assay that is specific and has a relatively rapid turn-around time, pyrosequencing offers information about the whole community, i.e., key members in the community as well members performing secondary tasks (not reduction of oxidized contaminants) like fermentation. The amount of a microbial group at a particular point can be measured and correlated to gene copies per ml of sample or

surface area of biofilm with a well-designed qPCR protocol. Pyrosequencing allows us to define microbial community structures through a taxonomical break down of thousands of sequences amplified from any given sample. In summary, by employing qPCR and pyrosequencing, key microorganisms can be monitored when either the reactor is operating successfully or when it is failing.

Besides the microbial ecology, a key constituent of my research is to monitor the reactor's performance, or the electron-acceptor removal rate. I use ion chromatography (IC) analysis to detect the influent and effluent concentrations of NO_3^-, ClO_4^-, and SO_4^{2-}. IC works based on the separation of ions or polar molecules due to their charges. These ions are retained in a stationary phase, and detected at a specific time after injecting the sample through the equipment. IC not only detects several compounds within a sample, but also reports the concentrations of those compounds. This analysis allowed me to measure the microbial community function in the MBfR, and it complements the output of qPCR and pyrosequencing to better relate microbial community structure and function.

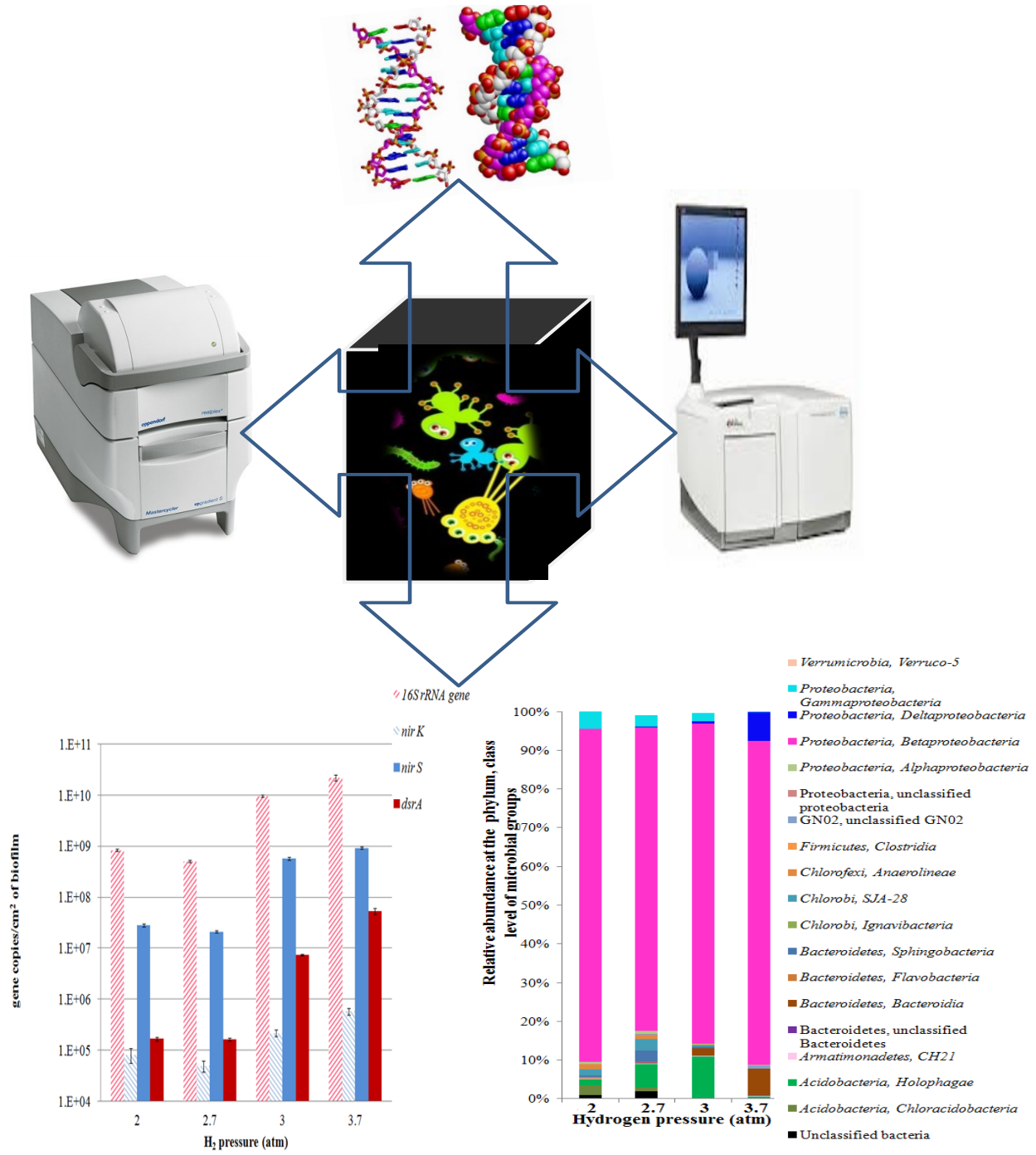

Figure 1.5 Opening the black box of microbial ecology by qPCR and pyrosequencing. The two analyses done in concert provide a comprehensive understanding of the microbial community function and structure.

1.5 Objectives and content of the dissertation

The over-arching objective of my dissertation is to understand the competitive and synergistic relationships in mixed microbial communities in MBfR biofilms used to manage the reductions of NO_3^- and ClO_4^-in the presence of SO_4^{2-}. I studied different combinations of these electron acceptors in a series of complementary studies, each of which comprises a chapter of the dissertation. In all the studies, I related the microbial community structure with the function in the MBfR. I tested and applied several strategies to achieve successful removal of the oxidized contaminants NO_3^- and ClO_4^- while controlling SO_4^{2-} reduction. I also provide insightful analysis on how pilot MBfRs reactors must be operated to achieve complete microbial reduction of NO_3^- and ClO_4^- while holding SO_4^{2-} reduction from being active. I describe below the themes and objectives of each chapter.

Chapter 2. The objective is to understand how DB and SRB are able to establish competitive or co-existence relationships. I use two MBfRs and modify either the electron donor availability (H_2 pressure) or the electron acceptor (i.e. NO_3^-) surface loading, and I evaluate the reduction of NO_3^- and SO_4^{2-} along with the abundances of DB and SRB (assayed by qPCR) at each steady state. The results allow me to address the question of whether DB and SRB compete for common resources or are able to co-exist despite of lack of SO_4^{2-} reduction. This research was published in an altered format in *Environmental Science and Technology* (Ontiveros-Valencia et al., 2012).

Chapter 3. To further investigate the ecological relationships between DB and SRB in the hydrogen-fed biofilms previously described in Chapter 2, I use high throughput sequencing (454 pyrosequencing). Here, I expand the findings of Chapter 2

beyond the presence of DB and SRB by researching which DB and SRB phylotypes were present in the MBfR. I also include the interactions of DB and SRB with other members in the biofilm community, evaluate the key drivers of the microbial community structure (i.e., electron donor availability and electron acceptor surface loading), and describe how the onset of SO_4^{2-} reduction alters the microbial community of the biofilm. This chapter was published in an altered format in *FEMS Microbial Ecology* (Ontiveros-Valencia et al., 2013a).

Chapter 4. Besides the ecological interactions between DB and SRB described in Chapters 2 and 3, I am interested in understanding the ecological interactions of a biofilm populated with PRB, SRB, and DB. This builds on my research for Chapter 2 and 3, and here I add a third electron acceptor, ClO_4^-, which has a very stringent treatment goal. I use a single-stage MBfR to treat a groundwater highly contaminated with ClO_4^- (~10000 μg ClO_4^-/L), a relatively low nitrate input (2 mg N/L), and significant SO_4^{2-} concentration (~60 mg/L). Thus, management of the ecological interactions among DB, PRB, and SRB becomes crucial to achieve the water reclamation goal. I discover a competitive relationship between PRB and SRB that prevented complete ClO_4^-reduction, (i.e., effluent ClO_4^- concentration < 4 μg/L). Hence, controlling this competition is necessary for achieving a ClO_4^- concentration below 4 μg/L. This research was published in an altered format in *Biotechnology and Bioengineering* (Ontiveros-Valencia et al., 2013b).

Chapter 5. Based on the findings of Chapter 4, my next objective is to clarify further the ecological interactions between PRB and SRB while aiming for complete ClO_4^- reduction from an atypically high ClO_4^- influent concentrations (~4000 μg ClO_4^-/L) in the presence of SO_4^{2-} (~55 mg/L). Because modifying the H_2 pressures and acceptors

surface loading in the single-stage MBfR described in Chapter 4 did not result in 100% ClO_4^- removal, I configure a two-stage MBfR (i.e., lead and lag MBfRs). The two-stage MBfR can attain 100% ClO_4^- removal, achieved by minimizing SO_4^{2-} reduction. I alter two key parameters of the MBfR (H_2 pressure and electron-acceptor surface loading) in ways to enhance the growth of PRB over SRB. During the process, I assess the microbial community structure of each stage (lead and lag) using qPCR and pyrosequencing. The results show that SRB compete strongly with PRB for space in the biofilm and also establish synergistic relationships with other members in the microbial consortia. This research was published in an altered format by *Water Research* (Ontiveros-Valencia et al., 2014a).

Chapter 6. This chapter is part of a pilot project that was a team effort involving researchers at ASU, CDM-Smith, and APTwater. It was a comprehensive project in which I took the lead for the ASU team. The goal of the pilot-scale MBfR, operated at Rialto, CA, was the production of drinking water after removal of two oxidized contaminants: NO_3^- and ClO_4^-. The research in Chapter 6 builds on the findings described in Chapters 4 and 5; however, the ratio between the NO_3^- and ClO_4^- concentrations is significantly higher at Rialto than for the groundwater treated in Chapters 4-5. In other words, Rialto's groundwater had NO_3^- as high as ~9 mg N/L and ClO_4^- as 160-200 µg/L. In this chapter, I report directly on one of my key strategies, characterizing the microbial community structure of the pilot two-stage MBfR by using pyrosequencing. Contrary to the MBfRs in Chapter 5, the pilot two-stage MBfR in Chapter 6 was operated in a way that facilitated SRB growth, and the two-stage MBfR could not consistently achieve complete ClO_4^- reduction. My pyrosequencing analysis

shows that the upswing in SRB was detrimental for achieving complete ClO_4^- removal in the pilot two-stage MBfR. Most importantly for this chapter, I show that the biofilms that had substantial SRB had higher diversity that came from other members besides the expected DB, PRB, and SRB – i.e., sulfur oxidizers and heterotrophs – that competed for space with PRB. This chapter has been submitted for publication (Ontiveros-Valencia et al., 2014b).

Chapter 7. In this chapter, I summarize the key behaviors I saw among DB, PRB, and SRB through Chapters 2-6, along the strategies to manage the community in the MBfR biofilm. I also propose several studies to extend on the competition between SRB and PRB observed in the MBfR, along with ways to elucidate further the roles of other members in the biofilm. Finally, I recommend how to look "outside of the box", and assess the sustainability of the MBfR.

Chapter 2

INTERACTIONS BETWEEN NITRATE-REDUCING AND SULFATE-REDUCING BACTERIA COEXISTING IN A HYDROGEN-FED BIOFILM.

This chapter was published in an altered format in *Environmental Science and Technology* (Ontiveros-Valencia et al., 2012)

2.1 Introduction

To assess the ecological interactions of microorganisms in the MBfR, I started with a series of experiments designed to understand competition or coexistence behaviors between DB and SRB. I used qPCR to relate the biofilm community structure with the microbial community function when NO_3^- and SO_4^{2-} were present at the same time.

Common sources of NO_3^- and nitrite (NO_2^-) are agricultural run-off, wastewater discharges, and leaching from septic tanks. Infants are particularly at high risk because ingestion of NO_3^- and NO_2^- can lead to methemoglobinemia. Hence, the US Environmental Protection Agency (EPA) has established maximum contaminant levels (MCLs) of 10 mg N/L for NO_3^- and 1 mg N/L for NO_2^- (US EPA, 2012a). Because NO_3^- and NO_2^- serve as nutrients for photoautotrophs, the accumulation of these two oxidized contaminants also threatens surface-water quality and spurs eutrophication of water bodies. Concentrations much less than 1 mgN/L often are necessary to preclude eutrophication (World Health Organization, 2002).

Microbial reduction of NO_3^- and NO_2^- is a promising biological alternative for remediating water contaminated with these compounds. Denitrification, the microbial reduction of NO_3^- and NO_2^- to form N_2 gas, involves the stepwise reduction from the most oxidized form, NO_3^-, to N_2 gas. The reduction pathway is driven by a series of

enzymes which is showed in Figure 1.1 in Chapter 1. NO_3^- reductase reduces NO_3^- to NO_2^-, and NO_2^- reductase converts NO_2^- to nitric oxide (NO), which is further reduced by NO reductase to nitrous oxide (N_2O). Finally, N_2O is reduced to N_2 gas by a N_2O reductase (Rittmann and McCarty, 2001). This process involves a total transfer of 5 electrons from the electron donor per mole of NO_3^- and allows the DB to gain a total energy yield of -112 KJ/e^- eq, which is only slightly lower than respiration of O_2 (Rittmann and McCarty, 2001).

SO_4^{2-} is another respiratory electron acceptor for microorganisms commonly found in water and wastewater. Figure 1.3 in Chapter 1 explains in detail the dissimilatory SO_4^{2-} reduction process. In short, SRB spend one molecule of ATP to activate SO_4^{2-} by an ATP sulfurylase, producing APS and pyrophosphate (Peck, 1959). After the activation, APS is reduced by an APS reductase to form SO_3^{2-} and adenosine monophosphate (AMP). SO_3^{2-} is then reduced by a sulfite reductase to form H_2S. This process involves a total transfer of 8 electrons from the electron donor to reduce SO_4^{2-} to H_2S and allows SRB to gain a total energy yield of -18.3 KJ/e^- eq (Madigan et al., 2009). Hence, SO_4^{2-} reduction yields ~16% of the energy of denitrification, and SRB grow proportionally slower than do DB (Rittmann and McCarty, 2001).

While NO_3^- is a water contaminant, SO_4^{2-} is not normally considered a health concern, and no MCL has been established for SO_4 (US EPA, 2012c). However, the US EPA has a secondary standard that is based on deleterious aesthetic effects (taste and odor) from SO_4^{2-} and potential for causing diarrhea in humans when SO_4^{2-} is at concentrations higher than 250 mg/L. Perhaps even more important is that SO_4^{2-}

reduction produces H_2S, a corrosive, odorous, and toxic substance. Thus, SO_4^{2-} reduction usually is an unwanted process.

The H_2-based MBfR has been used to achieve the microbial reduction of a broad spectrum of oxidized contaminants (Lee and Rittmann, 2002; Nerenberg and Rittmann 2004; Chung et al., 2007b; Ziv-El and Rittmann, 2009). In the MBfR, H_2 gas diffuses through the walls of hollow-fiber membranes and serves as the electron donor for autotrophic bacteria that grow as biofilm on the membrane's outer surface. The H_2-oxidizing bacteria reduce one or more oxidized contaminants, transforming them into innocuous forms. For instance, NO_3^- and NO_2^- are converted to N_2 gas.

The bio-reduction of NO_3^- has been studied extensively in H_2-fed biofilms over a range of operating conditions (e.g., H_2 pressure, surface loadings, and pH) either as a sole contaminant (Lee and Rittmann, 2002) or with simultaneous reduction of other oxidized contaminants (Nerenberg and Rittmann, 2004; Chung et al., 2006b, c; Ziv-El and Rittmann, 2009). These studies concluded that H_2 availability (controlled by adjusting the H_2 pressure) provides sensitive control over the rate and extent of microbial reduction of NO_3^- in the H_2-fed biofilms. A higher H_2 pressure can increase the delivery rate of H_2 to the biofilm and the kinetics of denitrification. But also, a higher H_2 availability also raises the chances for SO_4^{2-} reduction, because H_2 can remain after denitrification is complete.

The literature on SO_4^{2-} reduction points out that NO_3^- inhibits SO_4^{2-} reduction due to electron donor competition, accumulation of denitrification intermediates, and high NO_3^- loadings (Zhang et al., 2008). In fact, NO_3^- addition has been used as strategy to control unwanted SO_4^{2-} reduction in various settings (Jenneman et al., 1986; McInerney

et al., 1996; Londry and Suflita, 1999). In H_2-fed biofilms, SO_4^{2-} reduction usually has been minimal, as most H_2-based MBfRs have been operated to just accomplish denitrification (e.g. Lee and Rittmann, 2002). However, SO_4^{2-} reduction in the H_2 based-MBfR occurred during co-reduction of other oxidized contaminants, such as arsenate (Chung et al., 2006a), selenate (Chung et al., 2006b), chromate (Chung et al., 2006c), and chlorinated solvents (Chung and Rittmann, 2008; Zhang et al., 2010). In some cases, H_2S production was encouraged in order to precipitate toxic compounds such as arsenic (Chung et al., 2006a), zinc (Scharwz and Rittmann, 2007a, b), hexavalent uranium (Marsili et al., 2005), and cadmium (Wang et al., 2000). Some SRB also are capable of utilizing NO_3^- as an electron acceptor (Dalsgaard and Bak, 1994) by using a perisplasmic nitrate reductase (Nap) to reduce to NO_2^-, which is further reduced to ammonium (NH_4^+) by a cytochrome c nitrite reductase (ccNir) (Moura et al., 2007).

Because SO_4^{2-} reduction is undesirable in most cases, but desired in special cases, it is important to understand how to control it in H_2-fed biofilms. Part of that understanding is defining the microbial community formed by DB and SRB; we used qPCR to determine how DB and SRB defined the structure of the biofilm community in the H_2-based MBfR and how the structure related to operational conditions, such as H_2 availability and acceptor surface loading. Because NO_3^- is a more thermodynamically favorable electron acceptor than SO_4 (Rittmann and McCarty, 2001; Madigan et al., 2009) we hypothesize that SRB will be outcompeted by DB when H_2 is the limiting factor in the MBfR. The corollary is that decreasing the NO_3^- loading will enhance SO_4^{2-} reduction for a fixed donor delivery.

Due to the substantial phylogenetic diversity of DB and SRB, quantification of these two groups using only 16S rRNA gene is not reliable. Hence, targeting functional genes to determine DB and SRB in a mixed community is a more realistic approach. Braker et al. (2000) proposed two nitrite reductases − the Cu-containing nitrite reductase (*nirK*) and cytochrome cd1 nitrite reductase (*nirS*) -- as molecular markers for DB. These two enzymes have been applied widely in environmental samples (Kandeler et al., 2006; Yoshida et al., 2009; Bárta et al., 2010) including H_2-fed biofilms (Zhao et al., 2011). Based on current understanding in the literature, DB have either NirK or NirS as their NO_2^- reductase enzyme, since a strain having both genes has not been identified (Knowles, 1982; Philipppot et al., 2007). To target SRB in mixed communities, the functional gene for the α-subunit of the dissimilatory sulfite reductase (*dsrA*) has been applied to quantify SRB in aquatic samples (Kondo et al., 2004, 2008) industrial wastewater (Ben-Dov et al., 2007), petroleum-contaminated marine sediments (Chin et al., 2008), soda lakes (Foti et al., 2007), and the intestines of non-human primates (Nakamura et al., 2009) and humans (Pereyra et al., 2010) but not before in H_2-fed biofilms.

This chapter focused on what controls competition versus coexistence of DB and SRB in the H_2-based MBfR. I evaluated NO_3^- and SO_4^{2-} reduction kinetics (i.e., the community function) and the community structure of the MBfR biofilm in a series of experiments designed to determine how different loadings of NO_3^- and different H_2 pressures (controlling H_2 availability) promote or inhibit SO_4^{2-} reduction.

2.2. Materials and Methods

Reactor configuration

I used two MBfRs with a set up similar to Ziv-El and Rittmann (2009). Each MBfR was composed of two glass tubes interconnected with Norprene tubing (Masterflex, model 06404-15, 16, 26) and plastic fittings (Figure 1.2). In one glass tube, I inserted a set of 49 25-cm long, non-porous polypropylene membranes (Teijin, Ltd., Japan) that were potted at their end with glue. The polypropylene fibers have a H_2 permeation coefficient of 0.0014cm^2/d (Tang et al., 2012d). In the other glass tube, I inserted 10 "coupon" membranes for biomass sampling which were potted on one end; the membrane type was the same as for the main bundle. The MBfR total volume was 60 mL. H_2 was delivered to the lumen of the fibers at a controlled pressure, and it diffused through the walls of the non-porous polypropylene membranes. The MBfRs Electron-donor-varied steady state (EDvSS) and Electron-acceptor-varied steady state (EAvSS) were operated in a continuous mode with influent flow rates of 0.67 and 0.17 mL/min, respectively, with a recirculation rate of 150 ml/min in each MBfR which allowed for complete mixing of the liquid. The corresponding hydraulic retention times (HRTs) were 89 and 352 min. Table 2.1 summarizes the operating conditions for both MBfRs. For EDvSS, the only variable was the H_2 pressure, which was stepwise increased once the NO_3^- effluent concentrations reached a steady state. A steady state was defined when the variations of NO_3^- and SO_4^{2-} effluent concentrations were less than 10% over at a minimum of three HRTs. Each steady state had a duration of at least 20 days. For EAvSS, all operating conditions were kept constant except for the NO_3^- influent concentration, which was changed once the MBfR performance reached steady state.

Table 2.1 Experimental conditions for EDvSS and EAvSS

Steady states	EDvSS			EAvSS		
	H_2 pressure atm	**Influent NO_3^- concentration mg NO_3^- as N/L***	**Influent SO_4^{2-} concentration mg/L***	**H_2 pressure atm**	**Influent NO_3^- concentration mg NO_3^- as N/L***	**Influent SO_4^{2-} concentration mg/L***
1	1.7	10	46	2.7	10	46
2	2.0	10	46	2.7	20	46
3	2.7	10	46	2.7	5	46
4	3.0	10	46	2.7	1	46
5	3.4	10	46	2.7	10	46
6	3.7	10	46	2.7	25	46

*Variations in the influent concentrations are shown in Figures 2.1 and 2.3.

Notes:
(1) Pressure in atm = (psig/14.7) + 1. Pressure in kPa =atm*101.32.
(2) The maximum H_2 flux for all the pressures tested in these experiments was calculated as described by Tang et al. (2012d).
(3) Samples were run chronologically as they are presented in this table.
(4) Both reactors were operated at room temperature (25°C).

Medium, inoculation, and continuous operation

I fed the reactors with a synthetic medium similar the one used by Chung et al. (2006c). The composition of the feed medium was (g/l): KH_2PO_4, 0.128; Na_2HPO_4, 0.434; $MgSO_4 \cdot 7H_2O$ 0.109; $NaNO_3$ as N, 0.0607, $CaCl_2 \cdot 2H_2O$, 0.001; $FeSO_4 \cdot 7H_2O$, 0.001; $MgCl_2$, 0.0034; and 1 ml of trace mineral solution. I adjusted the pH to 7.2$\pm$0.1 with 10% HCl. For both MBfRs, I kept the SO_4^{2-} influent concentration constant (~46 mg/L; the actual concentration in the influent varied slightly and was measured).

I inoculated both MBfRs with 1 ml of activated sludge from the Mesa (Arizona) Northwest Wastewater Treatment Plant. Before inoculating the reactors, I diluted 1 ml of activated sludge into 59 ml of synthetic medium. I left the reactors in batch operation for 24 h after inoculation, and then I put the reactors into continuous operation according to the first phase of Table 2.1.

Nitrate, nitrite, and sulfate analyses

I took 1-mL influent and effluent samples and filtered them immediately through 0.2-μm membrane filters (LC+PVDF membrane, Pall Life Sciences Acrodisc Syringe Filters, USA). I assayed for influent and effluent concentrations of NO_3^-, NO_2^-, and SO_4^{2-} by using an anion IC (Dionex ICS 3000). The IC had an AG18 pre-column, an AS18 column, an eluent of 22-35 mM potassium hydroxide (KOH), and an eluent flow rate of 1 ml/min. To monitor the possible use of NO_3^- as an electron acceptor for the SRBs, NH_4^+ was analyzed with a cation IC (Dionex 3000). I analyzed the pH of the influent and effluent samples with a pH meter (Orion Star, USA). The pH for effluent samples was maintained stable in the range of 7.5-7.8.

Oxygen analysis

Since oxygen (O_2) was not removed from the influent medium, O_2 was an electron acceptor. O_2 influent concentrations were measured with a dissolved oxygen (DO) probe (Orion Star, USA). The range of O_2 in the medium was 7.8-8.0 mg/L. Effluent O_2 concentrations were assumed to be negligible (Lee and Rittmann, 2002; Nerenberg and Rittmann, 2004; Ziv-El and Rittmann, 2009).

NO_3^-, SO_4^{2-}, and O_2 removal fluxes

I calculated the NO_3^-, SO_4^{2-}, and O_2 removal fluxes (J, in g/m^2-d) based on equation 2.1:

$$J = \frac{Q \times (S^\circ - S)}{A} \qquad \text{(Equation 2.1)}$$

where Q = volumetric flow rate (L/day), A = membrane surface area (m^2), and S° and S were the influent and effluent concentrations (g/L) for the electron acceptor: NO_3^-, SO_4^{2-}, or O_2. To establish if the delivery rate of the electron donor was limiting or sufficient, I calculated the experimental H_2 flux from the stoichiometry given in equations 2.2 to 2.4 (Rittmann and McCarty, 2001; Tang et al., 2012a):

$$NO_3^- + 3.0\ H_2 + 0.23\ CO_2 + H^+ = 0.48\ N_2 + 0.046\ C_5H_7O_2N + 3.4\ H_2O$$

(Equation 2.2)

$$SO_4^{2-} + 4.2\ H_2 + 0.015\ NO_3^- + 0.075\ CO_2 + 1.515\ H^+ = 0.5\ H_2S + 0.5\ HS^- + 4.17\ H_2O + 0.015\ C_5H_7O_2N$$

(Equation 2.3)

$$O_2 + 2.4\ H_2 + 0.028\ NO_3^- + 0.14\ CO_2 + 0.028\ H^+ = 0.028\ C_5H_7O_2N + 2.3\ H_2O$$

(Equation 2.4)

I then computed the total flux by summing the H_2 fluxes for all acceptors and compared the experimental H_2 flux with the theoretical maximum H_2 flux through the polypropylene fibers for the given H_2 pressure calculated according to Tang et al. (2012d).

DNA extraction

Once the reactors showed steady state reduction of either NO_3^- only or NO_3^- and SO_4^{2-}, I sampled the fiber biofilm by cutting a ~12 cm-long section of a coupon fiber and tied a knot at the end of the remaining fiber. I followed the procedures described by Zhao et al. (2011) to detach the biofilm from the fiber and to form biomass pellets, which were stored overnight at -20˚C. To achieve high DNA yields, I added to the thawed biomass pellets a fresh lysis buffer, slightly modified from Ziv-El et al., (2011) which contained 20 mM Tris·HCl, 2 mM EDTA, and 20 mg/ml of lysozyme. Incubation of biomass pellets and further clarification were as described by Ziv-El et al. (2011). I extracted the DNA according to the procedures described in the DNeasy Blood and Tissue kit (QIAGEN, USA), measured the DNA concentrations with a spectrophotometer (Nanodrop ND-1000, Nanodrop Technologies, USA), checked the quality of the DNA by PCR targeting the 16S rRNA gene (Lee HS et al., 2008), and stored the samples at -20˚C until qPCR and pyrosequencing analyses (Ontiveros-Valencia et al., 2013a).

Quantitative Polymerase Chain Reaction (qPCR)

I established standard curves (serial dilutions from 10^7 to 10^1 gene copies) from plasmids containing target fragments of the functional genes *dsrA, nirK, nirS*, and 16S rRNA gene as described in Zhao et al. (2011). The gene copy numbers were calculated based on the concentration and size of the extracted plasmids. Table 2.2 summarizes the

primers used for this study (Braker et al., 1998; Maeda et al., 2003; Throbäck et al., 2004; Kondo et al., 2008) and the qPCR protocols.

I used the SYBR Premix Ex Taq Kit (Takara Bio, Inc, Japan) and performed the qPCR reactions in a final volume of 20 µL: 10 µL SYBR, 8.6 µL H2O, 0.2 µl of each forward and reverse primer (10 pmol/µl), and 1 µL of DNA template. Negative controls had water instead of DNA templates, and all qPCR reactions were carried out in triplicate. I ran melting curves in all qPCR protocols to confirm amplification specificity and the absence of primer dimers.

To interpret the abundance of each gene in the biofilm, I converted gene copy numbers to cell numbers. I considered that one *nirK* gene (Philippot, 2006) corresponds to one microbial cell and two *nirS* genes correspond to one cell for DB (Coates et al., 2001). I also assumed that one *dsrA* gene copy number corresponds to one cell for SRB (Kondo et al., 2004); however, this normalization to cells/cm^2 biofilm might overestimate SRB, given that some SRB strains have showed more than one *dsrA* gene (Kondo et al., 2004).

Lastly, I converted the gene copies of 16S rRNA gene to microbial cells based on the major phylum, class, order, family, and genus revealed by the pyrosequencing results of each DNA sample (Ontiveros-Valencia et al., 2013a). The number of 16S rRNA gene copies of the dominant taxonomic hierarchies were based on Klappenbach et al. (2001) and Lee ZM-P et al. (2008).

Table 2.2 Primer sets and protocols used for qPCR analyses

Target gene	Primer name	Sequence	PCR protocol	Reference	Calibration curve parameters		
					Slope	Y-intercept	R^2
nirK	nirK1F nirK5R	5'- GGMATGGTKCCSTGGCA-3' 5'- GCCTCGATCAGRTTRTGG -3'	95°C 2 min 40 cycles 94°C 30 sec 60°C 60 sec 72°C 60 sec 72°C 5 min	Braker et al. (1998)	-3.58	36.3	0.997
nirS	cd3af R3cd	5'-GTSAACGTSAAGGARACSGG-3' 5'-GASTTCGGRTGSGTCTTGA-3'	95°C 2 min 40 cycles 94°C 60 sec 57°C 60 sec 72°C 60 sec 72°C 10 min	Throbäck et al. (2004)	-3.47	33.2	1
dsrA	dsr1F+ dsrR	5'-ACSCACTGGAAGCACGGCGG-3' 5'- GTGGMRCCGTGCAKRTTGG-3'	94°C 4 min 40 cycles 94°C 40 sec 60°C 40 sec 72°C 40 sec 72°C 10 min	Kondo et al. (2008)	-3.24	33.4	0.993
16S rDNA		**5'**-GTGSTGCAYGGYTGTCGTCA-3' 5'-ACGTCRTCCMCACCTTCCTC-3'	95°C 10 min 40 cycles 95°C 15 sec 60°C 60 sec	Maeda et al. (2003)	-3.44	35.365	0.997

2.3 Results and Discussion

NO_3^- and SO_4^{2-} reduction kinetics

I calculated the average influent and effluent NO_3^- and SO_4^{2-} concentrations for EDvSS. Figure 2.1 shows that the degree of denitrification steadily increased with higher H_2 pressure, and EDvSS accomplished full denitrification at H_2 = 3 atm. For the operating conditions tested in EDvSS, SO_4^{2-} reduction began at H_2 = 3.4 atm, and ~55% reduction was achieved at H_2 = 3.7 atm. NO_2^- production was not observed in EDvSS1, 3, 4, 5, and 6; however, EDvSS2 (H_2 = 2 atm) showed a small accumulation of NO_2^-. Accumulation of NO_2^- is a sign of H_2 limitation, (Lee and Rittmann, 2000, 2002) and this was likely the case due to the increased NO_3^- removal flux in EDvSS2 compared to EDvSS1.

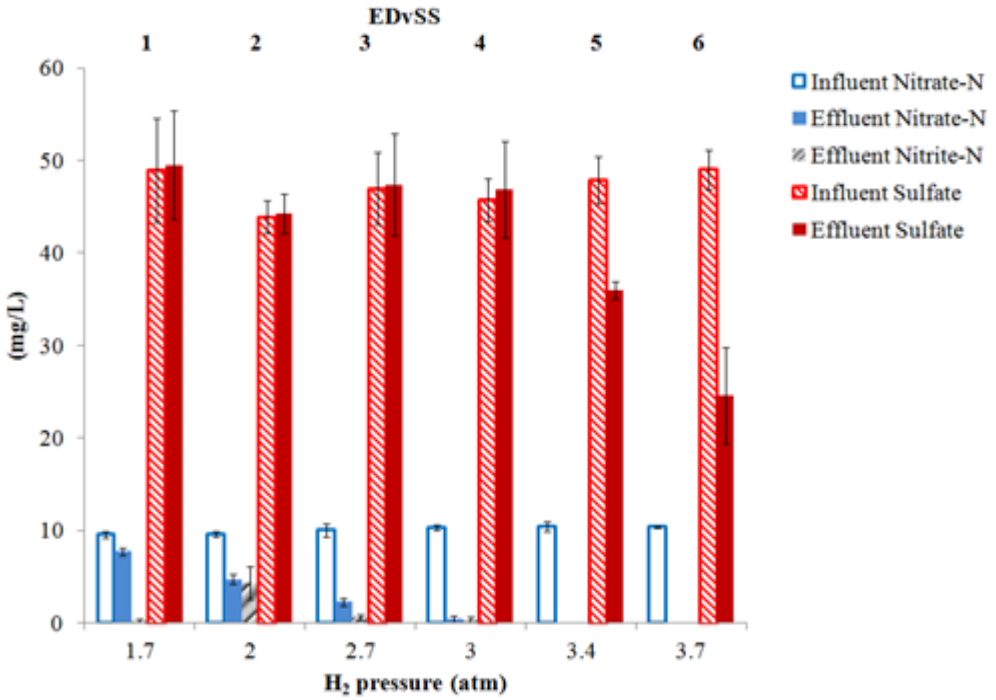

Figure 2.1 Steady-state concentrations of NO_3^- and SO_4^{2-} for EDvSS. Operating conditions are in Table 2.1. Denitrification was complete with a H_2 pressure of 3 atm, and SO_4^{2-} reduction began at 3.4 atm. The steady states were obtained in the order shown.

Figure 2.2 presents the experimental NO_3^-, SO_4^{2-}, and H_2 fluxes and compares them to the maximum possible H_2 fluxes that can be delivered by the polypropylene fibers with the pressures tested for this study: 1.7 - 3.7 atm (Tang et al., 2012d). Figure 2.2 also compares the maximum H_2 fluxes based on 100% reduction of the electron acceptor loading (either NO_3^- or SO_4^{2-}). The NO_3^- flux plateaued for H_2 pressure ≥ 3 atm, since EDvSS had 100% denitrification. The experimental SO_4^{2-} flux never exceeded 50% of the maximum removal flux for SO_4^{2-}. An unquestionable sign of the importance of H_2 limitation in EDvSS is the tight match between the experimental H_2 fluxes with the maximum H_2 fluxes for EDvSS5 and 6, and the correlation between the H_2 fluxes for EDvSS1-4. This reinforces that the H_2 delivery rate was limiting in EDvSS.

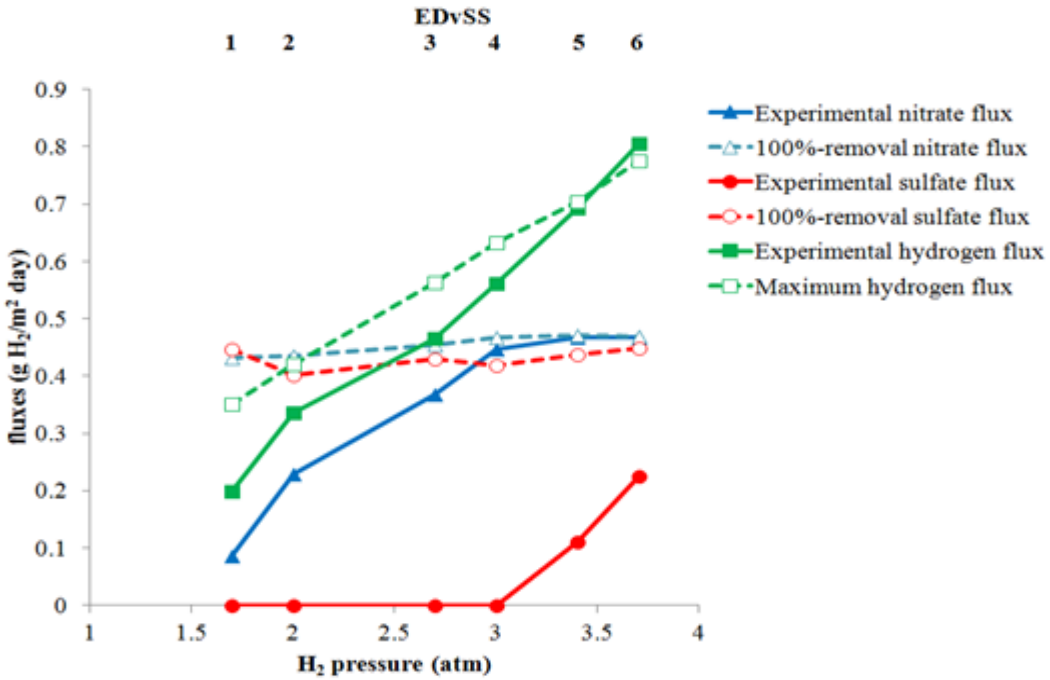

Figure 2.2 Removal fluxes of NO_3^- and SO_4^{2-} for EDvSS, 100%-reduction fluxes for these acceptors, the total H_2 removal flux for all acceptors, and the maximum H_2 flux deliverable within the range from 1.7 to 3.7 atm. All fluxes are expressed as H_2 equivalents. The H_2 flux due to O_2 reduction of 0.12 g H_2/m^2-day for each EDvSS is included in the total H_2 flux.

I averaged the NO_3^- and SO_4^{2-} concentrations for the influent and effluent of EAvSS. Figure 2.3 shows that NO_3^- was completely reduced for EAvSS1, 3, 4, 5, and 6, even though the NO_3^- loading varied widely; EAvSS2 showed about 75% NO_3^- reduction. Incomplete NO_3^- removal in EAvSS2 might be explained by an insufficient number of DB cells in the biofilm to carry out full NO_3^- reduction for its high NO_3^- loading (~0.53 g N/m^2 day); I addressed this interpretation in the section that presents the qPCR results. NO_2^- accumulation was not observed for any EAvSSs, supporting that the reactor was not H_2-limited.

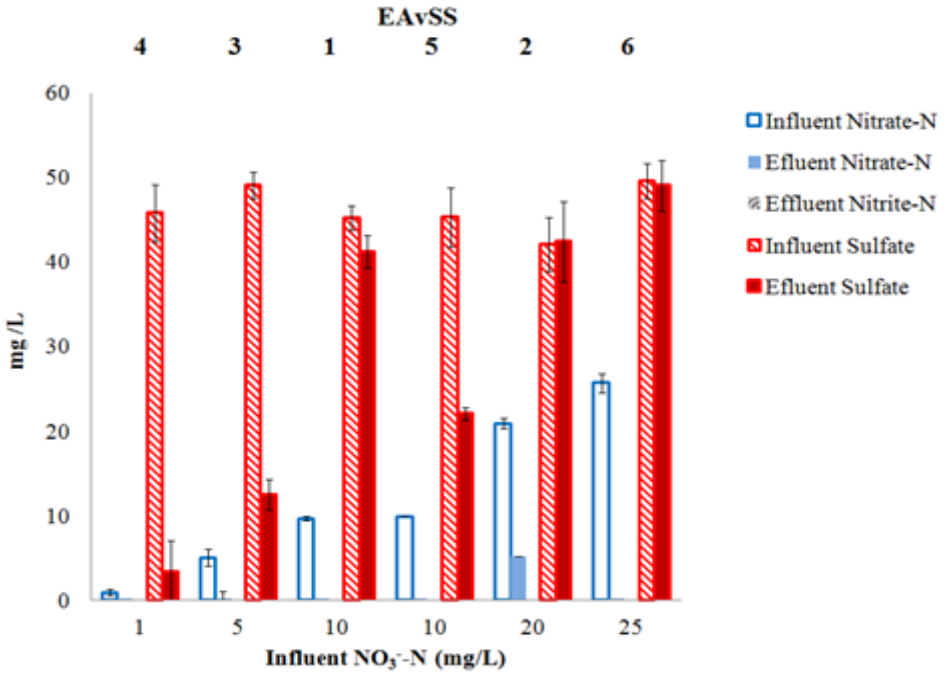

Figure 2.3 Steady-state concentrations of NO_3^- and SO_4^{2-} for EAvSS with a H_2 pressure of 2.7 atm throughout the experiments. Operating conditions are in Table 2.1. SO_4^{2-} reduction changed with the NO_3^- loading. The EAvSS numbers indicate the chronological order of the experiments. The results are presented here in ascending order of influent NO_3^- concentration.

Figure 2.4 presents the experimental NO_3^-, SO_4^{2-}, and H_2 fluxes and compares them to the H_2 fluxes for 100% removal of NO_3^- and SO_4^-, as well as the maximum H_2

flux that can be delivered by the fibers with a pressure of 2.7 atm (Tang et al., 2012d). The experimental SO_4^{2-} and NO_3^- removal fluxes showed an inverse relationship: when the NO_3^- removal flux increased, the SO_4^{2-} removal flux decreased and *vice versa*. Hence, the highest SO_4^{2-} removal fluxes occurred for EAvSS3 and 4, when the NO_3^- substrate loadings were the smallest. Figure 2.4 also shows how the experimental NO_3^- experimental removal flux coincided with the NO_3^- 100%-removal fluxes for all EAvSSs except for EAvSS2. The substantial gap between the maximum H_2 flux (0.56 gH_2/m^2-day for a H_2 pressure of 2.7 atm) and the total experimental H_2 fluxes for all EAvSSs (the highest flux was 0.33 gH_2/m^2-day) proves that the reactor did not experience severe limitation from H_2 availability in any EAvSSs. Nevertheless, SO_4^{2-} was never 100% removed. The degree of SO_4^{2-} reduction changed according to the NO_3^- loading. At the two lowest NO_3^- loadings (EAvSS3 and 4), SO_4^{2-} reduction was ~75% and 93%, but steady states with higher NO_3^- loadings (EAvSS1, 2, and 6) had $\leq$ 8% SO_4^{2-} removal. EAvSS5, which had a NO_3^- loading similar to EAvSS1, showed ~51% SO_4^{2-} reduction despite the reintroduction of NO_3^- to the medium, although SO_4^{2-} reduction was much less than in EAvSS4. This difference reflects the capability of SRB to persist even after the NO_3^- loading was increased (from EAvSS4 to EAvSS5). In contrast, EAvSS1 (with the same NO_3^- loading as EAvSS5) did not have SO_4^{2-} reduction activity because of the lack of previous "enrichment of SRB."

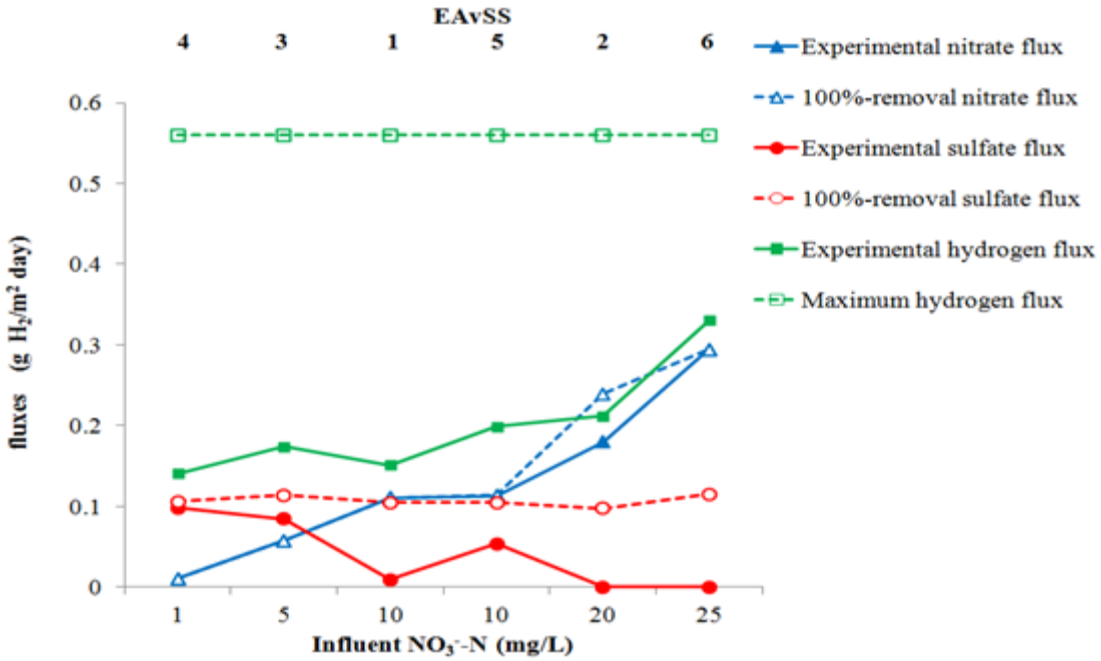

Figure 2.4 Removal fluxes of NO_3^- and SO_4^{2-} for EAvSS, 100%-removal fluxes for these acceptors, the total H_2 removal flux for all acceptors, and the maximum H_2 flux deliverable with a H_2 pressure of 2.7 atm. All fluxes are expressed as H_2 equivalents. The H_2 flux due to O_2 reduction of 0.03 g H_2/m^2-day for each EAvSS is included in the total H_2 flux. The EAvSS numbers indicate the chronological order of the experiments. The results are presented here in ascending order of influent NO_3^- concentration.

Abundance of different microbial populations (qPCR results)

I synthesized in Figure 2.5 the qPCR results normalized to cells/cm^2 of biofilm for EDvSS, along with the correlation between H_2 consumption by each electron acceptor (including O_2). Total bacteria increased in response to the increase of H_2 pressure and H_2 total flux. DB (especially DB containing the *nirS* functional gene) were positively correlated to the increase of electron-donor availability when H_2 availability was limited.

A strong increase in SRB was observed at higher H_2 pressures, when SO_4^{2-} reduction consumed H_2. The qPCR results for *dsrA* indicate that the reactor contained SRB and, therefore, the potential for SO_4^{2-} reduction at pressures lower than 3 atm, even

though SO_4^{2-} reduction was negligible except for H_2 pressures higher than 3 atm (Fig. 2.2). Apparently, DB were stronger competitors for the electrons donated by H_2, not allowing SRB access to the electrons. This result is consistent with the redox potential of denitrification (-112 KJ/e^- eq) vs SO_4^{2-} reduction (-18.3 KJ/e^- eq) when H_2 is the electron donor. Extensive literature on SRB indicates that some strains are able to persist under denitrification conditions, particularly within the genus *Desulfovibrio* (Mohanakrishnan et al., 2011). SRB also were found by Santegoeds et al. (1998) in sulfidogenic biofilms despite a lack of SO_4^{2-} reduction. Muyzer and Stams (2008) also pointed out that a relatively high abundance of SRB does not always correlate with high SO_4^{2-} reduction rates, since SRB can rely on different metabolic activities: e.g., O_2 respiration (Dilling and Cypionka, 1990; Marschall et al., 1993), fermentation of organics (e. g., fumarate and malate) (Widdel and Hansen, 1991), and NO_3^- reduction to NH_4^+ (Dalsgaard and Bak, 1994). In the H_2-based MBfR, O_2 and NO_3^- were electron acceptors that potentially could have been used by some SRB strains. However, ammonium production was not detected in this study (data not shown). In addition, the presence of a functional gene need not correspond to enzymatic activity; it only testifies that the microorganisms that harbor this gene are present. Also, the presence of *dsrA* genes in denitrifying conditions could be explained by the fact that some DB harbor the *dsrA* gene, as discovered by Wu et al., (2005) who found novel *dsr* sequences in denitrifying biomass.

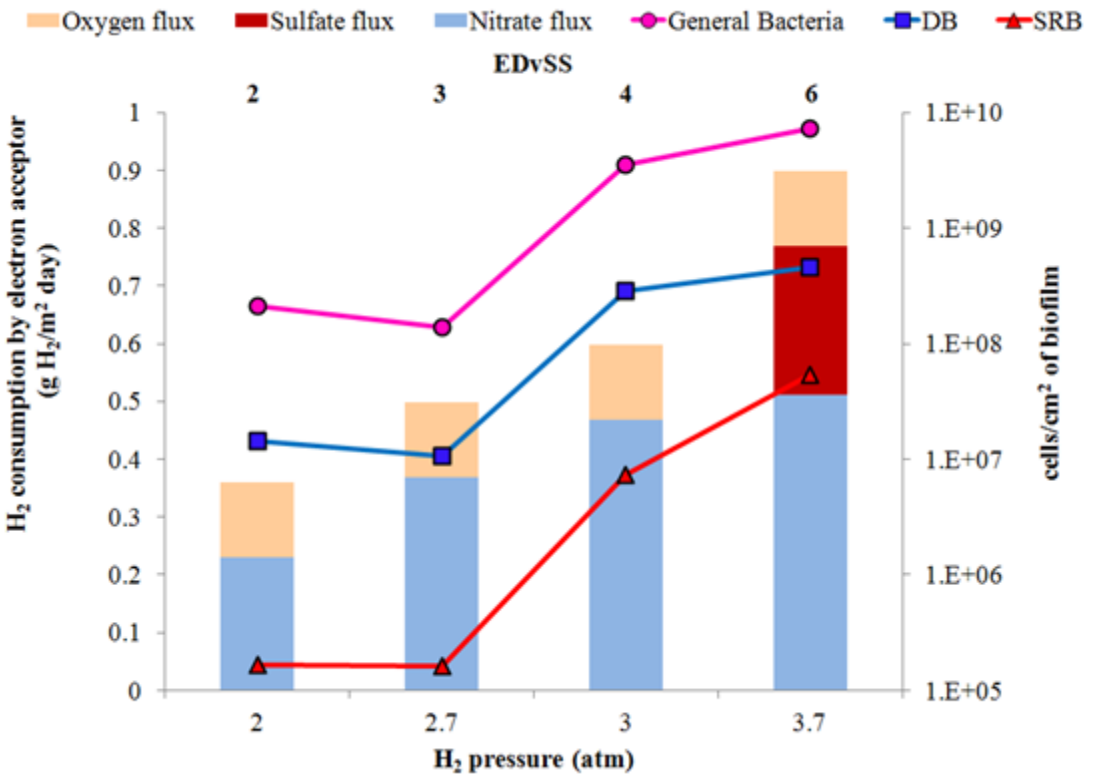

Figure 2.5 Abundances (in cells/cm^2) of DB (sum of *nirS* and *nirK* genes), SRB, and general bacteria for four biofilm samples from EDvSS, along with the H_2 consumption rate by each electron acceptor.

I summarized in Figure 2.6 the qPCR results normalized to cells/cm^2 of biofilm as a function of different NO_3^- influent concentrations for EAvSS, along with the H_2-consumption fluxes by each electron acceptor (including O_2). The greatest electron sink was denitrification in EAvSS1, 2, and 6, although SO_4^{2-} reduction competed for electrons during EAvSS5 and was the largest electron sink when the NO_3^- loading decreased in EAvSS3 and 4. The abundance of general bacteria remained stable for EAvSS1 through 4, but increased in EAvSS5 and 6, implying an increase in biofilm growth when the NO_3^- removal flux increased. EAvSS2 showed 2-fold lower level of DB cells in comparison with EAvSS6. This difference likely was the reason for the 75% NO_3^- reduction

observed at EAvSS2, since a low biomass density can impair biofilm performance (Rittmann and McCarty, 2001). The *dsrA* cell numbers per cm^2 were similar (~10^7 gene copy numbers per cm^2) for all EAvSSs, even though the SO_4^{2-} flux was much larger for EAvSS3 and 4, when NO_3^- fluxes were smallest. This ubiquitous presence of SRB is expected, since SRB are versatile microorganisms that can carry out metabolisms other than SO_4^{2-} reduction, as pointed out previously. Also, *dsrA* genes could be attributed to DB (Wu et al., 2005). A possible explanation for lack of growth of SRB with SO_4^{2-} fluxes might be the competition for space in the biofilm. As seen in Figure 2.6, DB were the major microorganisms in the biofilm and may have exerted control over the growth of SRB. Competition for space, a typical phenomenon in multispecies biofilms, forces some microorganisms to live in locations in which the impact of mass transport resistance is greater, lowering their substrate concentration and subsequently slowing their growth (Rittmann and Manem, 1992). The competition for space between DB and SRB in the biofilm is particularly important at the fiber surface, which is the source of H_2. Modeling results (Tang et al., 2012a) indicate that this competition becomes more favorable for SRB only when the growth rate of inherently faster-growing DB slows down and approaches the growth rate of SRB.

The fact that SRB cells/cm^2 did not increase as the SO_4^{2-}-reduction rate increased also might be related to toxicity effects from H_2S production and accumulation, since H_2S can stop electron-transport activity of SRB (Okabe et al., 1992). At the highest SO_4^{2-} reduction rate, sulfide production (i.e., $H_2S + HS^-$) calculated by stoichiometry (eq. 2.3) was ~14 mg S/L. As reviewed by Hao et al., (1996) the range of toxicity from sulfide is from 60 to 1000 mg S/L, depending on the electron donor (organic substances in all

reported values) (Maillacheruvu et al., 1993). The low sulfide level (Hao et al., 1996) makes it unlikely that sulfide toxicity was an important factor, compared to competition for space.

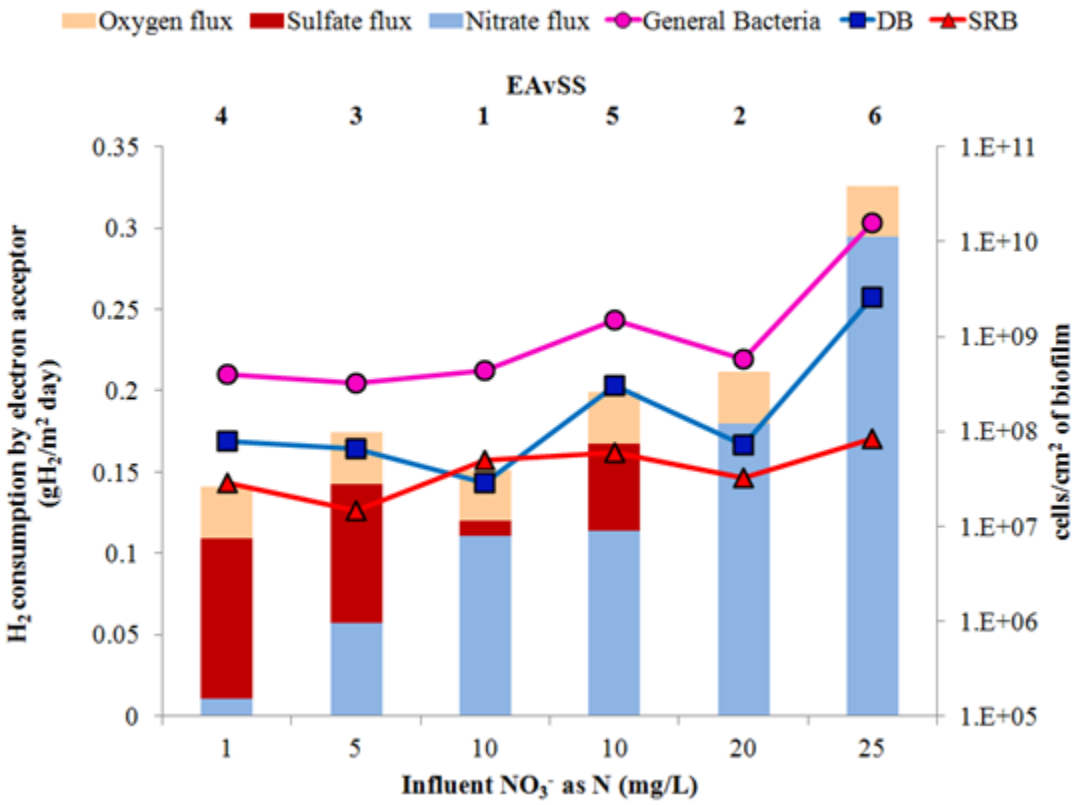

Figure 2.6 Abundances (in cells/cm^2) of DB (sum of *nirS* and *nirK* genes), SRB, and general bacteria for six biofilm samples from EAvSS, along with the H_2 consumption rate by each electron acceptor. As shown in Figure 2.8, gene copies from *nirS* dominated those from *nirK*. The EAvSS numbers indicate the chronological order of the experiments. The results are presented here in ascending order of influent NO_3^- concentration.

The cells/cm^2 abundances of DB and SRB showed significant differences between EDvSS (Fig. 2.5) and EAvSS (Fig. 2.6). When the electron donor was limited (EDvSS), DB clearly were the major fraction of microorganisms within the biofilm, while SRB were one to two orders of magnitude lower than DB. In EAvSS, in which the delivery of the electron donor was sufficient, SRB cells/cm^2 were less than one order of magnitude

smaller than for DB. This supports that the competition for electron donor (EDvSS) provided a stronger advantage to DB over SRB than did competition for space in the biofilm (EAvSS). Another potential reason for a higher number of DB than SRB cells could be O_2 respiration by DB. While most DB respire O_2, most SRB are inhibited by O_2. Despite the significant O_2 loading in EDvSS and EAvSS, the results show that the NO_3^- loading was the controlling factor that allowed or prevented SO_4^{2-} reduction: SO_4^{2-} reduction only happened once denitrification was complete and when the NO_3^- loading was reduced.

I show in Figures 2.7 and 2.8 all the qPCR data in gene copies/cm^2 for EDvSS and EAvSS, respectively. DB containing the *nirS* functional gene were 3-fold greater than DB with the *nirK* functional gene. In another MBfR study, Zhao et al. (2011) also reported a higher abundance of DB with *nirS* than *nirK*; this consistency might imply that autotrophic denitrification in the MBfR favors DB with *nirS* gene over those with *nirK*. Kandeler et al. (2006) found that *nirK* genes were relatively lower in comparison to *nirS* when organic substrate was limited in a heterotrophic denitrifying community of a glacier foreland. Bàrta et al. (2010) concluded that DB with *nirK* genes were higher in abundance in soils with high availability of phosphorus (P) and with higher dissolved organic matter (DOM) than 4.8 mM/kg soil. These two studies suggest that *nirK* genes are less adaptive for conditions of nutritional limitation, but respond favorably to a high availability of electron donor to support microbial growth.

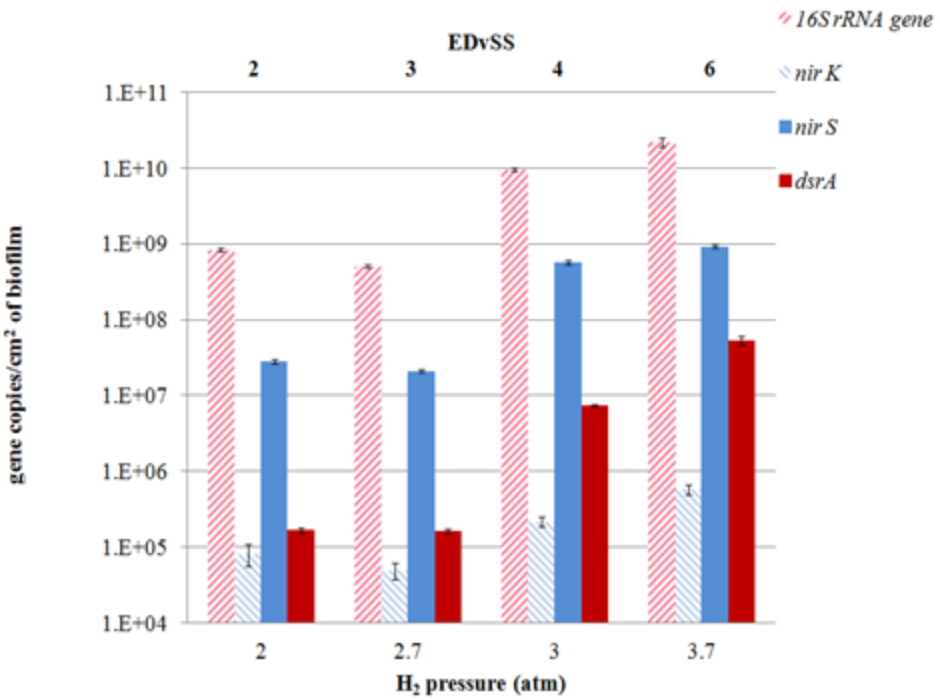

Figure 2.7 Abundances (in gene copies/cm^2) of all functional genes and the 16Sr RNA gene for the 4 sampled steady states for EDvSS.

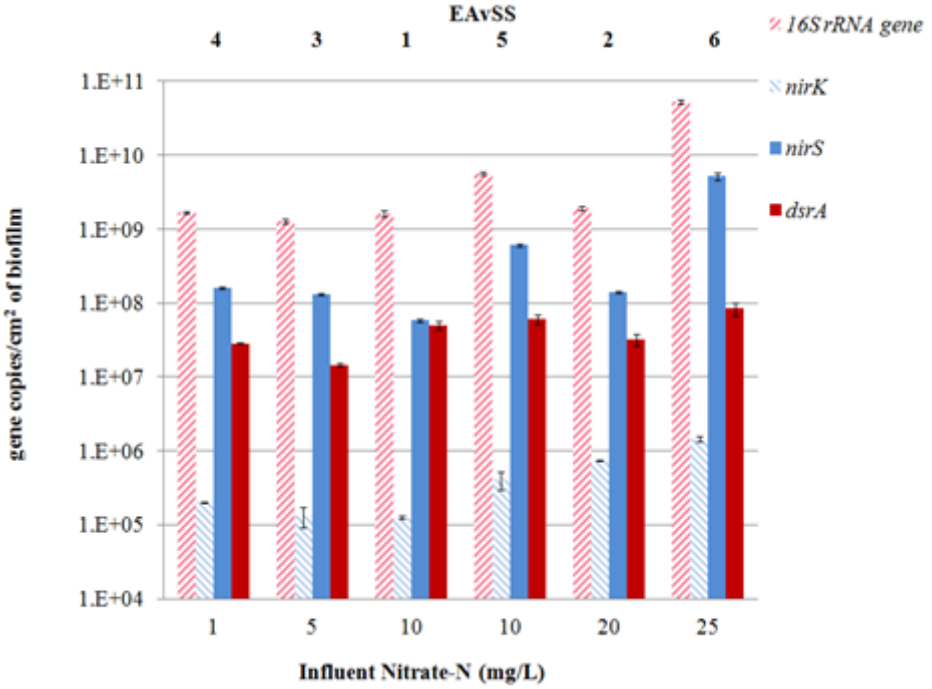

Figure 2.8 Abundances (in gene copies/cm^2) of all functional genes and the 16Sr RNA gene for EAvSS. The EAvSS numbers indicate the chronological order of the experiments. The results are presented here in ascending order of influent NO_3^- concentration.

2.4 Conclusions

I gained insight into the relationships between structure and function of H_2-oxidizing biofilms by combining qPCR analyses directed towards functional genes with measurements of donor and acceptor fluxes. DB clearly out-competed SRB for H_2 when effluent NO_3^- was $\geq \sim 0.1$ mg N/L (Figs. 2.1 and 2.3). Thus, SRB started to compete for the electrons donated by H_2, allowing the onset of SO_4^{2-} reduction, only after nearly complete denitrification was achieved. Even when the availability of the H_2 electron donor was not limited (EAvSS), SO_4^{2-} reduction occurred only when the consumption of H_2 by denitrification was $\leq$0.06 g H_2/m^2 day (NO_3^- loading of $\leq$0.13 g N/m^2 day), so that the NO_3^- concentration in the effluent was $\leq$ 0.1 mg N/L. Nevertheless, SRB were present in the biofilm in all EDvSSs and EAvSSs, likely carrying out metabolism other than SO_4^{2-} reduction. While the number of DB in the biofilm responded to increasing or decreasing NO_3^- removal fluxes in both MBfRs, SRB were nearly unresponsive to the SO_4^{2-} reduction rate when the H_2 availability was not limited (EAvSS). Thus, SRB showed sufficient metabolic flexibility to persist in the biofilm of EAvSS under non-favorable conditions. Once competition for H_2 was relieved by nearly complete removal of NO_3^-, the SRB were able to initiate strong SO_4^{2-} reduction. This knowledge can lead to management strategies for targeted reduction of electron acceptors.

Chapter 3

PHYLOGENETIC ANALYSIS OF NITRATE AND SULFATE-REDUCING BACTERIA IN A HYDROGEN-FED BIOFILM

This chapter was published in an altered format in *FEMS Microbial Ecology* (Ontiveros-Valencia et al., 2013a)

3.1 Introduction

This chapter builds on the findings reported in Chapter 2 about the ecological interactions between DB and SRB; here, I used pyrosequencing to search for the most abundant DB and SRB phylotypes in the H_2-fed biofilms and their relationships with other members in the microbial community.

NO_3^- and SO_4^{2-} often coexist in water due to anthropogenic activities (e. g., agricultural leaching of fertilizers; wastewater discharges), natural mineralogy (e. g., SO_4^{2-} minerals such as sodium sulfate, magnesium sulfate, and calcium sulfate), and atmospheric deposition of SO_2 or NO_x (Van Bremen and Van Dijk, 1988; Lovett, 1994). Given the common co-occurrence of NO_3^- and SO_4^{2-} in water and that many bacteria utilize NO_3^- and SO_4^{2-} as electron acceptors to generate energy for their growth, studies focusing on interactions of these two oxyanions are of high relevance for water-quality improvement by microbiological means. Denitrification, the respiratory reduction of NO_3^- to N_2 gas, is a step-wise process catalyzed by a set of well-known reductase enzymes (Payne, 1973; Knowles, 1982; Rittmann and McCarty, 2001). Respiratory SO_4^{2-} reduction relies on a different set of reductases to stepwise reduce SO_4^{2-}, ultimately generating H_2S (Peck, 1959), which is a corrosive and toxic substance.

DB are spread in many phylogenetic genera that include autotrophs and heterotrophs (Payne, 1981; Mateju et al., 1992). Some common autotrophic denitrifiers are in the genera *Thiobacillus, Paracoccus, Ferrobacillus,* and *Leptothrix*. *Pseudomonas* and *Azonexus* are examples of heterotrophic denitrifiers, while facultative DB are represented by *Hydrogenophaga*. Muyzer and Stams (2008) summarized the more relevant SRB and their phylogenetic relationships. Typical SRB belong to the orders *Desulfovibrionales, Desulfobacterales, Syntrophobacterales, Desulfotomaculum, Desulfosporomusa,* and *Desulfosporinus.* Also, SR microorganisms are present in the Archaea domain: *Archaeoglobus*, *Caldivirga*, and *Thermocladium* are some representative examples.

The chance of DB and SRB to coexist is determined by differences of their growth rates (Tang et al., 2012a) and thermodynamics (Rittmann and McCarty, 2001). Because NO_3^- respiration is energetically more favorable than SO_4^2 respiration, DB growth rates are faster than SRB growth rates (Tang et al., 2012a), and this provides DB an advantage over SRB when they compete for common resources, such as an electron donor and space (Ontiveros-Valencia et al., 2012). The selection of DB over SRB in mixed communities has been a practical strategy to control SRB, and the addition of NO_3^- has been used to minimize SO_4^{2-} reduction and H_2S production in sewers (Bentzen et al., 1995; Garcia de Lomas et al., 2005). However some SRB strains, such as *Desulfovibrio* and *Desulfomicrobium,* were able to remain in biofilms exposed to NO_3^-, even though others (e. g., *Desulfobacter* and *Desulfobulbus*) disappeared immediately after NO_3^- addition, leading to rapid DB enrichment in sulfidogenic biofilms (Mohanakrishnan et al.,

2011). Thus, the response of SRB to NO_3^- addition appears to be genus specific, with some SRB strains able to coexist despite selective pressure from NO_3^-.

The H_2-based MBfR has been successfully applied for microbial reduction of diverse sets of oxidized contaminants (e.g., Lee and Rittmann, 2002; Nerenberg and Rittmann, 2002; Chung et al., 2006a, b; Chung et al., 2007b; Ziv-El and Rittmann, 2009; Zhang et al., 2010). In the MBfR, H_2 is delivered to autotrophic bacteria by diffusion through the wall of bubbleless gas-transfer membranes. The outside of the membrane wall provides an ideal habitat for H_2-oxidizing bacteria, which form a strong and stable biofilm (Lee and Rittmann, 2002; Nerenberg et al., 2008; Ziv-El and Rittmann, 2009). The microbial ecology of biofilms in H_2-fed biofilms has been studied for many different sets of electron acceptors (Chung et al., 2008; Nerenberg et al., 2008; Zhang et al., 2010; Van Ginkel et al., 2010; Zhao et al., 2011), but most of the previous studies have not addressed the presence and diversity of SRB.

By using qPCR Ontiveros-Valencia et al. (2012) studied the coexistence of DB and SRB in H_2-fed MBfR biofilms. Higher electron availability (controlled by the H_2 pressure supplied to the membrane) led to complete denitrification and an increase in DB (quantified by nitrite-reductase genes). SO_4^{2-} reduction occurred only when the NO_3^- effluent concentration was driven below 0.1 mg N/L, and SRB increased (as assayed by targeting the dissimilatory sulfite reductase alpha subunit gene or *dsrA*) at higher H_2 pressures when H_2 availability was limiting. However, SRB were present in the H_2-fed biofilms whether or not SO_4^{2-} was being reduced because of their metabolic diversity (Ontiveros-Valencia et al., 2012).

Here, I expanded the understanding of the microbial ecology beyond the presence and abundance of SRB and DB in the biofilms of the H_2-based MBfR. I evaluated the microbial-community structure and the factors producing changes in the important genera/orders of autotrophic-founded biofilms containing DB and SRB. In particular, I identified SRB that are especially able to coexist in DB-dominated biofilms, including in situations in which SO_4^{2-} reduction does not occur, and I showed how the onset of SO_4^{2-} reduction affects some DB taxonomic groups more than others.

3.2 Materials and Methods

Reactor configuration and continuous operation

Following Ontiveros-Valencia et al. (2012), I set up two MBfRs each composed of two glass tubes interconnected with Norprene tubing (Masterflex, USA model 06404-1 5,16, 26) and plastic fittings. The total membrane surface area of each MBfR was 94 cm^2, which was distributed in a main bundle of 49-25 cm long polypropylene fibers (Teijin, Ltd, Japan) and 10-25 cm long for "coupon" fibers for biofilm samples. The total liquid volume of each MBfR was 60 mL and the liquid was circulated through both MBfRs at a rate of 150 ml/min. Both reactors were operated at room temperature (25±1°C). I analyzed biofilm samples from the two MBfRs described in Ontiveros-Valencia et al. (2012). Both MBfRs were inoculated with activated sludge from the Mesa Northwest Wastewater Treatment Plant, for which the microbial composition has been described previously (Li et al., 2011). Table 3.1 summarizes the operating conditions for both MBfRs. The SO_4^{2-} influent concentration was held constant for both MBfRs (~46 mg/L). One MBfR was operated with a set of increasing H_2 pressures, which allowed me

to control the electron-donor (i.e., H_2) availability for a fixed ratio of the two acceptors. This set of experiments is identified as the electron-donor-varied steady states, EDvSS. For the second MBfR, the input concentration of NO_3^- was varied, while the SO_4^{2-} concentration and H_2 pressure were held constant. This allowed me to evaluate the effect of electron-acceptor availability, and this set of experiments is identified as the electron acceptor-varied steady states, EAvSS. EDvSS and EAvSS were operated with continuous influent flow rates of 0.67 and 0.17 mL/min, respectively. The corresponding hydraulic retention times were 89 and 352 min. Due to the higher flow rate in EDvSS, electron-acceptors-loading rates for this reactor were higher for EDvSS than for EAvSS (Table 3.1); this led to H_2 limitation in EDvSS, but not in EAvSS.

I monitored the concentrations and reduction kinetics for NO_3^- and SO_4^{2-}, as described in Ontiveros-Valencia et al. (2012). Once the reactors reached a steady-state condition (5-10% variation in NO_3^- and SO_4^{2-} effluent concentrations over at a minimum of 10 days), I took samples of the biofilm for DNA extraction (Ontiveros-Valencia et al., 2012). The biofilm samples represented an area of 0.8-1 cm^2, which is large enough that localized heterogeneities did not bias the phylogenetic distributions (Ziv-El et al., 2012).

Pyrosequencing and sequence analysis

To investigate the major DB and SRB phylotypes in the biofilm and their relationship with the bioreactors performance, I sent all DNA samples for pyrosequencing at the Research and Testing Laboratories LLC (Texas, USA), which performed amplicon pyrosequencing using a standard 454/GS-FLX Titanium (Sun et al., 2011). The Bacteria domain was targeted by selecting the V6 and V7 regions of the 16S rRNA gene with primers 939F (5'-TTGACGGGGGCCCGCAC-3') and 1492R

(5'TACCTTGTTACGACTT-3') (Zhao et al., 2011). The potential presence of Archaea was not determined. I processed the raw data using QIIME 1.4.0 suite (Caporaso et al., 2010a) and removed sequences having fewer than 200 bps, homopolymers of more than 6 bps, primer mismatches, or an average quality score lower than 25. I picked the operational taxonomic unit (OTUs) using the Greengenes 16S rDNA database with *uclust* (Edgar, 2010) based on ≥ 97% identity, removed OTUs that contain less than two sequences (singletons) from the analysis, and aligned the representative sequence of each OTU to the Greengenes Database using *PyNast* (DeSantis et al., 2006; Caporaso et al., 2010b). The potentially chimeric sequences were identified by using ChimeraSlayer (Haas et al., 2011), and a python script in QIIME was employed to remove the chimeric sequences. To assign taxonomy to OTUs, I used the ribosomal database project (RDP) classifier with a 50% confidence threshold (Wang et al., 2007). I constructed Newick-formatted phylogenetic trees using FastTree (Price et al., 2009).

For the purpose of eliminating heterogeneity related to having different numbers of sequences among the samples, I sub-sampled the OTU table by randomly selecting ten different times 740 sequences per sample, which was the lowest number of sequences found in one sample. I created 10 iterations for every 10 sequences and repeated this process until reaching 740 selected sequences in each sample. The diversity and evenness within each sub-sample of 740 sequences was calculated from rarified OTU tables with the mean of the last ten iterations of each sample. I averaged the estimates for the 10 iterations I created for every 10 sequences, compiled the averages, and produced rarefaction plots.

Table 3.1 Operating conditions and function metrics for EDvSS and EAvSS. The tested variables are indicated by the shaded squares. Experimental H_2 fluxes and electron-acceptor (NO_3^- and SO_4^{2-}) removal fluxes are from Ontiveros-Valencia et al. (2012). The maximum H_2 delivery capacities of the polypropylene fibers at a given pressure were calculated from Tang et al. (2012d).

Reactor	Sample ID	H_2 pressure atm	Maximum H_2 delivery capacity g H_2/m^2 day	Experimental H_2 flux g H_2/m^2 day	NO_3^- influent concentration mg N/L	NO_3^- loading g N/m^2 day	SO_4^{2-} loading g SO_4^{2-}/m^2day	NO_3^- removal flux g N/m^2 day	SO_4^{2-} removal flux g SO_4^{2-}/m^2day
EDvSS	1a	2.0	0.42	0.34	10	1.04±0.04	4.9±0.21	0.51	0
	1b	2.7	0.56	0.47				0.81	0
	1c	3.0	0.63	0.56				1.04	0
	1d	3.7	0.78	0.80				1.08	2.56
EAvSS	2a	2.7	0.56	0.15	10	0.26	1.2±0.07	0.26	0
	2b			0.21	20	0.55		0.42	0
	2c			0.17	1	0.13		0.13	0.97
	2d			0.14	5	0.02		0.02	1.12
	2e			0.20	10	0.26		0.26	0.61
	2f			0.33	25	0.68		0.68	0

I used a set of metrics to characterize the microbial communities of the two MBfRs in terms of diversity and evenness. While a higher value for the Shannon diversity index indicates greater microbial diversity, a value for the Simpson metrics near one shows an even distribution of bacterial groups within the sample. The OTU richness was estimated by calculating Chao1, which determines the asymptote on an accumulative curve, predicting how many OTUs would be present if a high number of sequences had been collected, and the phylogenetic relationships by using PD (Faith, 1992), which estimates the cumulative branch lengths from random OTUs.

To evaluate the overall community composition, I quantified the fraction of unique branch lengths from the total branch length of the phylogenetic tree using the unweighted UniFrac distance matrix (Lozupone et al., 2006). The unweighted option accounts only for the presence or absence of microbial phylotypes. I generated principal coordinate analysis (PCoA) plots and Unweighted Pair Group Method Arithmetic Mean (UPGMA) plots (Lozupone et al., 2006) using jack-knifed beta diversity that subsampled each sample at a depth of 740 sequences. Sequence data sets are available at NCBI/Sequence Read Archive (SRA) under study with accession number SRP018321. Individual sample files have the following accession numbers: SAMN01902537 - SAMN01902546.

3.3 Results and discussion

Community function

Table 3.1 summarizes the results of the reduction of NO_3^- and SO_4^{2-} for EDvSS and EAvSS for the steady states when DNA samples were taken. The <10% differences

between the experimental H_2 fluxes and the maximum H_2 delivery fluxes point out that H_2 was limiting in EDvSS (Ontiveros-Valencia et al., 2012). Thus, the reductions of NO_3^- and SO_4^{2-} depended on the H_2 pressure applied to the membranes in EDvSS. Starting with the lowest H_2 pressure, the removal flux for NO_3^- increased with greater H_2 pressure until NO_3^- was completely removed. Then, SO_4^{2-} was reduced as H_2 became available for the SRB (EDvSS 1d).

In EAvSS, the experimental H_2 flux always was at least 20% less than the maximum H_2 delivery flux (Tang et al., 2012d), which indicates that H_2 delivery was not limiting in the biofilm. While the H_2 concentration changes within the biofilm (e. g., being at higher concentrations near the fiber surface than near the liquid side), the H_2 that could be delivered at the gas pressures utilized in EAvSS was more than enough to supply all the H_2 needed by the DB and SRB in the biofilm. In all the cases except EAvSS 2b, the NO_3^- removal flux equaled the NO_3^- loading (Table 3.1), which means that denitrification was complete. Significant rates of SO_4^{2-} reduction occurred only for the three lowest NO_3^- loadings (EAvSS 2c, 2d and 2e).

Forces driving the biolfilm microbial community structure elucidated by UniFrac and PCoA

Pyrosequencing generated a total of 48,524 high-quality sequences with a median length of 355 bp for 16S rDNA for all the biomass samples of EDvSS and EAvSS. Figure 3.1 shows the results of the unweighted UniFrac analysis for an overall community comparison. All biofilm samples from EAvSS formed a cluster (highlighted in red), while three of four biofilm samples from EDvSS (1a, 1b, and 1c) formed another cluster (highlighted in blue). Sample 1d, which clustered closer to the samples from

EAvSS, was the only steady state in which SO_4^{2-} reduction was observed for EDvSS; hence, the overall community was dramatically affected when SO_4^{2-} reduction took place. The blue group corresponds solely to biofilm samples with denitrification as the predominant microbial respiratory process (Table 3.1, samples 1a-1c).

Figure 3.2 shows the unweighted PCoA, which is based only on the presence or absence of phylotypes. Again, all the samples from EAvSS grouped together, having relatively low values of PC1. The biofilm sample with the highest removal flux for NO_3^- (EAvSS 2f) was slightly distant from the rest of the samples on the PC2 vector. For EDvSS, the effect of H_2 availability on the biofilm structure showed a clear gradient (1a→1b→1c→1d), in which the samples with the least H_2 availability (samples 1a and 1b) showed the highest magnitudes for PC1, while the samples with the greatest H_2 availability became more like EAvSS on the PC1 axis.

Ontiveros-Valencia et al. (2012) concluded that H_2 availability for EDvSS and electron-acceptor loading (or NO_3^- influent concentration in these experiments with a constant influent flow rate) for EAvSS, respectively, were the critical factors affecting the removal fluxes for NO_3^- and SO_4^{2-}. The UniFrac and PCoA analyses support these conclusions, but also reflect how the community structure behaved. PCoA analysis demonstrates that H_2 availability caused greater variance among the samples than electron acceptor loading, which is well illustrated by the trends along the PC1 axis. UniFrac showed evidence for microbial community clustering in the two MBfR reactors when SO_4^{2-} reduction was significant within the biofilm.

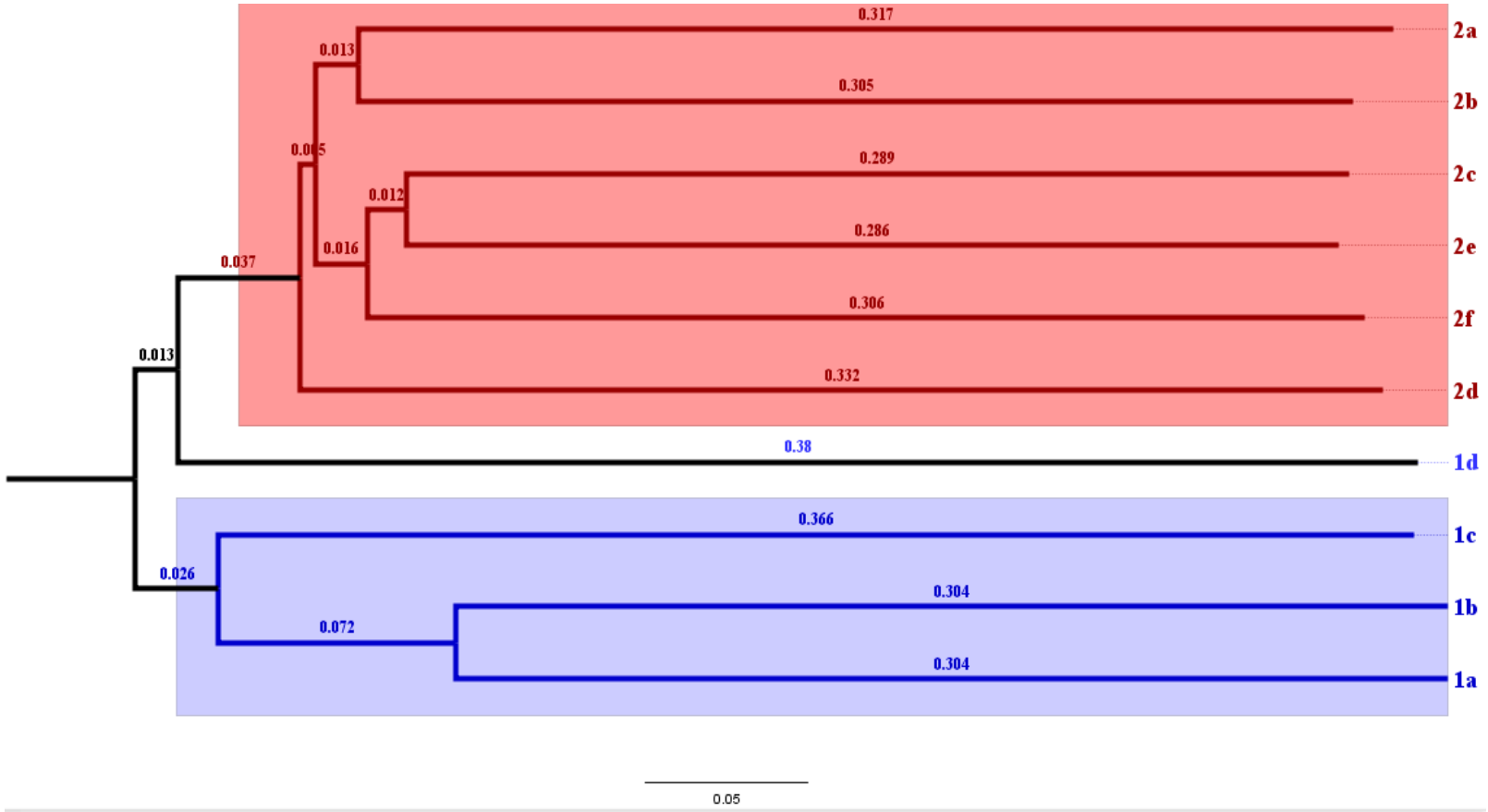

Figure 3.1 Clustering based on the unweighted UniFrac analyses for EDvSS and EAvSS. The branch length represents the distance between biofilm samples in UniFrac units, as indicated by the scale bar. 1a-1d correspond to EDvSS, with 1a = 0.42 g H_2/m^2 day, 1b = 0.56 g H_2/m^2 day , 1c = 0.63 g H_2/m^2 day, and 1d = 0.78 g H_2/m^2 day. 2a-2f correspond to EAvSS, with 2a = 10 mg N/L, 2b = 20 mg N/L, 2c = 5 mg N/L, 2d = 1 mg N/L, 2e = 10 mg N/L, and 2f = 25 mg N/L.

Along with electron-donor availability and electron-acceptor loading rates, other factors affect the structure of the microbial community in the biofilm. For instance, the profiles of dissolved components such as H_2, NO_3^-, and SO_4^{2-} also have significance. As modeled by Tang et al. (2012a), the H_2 concentrations are higher near the fiber surface, allowing a higher concentration of DB and SRB than at the liquid side, which is mostly populated by inert compounds and heterotrophs. The profiles of the electron acceptors NO_3^- and SO_4^{2-} vary accordingly the respective biomass fractions of DB and SRB: The NO_3^- concentration non-linearly declines from the liquid side to the fiber side of the biofilm due to the high density of DB near the fiber surface, but the SO_4^{2-} concentrations do not decline much in the biofilm because of a smaller fraction of SRB than DB.

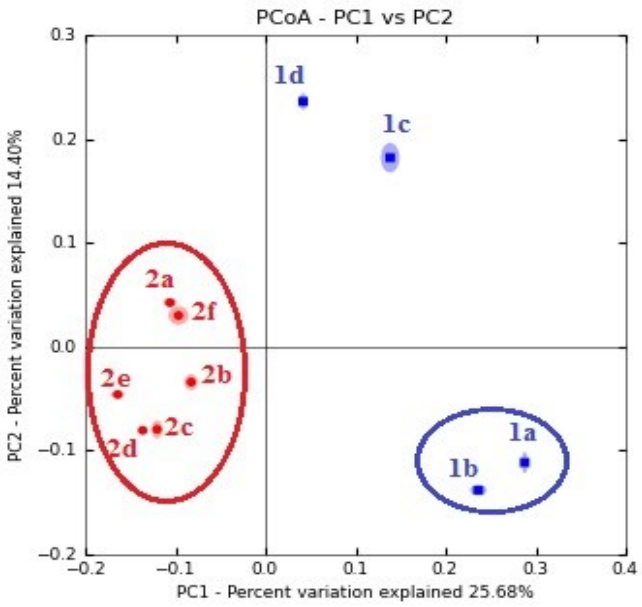

Figure 3.2 PCoA based on the unweighted UniFrac analyses for EDvSS and EAvSS. PC1 and PC2 axes represent 25.68% and 14.40% of the variance within the microbial community. 1a-1d correspond to EDvSS, with 1a = 0.42 g H_2/m^2 day, 1b = 0.56 g H_2/m^2 day , 1c = 0.63 g H_2/m^2 day, and 1d = 0.78 g H_2/m^2 day. 2a-2f correspond to EAvSS, with 2a = 10 mg N/L, 2b = 20 mg N/L, 2c = 5 mg N/L, 2d = 1 mg N/L, 2e = 10 mg N/L, and 2f = 25 mg N/L.

As discussed above, H_2 availability and electron acceptor loading rates allow a higher or lower abundance of DB and SRB within the biofilm. For example, higher H_2 availability leads to more accumulation of DB. However, once complete denitrification is achieved, SRB are able to compete with DB for H_2 and space near the fiber surface.

The sequential order of the experiments influenced the community structure. Following the steady states favoring SO_4^{2-} reduction (EAvSS2c and 2d), the biofilm community retained SRB despite the introduction of NO_3^- and were still capable of reducing SO_4^{2-} (EAvSS2e). The SRB also remained in the biofilm in a subsequent steady state without SO_4^{2-} reduction (EAvSS2f).

Figure 3.3 and Table 3.2 show that the microbial diversity was higher for EAvSS over EDvSS based on number of OTUs, Chao1, and Shannon indices. Thus, H_2 limitation restricted diversity and led to fewer dominant phylotypes. Lastly, the evenness and PD was higher for EAvSS than for EDvSS (Table 3.2 Simpson metrics and Figure 3.4 respectively).

Table 3.2 Diversity and evenness metrics for EDvSS and EAvSS at a similarity level of 95%. 1a-1d correspond to EDvSS, with 1a = 0.42 g H_2/m^2 day, 1b = 0.56 g H_2/m^2 day, 1 c= 0.63 g H_2/m^2 day, and 1d = 0.78 g H_2/m^2 day. 2a-2f correspond to EAvSS, with 2a = 10 mg N/L, 2b = 20 mg N/L, 2c = 5 mg N/L, 2d = 1 mg N/L, 2e = 10 mg N/L, and 2f = 25 mg N/L.

SAMPLE ID	Chao1	Phylogenetic diversity	Shannon	Simpson
1a	96±20.5	3.5±0.3	2.8±0.1	0.64±0.02
1b	122±18	4.5±0.3	4.4±0.07	0.9±0.01
1c	120±29	3.3±0.3	3.6±0.05	0.83±0.01
1d	109±20	3.0±0.2	3.4±0.08	0.77±0.01
2a	149±12	6.6±0.3	5.0±0.08	0.94±0.004
2b	211±32	6.4±0.5	4.8±0.07	0.91±0.01
2c	200±45	5.7±0.5	4.7±0.09	0.91±0.004
2d	88±1	5.0±0.	4.2±0.01	0.89±0.0004
2e	219±36	6.2±0.3	4.5±0.06	0.86±0.01
2f	220±62	5.4±0.5	4.2±0.1	0.89±0.01

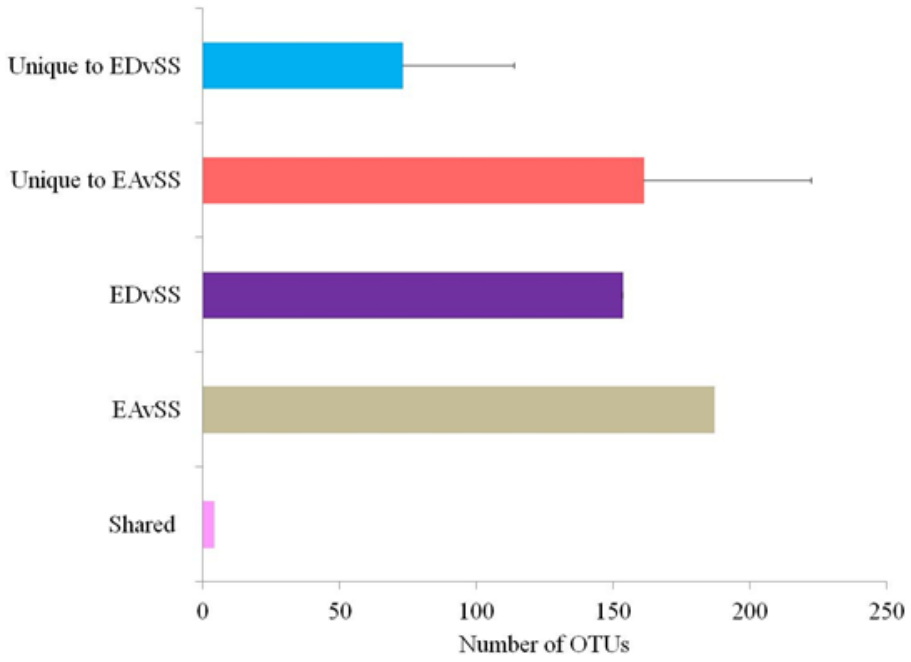

Figure 3.3 Number of unique, shared, and total OTUs per reactor. "Shared" indicates the occurrence of OTUs present in all biofilm samples from both MBfRs.

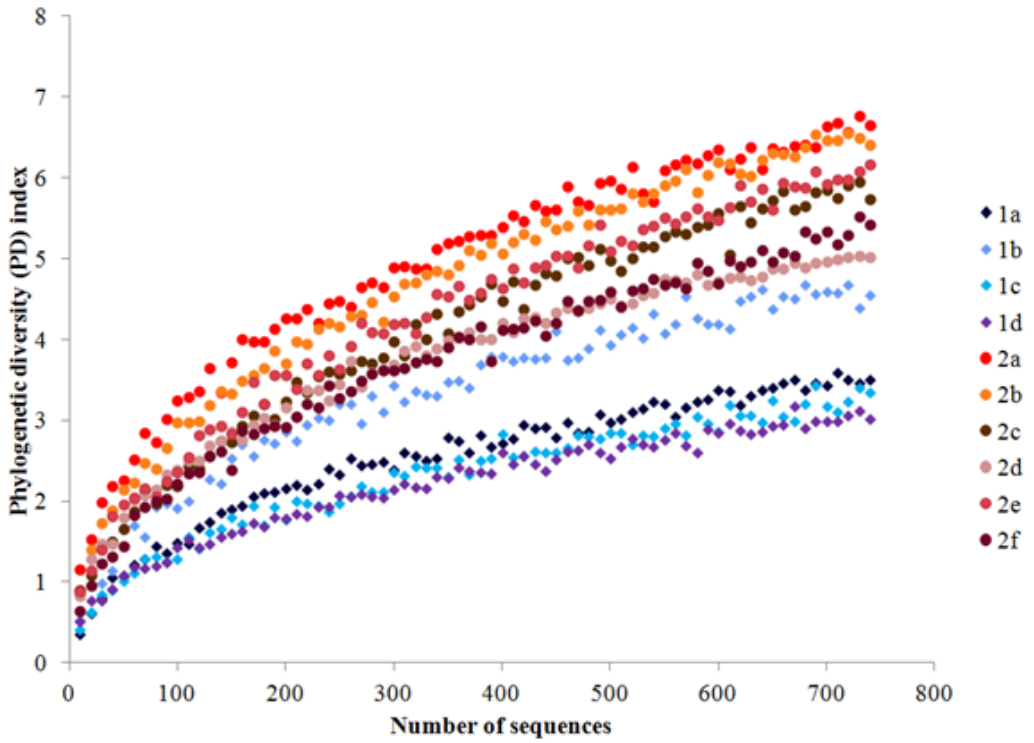

Figure 3.4 Rarefraction curves at 95% confidence. 1a-1d correspond to EDvSS, with 1a = 0.42 g H_2/m^2 day, 1b = 0.56 g H_2/m^2 day, 1c = 0.63 g H_2/m^2 day, and 1d = 0.78 g H_2/m^2 day. 2a-2f correspond to EAvSS, with 2a = 10 mg N/L, 2b = 20 mg N/L, 2c = 5 mg N/L, 2d = 1 mg N/L, 2e = 10 mg N/L, and 2f = 25 mg N/L.

Heterotrophic and autotrophic DB dominance

The different degrees of H_2 availability for EDvSS and EAvSS led to different microbial communities (Figure 3.5). The community of EDvSS was dominated by mostly heterotrophic DB (*Burkholderiales*) when H_2 was severely restricted (EDvSS 1a and 1b); however, once the limitation for H_2 was relieved, DB capable of autotrophic metabolism, such as *Hydrogenophilales* (chemoautotrophic bacteria that respire NO_3^- and oxidize H_2) and *Rhodocyclales* (a highly versatile microbial group with representative chemolithoautotrophic bacteria such as *Paracoccus denitrificans* and *Methyloversatilis*) out-competed the heterotrophic ones (EDvSS 1c and 1d). The dominance of heterotrophic *Burkholderiales* when H_2 was severely limited suggests that the community relied more on organic donors available from soluble microbial products (SMP) released by the autotrophs (Ni et al., 2011; Merkey et al., 2009). The growth of heterotrophic bacteria has been associated with the production of SMP by autotrophic bacteria (e.g., Kindaichi et al., 2004; Ni et al., 2011; Tang et al., 2012a). The abundance of heterotrophic bacteria has even reached 50% in an autotrophic nitrifying biofilm (Kindaichi et al., 2004).

Without restrictions on H_2 for EAvSS, the largest DB representation was by phylotypes related to *Rhodocyclales* and *Hydrogenophilales*, with *Burkholderiales* was in third place, but at significantly lower abundance. This indicates that the biofilm community of DB in EAvSS was predominantly autotrophic.

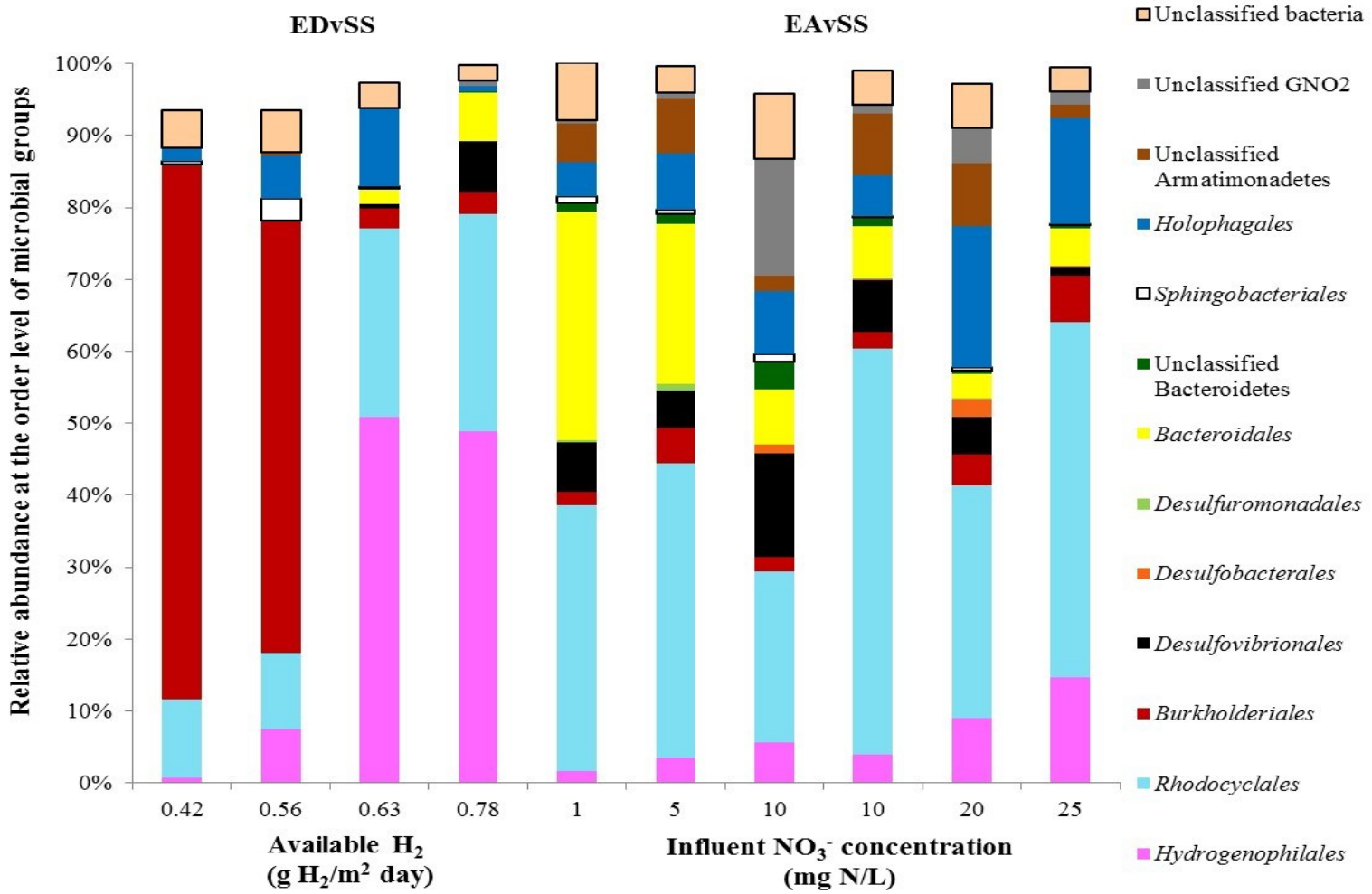

Figure 3.5 Relative abundances of the most abundant microbial phylotypes at the order level for EDvSS and EAvSS. The EDvSS and EAvSS letter and number codes show the chronological order of samples. Samples for EAvSS are shown according to increasing NO_3^- concentration. The sum does not add up to 100% in all cases because minor phylotypes are not shown.

The heterotrophic and autotrophic DB phylotypes in EDvSS and EAvSS are represented at the genus level in Figure 3.6. For EDvSS, heterotrophic microorganisms, including *Aquabacterium*-like phylotypes (sample 1b) and *Dechloromonas*-like phylotypes (1a – 1b), were prevalent with severe H_2 limitation, while *Methyloversatilis*-like phylotypes (methylotrophic microorganisms capable of utilizing CO_2 as carbon source) increased with increasing H_2 availability (1b to 1d). Zhao et al. (2011) similarly found that the microbial community moved towards mixotrophic in a H_2-fed biofilm when H_2 delivery was limited in a denitrifying and perchlorate-reducing community. In EAvSS, *Methyloversatilis* was the most abundant DB genus, reinforcing the autotrophic conditions under H_2 non-restriction, and it showed a positive correlation with the increase of NO_3^- concentration.

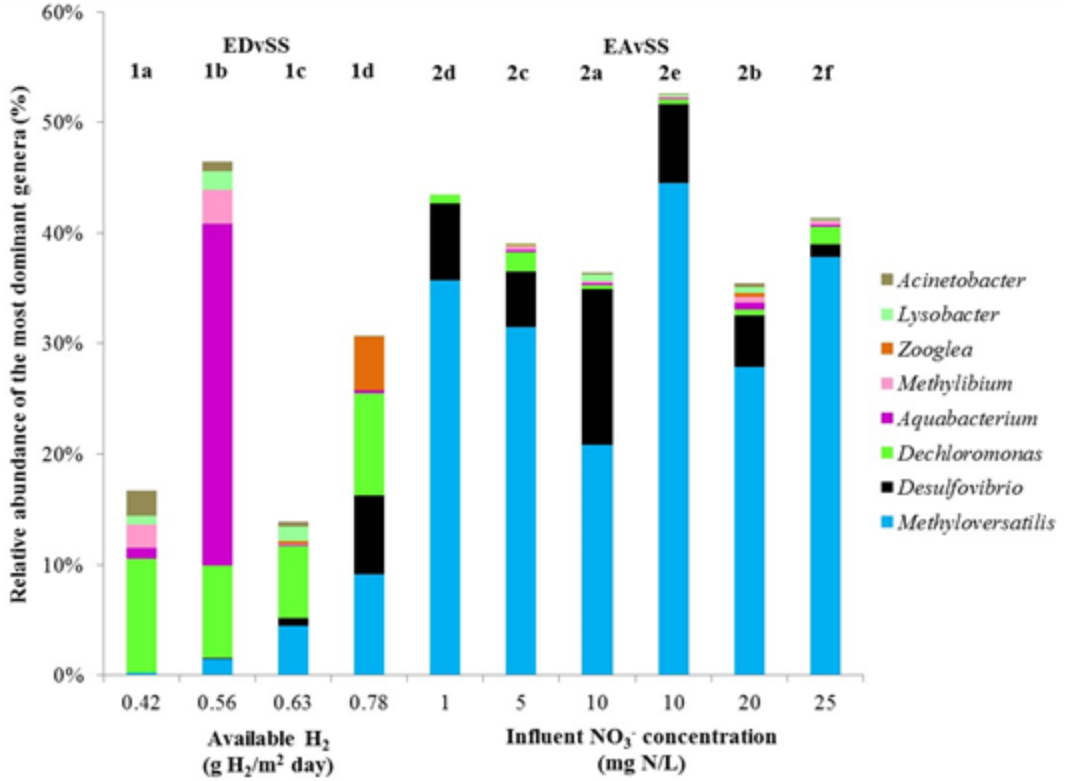

Figure 3.6 Relative abundances of the most abundant microbial phylotypes at the genus level for EDvSS and EAvSS. The EDvSS and EAvSS letter and number codes show the chronological order of samples. Samples for EAvSS are shown according to increasing NO_3^- concentration.

Competition between DB and SRB: a deeper insight by pyrosequencing analysis

In EAvSS, *Rhodocyclales*, *Hydrogenophilales*, and *Burkholderiale*s generally increased with higher NO_3^- concentration, but *Hydrogenophilales* and *Burkholderiales* declined as SO_4^{2-} reduction became more important (Figure 3.5). The DB community of EAvSS was clearly distinct from the DB community of EDvSS, and *Rhodocyclales* was the largest DB phylotype in EAvSS. In EDvSS, DB phylotypes were better competitors for H_2 than SRB (e.g., *Desulfovibrionales*), which only showed higher relative abundances once H_2 became available to them after complete denitrification (H_2 pressure >3 atm).

Using qPCR, Ontiveros-Valencia et al. (2012) reported a rise of *nirS*-containing denitrifiers with higher H_2 availability in EDvSS. However, pyrosequencing was able to reveal which phylotypes correlated with the increase of *nirS*-containing denitrifiers. The *nirS*-containing denitrifiers in our system were *Rhodocyclales*, *Hydrogenophilales*, and *Burkholderiale*s (Saunders et al., 2000; Matsuzaka et al., 2003; Beller et al., 2006; Yoshida et al., 2010). *Burkholderiales* decreased while *Hydrogenophilales* increased with greater H_2 availability. Hence, the increase of *nirS*-containing denitrifiers with higher H_2 availability observed by Ontiveros-Valencia et al. (2012) was correlated with the increase of *Hydrogenophilales*.

Despite lack of active SO_4^{2-} reduction, the biofilm samples of Ontiveros-Valencia et al. (2012) showed similar abundances of SRB in EAvSS. One possibility is that SRB were actively reducing NO_3^- in a process known as ammonification (Dalsgaard and Bak, 1994; Moura et al., 2007). However, NH_4^+ was not detected in the MBfR effluents, which suggests that the SRB potentially were respiring O_2 (Dilling and Cypionka, 1990;

Marschall et al., 1993) or fermenting organics (Widdel and Hansen, 1991). The apparent lack of SO_4^{2-} reduction also might be attributed to sulfide-oxidation by DB. However, sulfur-driven autotrophic denitrification (Shao et al., 2010), for which the final product of respiration is N_2, oxidizes sulfide to S° (Reyes-Avila et al., 2004; Chen et al., 2009a, b, 2010) or to SO_4^{2-} (Shao et al., 2010). Both cases were unlikely for our biofilm samples because (1) SO_4^{2-} reduction should have been suppressed by competition from denitrification (Tang et al., 2012a) and (2) pyrosequencing did not reveal DB known to do sulfide oxidation (e.g., *Thiobacillus denitrificans, Thiothrix, Thiomicrospira denitrificans, Sulfurimonas denitrificans, Paracoccus denitrificans* (Shao et al., 2010)). Furthermore, we did not observe the loss of SO_4^{2-}, which would have occurred if the oxidation product were S°. Although not carrying out denitrification or ammonification, SRB coexisted with DB even when NO_3^- suppressed SO_4^{2-} reduction.

Dominant SRB phylotypes and effect of SO_4^{2-} reduction on the microbial community

SRB were represented by phylotypes most closely related to *Desulfovibrionales* (Figure 3.5). In EDvSS, *Desulfovibrionales* became more prominent at the highest H_2 availability (EDvSS 1d), but *Desulfovibrionales* were significantly reduced as the NO_3^- concentration increased in EAvSS (from EAvSS 2d to 2f). *Desulfovibrionales,* which have high metabolic versatility (Dilling and Cipionka, 1990; Widdel and Hansen, 1991), could remain in the biofilm community even though it was dominated by DB and denitrification was happening (Figure 3.5 samples 2a, 2b, 2e, and 2f), a trend also seen in other systems (e.g., Gu et al., 2005; Fields et al., 2006; Mohanakrishnan et al. 2011). SRB-containing orders *Desulfobacterales* and *Desulfuromonadales* also were present (at <2% and <1% relative abundances) in EAvSS, but not in EDvSS (Figure 3.5); this

reflects the greater diversity of SRB in EAvSS. It also illustrates how pyrosequencing allowed us to detect subtle impacts of NO_3^- concentration on SRB; these abunbance trends correlated well with results with the qPCR assay of the *dsrA* gene (Ontiveros-Valencia et al., 2012).

Consistent with the UniFrac analysis (Figure 3.1), SO_4^{2-} reduction had a clear impact on framing the microbial community beyond DB and SRB. At the highest SO_4^{2-} reduction rates (EDvSS 1d and EAvSS 2c and 2d), the relative abundance of phylotypes similar to *Holophagales* decreased (Figure 3.5). *Holophagales* are homoacetogens also capable of utilizing NO_3^- as its electron acceptor (Drake et al., 2002; Coates et al., 1999a). The loss of *Holophagales* with high SO_4^{2-} reduction likely reflects a competition with SRB for H_2 in EDvSS and space within the biofilm in EAvSS. On the other hand, SO_4^{2-} reduction appeared to favor phylotypes closely related to *Bacteroidales* (in the phylum *Bacteroidetes*) (EDvSS 1d and EAvSS 2c and 2d). *Bacteroidales* participate in the mineralization of organic matter (Nagata, 2008), particularly proteins and carbohydrates (Church, 2008). The correlation of the abundances of *Bacteroidales* and *Desulfovibrionales* during SO_4^{2-} reduction suggests that these microorganisms established a cooperative relationship. Most likely, *Bacteroidales* utilized SMP (Ni et al., 2011) released by SRB like *Desulfovibrionales* during SO_4^{2-} reduction (Tang et al., 2012a). Ziv-El et al. (2012) also observed significant abundance of *Bacteroidales* and attributed their presence to the production of acetate by fermentation of complex organic molecules (e. g., decaying biomass and SMP).

3.4 Conclusions

H_2 availability and NO_3^- loading significantly shaped the microbial community structure in the MBfR. H_2 availability (in EDvSS) had a greater impact than NO_3^- loading (in EAvSS) on community structure; this included a decline in microbial diversity as H_2 delivery was restricted. Furthermore, the onset of SO_4^{2-} reduction strongly modified the microbial community, with communities experiencing SO_4^{2-} reduction being distinct from those without SO_4^{2-} reduction. When denitrification was the major microbial respiratory process due to H_2 restriction in EDvSS, DB (*Burkholderiales*, *Rhodocyclales*, and *Hydrogenophilales*) outcompeted SRB, although SRB were present (mostly *Desulfovibrionales)*. However, the DB phylotypes responded differently to H_2 availabilities, with the autotrophic phylotype *Methyloversatilis* becoming more important with greater H_2 availability. Under non-limiting H_2 conditions (in EAvSS), SRB declined with increasing NO_3^- loadings, but survived within the biofilm. Lastly, SO_4^{2-} reduction showed a negative impact on the homoacetogen *Holophagales*, which demonstrates competition between SRB for electron donor in EDvSS and space in EAvSS, and a positive impact on the heterotroph *Bacteroidales,* which might grow by utilizing SMP released during SO_4^{2-} reduction.

The findings reported here demonstrate relationships between DB and SRB, along with their interactions with other members of the microbial community. The biofilm community was affected by the availability of H_2 as an inorganic electron donor; the biofilm became more heterotrophic when the H_2 availability was below 0.56 g H_2/m^2 day. Likewise, a relatively low NO_3^- loading allowed more SO_4^{2-} reduction and caused the microbial community to shift to more SRB.

Chapter 4

PERCHLORATE REDUCTION FROM A HIGHLY CONTAMINATED GROUNDWATER IN THE PRESENCE OF SULFATE-REDUCING BACTERIA IN A HYDROGEN-FED BIOFILM

This chapter was published in an altered format in *Biotechnology and Bioengineering* (Ontiveros-Valencia et al., 2013b)

4.1 Introduction

Chapters 2 and 3 highlight the ecological interactions between DB and SRB in H_2-fed biofilms. In this Chapter, I introduce a new electron acceptor with very stringent reduction goal, ClO_4^-, and I study the ecology between SRB and PRB.

ClO_4^- is a chemical oxyanion naturally found in arid zones, the atmosphere, and the sea (Jackson et al., 2006). Anthropogenic activities -- such as production of rocket fuel, fireworks, munitions, and certain fertilizers -- have resulted in significant releases of ClO_4^- to the environment and water contamination (Gullick et al., 2001). Other sources of ClO_4^- are pharmaceutical, air bag, electronics, leather, paint, and enamel production industries (US EPA, 2005). Documenting the widespread presence of ClO_4^- contamination, the US EPA reported that 35 US states and Puerto Rico show ClO_4^- contamination of groundwater and surface water (US EPA, 2005). A typical scenario for contaminated groundwater is a ClO_4^- concentration < 100 μg/L, but with co-contamination from nitrate (NO_3^-) at ~20 mg/L (Herman and Frankenberger, 1999; Logan and LaPoint, 2002). In some cases, ClO_4^- has been detected at higher concentrations (US EPA, 2005): e.g., 800 μg/L in drinking water sources, 3,700 mg/L in groundwater, and 120 mg/L in surface water.

Because ClO_4^- has a strong affinity with the sodium-iodide symporter, which regulates the function of the thyroid, ClO_4^- interferes with the uptake of iodide into the thyroid gland. This disrupts the production of hormones in humans, which can impair the development of children (US EPA, 2005). Pregnant women and fetuses are even more sensitive to ingestion of ClO_4^- (Tiemann, 2006, 2008). Although a maximum contaminant level has not yet developed (US EPA, 2012b), a health-protective ClO_4^- reference dose of 0.7 µg-kg/day has been established (US EPA IRIS, 2005), and is expected to not present a health-risk in a lifetime. The reference dose translates to ~25 µg/L in drinking water. Some US states have established their own advisory levels for ClO_4^- contamination: e.g., 6 µg/L in California and 14 µg/L in Arizona (US EPA, 2005).

ClO_4^- can be treated by using physical/chemical methods such as ion exchange (Gu et al., 2000, 2001), carbon adsorption (Graham et al., 2004), and reverse osmosis (Urbansky and Schock, 1999); however, these methods do not destroy ClO_4^- and have considerable drawbacks. For instance, ion exchange and reverse osmosis generate significant high-salt waste streams, and reverse osmosis is energy intensive. In contrast, microbiological reduction generates harmless Cl^- and H_2O (Nerenberg et al., 2002).

PRB are microorganisms capable of stepwise reduction of ClO_4^- to Cl^- and H_2O, a biotransformation that requires a total of 8 electron equivalents per mole of ClO_4^- (Nerenberg et al., 2002). In Chapter 1, Figure 1.2 describes the microbial respiration pathway for ClO_4^- reduction. The first step, reduction of ClO_4^- to chlorate (ClO_3^-), requires two electron equivalents from an electron donor. The second step, reduction of ClO_3^- to chlorite (ClO_2^-), also needs two electron equivalents. Both steps are catalyzed by a ClO_4^--reductase (encoded by *pcrABCD)* (Coates and Achenbach, 2004). The next

step, the dismutation of ClO_2^- to form O_2 and Cl^-, does not consume electrons and is catalyzed by a ClO_2^- dismutase (*cld*) (Van Ginkel et al., 1996). The O_2 produced in the final step is reduced by the PRB, requiring four more electron equivalents to form H_2O.

PRB are phylogenetically diverse microorganisms that are present in the α, β, γ, and ε classes of the Proteobacteria phylum (Coates and Achenbach, 2004). Due to this phylogenetic diversity, targeting the genes involved in the microbial respiration of ClO_4^- makes it possible to quantify PRB. For PRB, *pcrA*, but not *cld*, is specific enough to quantify them (Nozawa Inoue et al., 2008) and has already been used successfully for hydrogen (H_2)-fed biofilms (Zhao et al., 2011).

The H_2-MBfR is among the technologies that can be used for biological reduction of ClO_4^- (US EPA, 2005; Rittmann et al., 2012). The principle of the MBfR is described in complete detail in Chapter 1. In short, H_2 serves as electron donor that can diffuse through the membrane wall, becoming available for bacteria that grow as biofilm on the membrane's outer wall. Bacteria utilize the electrons donated by H_2 to reduce ClO_4^- to H_2O and Cl^- (Nerenberg and Rittmann, 2002), NO_3^- to N_2 gas (Lee and Rittmann, 2002), SeO_4^{2-} to Se^0 (Chung et al., 2006b), and TCE to ethene and Cl^- (Chung et al., 2008; Ziv-El et al., 2012). The MBfR has been extensively tested at bench and pilot scales for ClO_4^- reduction in groundwater with the typical contamination scenario (e.g., Nerenberg et al., 2002; Adham et al., 2003; Ziv-El and Rittmann, 2009).

The contaminated groundwater tested in this study came from an industrial site associated with munitions manufacture. It deviates from the conventional scenario in that ClO_4^- is a more dominant oxidized contaminant than NO_3^-. Whereas the NO_3^- concentration is only 1-2 mg N/L in this groundwater, the ClO_4^- concentration is ~ 10

mg/L (10000 μg/L). Modeling (Tang et al., 2011b, c) and experimental research (Zhao et al., 2011) point out that concurrent microbial reductions of NO_3^- and ClO_4^- depend on their relative concentrations. In this study, the ratio between the NO_3^- and ClO_4^- influent concentration (0.2 g N: 1 g ClO_4^-) ought to have no effect on denitrification and ought to favor ClO_4^- reduction; this contrasts to the normally higher ratio between NO_3^- and ClO_4^-, which could inhibit ClO_4^- reduction (Zhao et al., 2011; Tang et al., 2011b, c).

In addition to ClO_4^- and NO_3^-, the groundwater contains SO_4^{2-} at ~ 60 mg/L SO_4^{2-} and O_2 at ~ 8 mg/L. While SO_4^{2-} is not a regulated contaminant, its high concentration makes SO_4^{2-} a potentially important electron acceptor in the MBfR. SO_4^{2-} reduction normally is an undesired process since it (1) consumes H_2, which increases the operating costs of the MBfR, (2) may lead to undesired competition with PRB, and (3) generates sulfide, which has a characteristic "rotten egg" odor and is corrosive and toxic (Odom, 1990). The relationships between SRB and PRB are not completely understood. While some studies (Attaway and Smith, 1993; Losi et al., 2002; Bardiya and Bae, 2005) showed no effect from SO_4^{2-} on ClO_4^- degradation, Waller (2002) found that high concentrations of SO_4^{2-} slowed the rate of ClO_4^- reduction. According to Waller (2002), the different microbial ecologies of the several consortiums were responsible for the diverse degradation rates of ClO_4^- and SO_4^{2-} when both electron acceptors were present. Clearly, the occurrence of SRB and their impacts on PRB must be identified for treating this groundwater with the MBfR when SO_4^{2-} is abundant.

The role of O_2 on ClO_4^- reduction is controversial. Some studies indicated inhibition of ClO_4^- reduction under aerobic conditions (Coates et al., 1999b; Chaudhuri et al., 2002), but others (Bardiya and Bae, 2005) reported microbial growth when O_2 was

used as an electron acceptor besides ClO_4^-. Coates and Anderson (2000) pointed out that O_2 is not toxic for PRB, because all PRB produce O_2 during the dismutation of ClO_2^- to Cl^-; the PRB are either microaerophilic or facultative.

The practical objective of this work was to test if a H_2-fed biofilm could remove ClO_4^- in a groundwater from ~10 mg/L to a very low concentration while minimizing SO_4^{2-} reduction. For example, achieving the Arizona advisory level of 14 μg/L (US EPA, 2005) would require greater than 99.8% ClO_4^- removal. More fundamentally, I evaluated how ecological interactions between PRB and SRB in the biofilm community were related to achieving ClO_4^- reduction and minimizing SO_4^{2-} reduction.

4.2 Materials and Methods

MBfR configuration

I employed a bench-scale, single-stage MBfR similar to Ontiveros-Valencia et al. (2012). The MBfR was composed of two glass tubes interconnected with Norprene tubing (Masterflex, model 06404-15, 16, 26) and plastic fittings (Ontiveros-Valencia et al., 2012). In one glass tube, I inserted a set of 32 25-cm long, composite and non-porous Mitsubishi-Rayon fibers (Model MHF200TL) that were potted at their end with glue. In the other glass tube, I inserted 10 "coupon" fibers for biomass sampling; the fiber type and potting method were the same as for the main bundle. The MBfR total volume was 60 mL. H_2 was delivered to the lumen of the fibers at a controlled pressure, and it diffused through the walls of the bubbleless gas-transfer fibers. Bubbleless operation was achieved by the hydrophobic and non-porous inner layer of polyurethane, which provides

a high bubble-point pressure. The recirculation rate was 150 ml/min, which allowed complete mixing of the liquid inside the entire MBfR.

The groundwater was bailed at a contaminated well from an industrial site in Arizona, and immediately shipped to the Swette Center for Environmental Biotechnology in ice containers. I inoculated the MBfR with 1 ml of activated sludge from the Mesa (Arizona) Northwest Wastewater Treatment Plant. Before inoculating the reactor, I diluted 1 ml of activated sludge into 59 ml of groundwater. I left the reactor in batch operation for 24 h after inoculation, and then I put the reactor in continuous operation. The MBfR was operated in a continuous-flow mode at room temperature (25°C) according to the series of conditions shown in Table 4.1. MBfR experimentation has demonstrated the role of H_2 availability and electron acceptor surface loading for optimal microbial reduction of oxidized contaminants (Lee and Rittmann, 2002; Ziv-El and Rittmann, 2009; Ontiveros-Valencia et al; 2012). Therefore, I evaluated the effect of H_2 (electron-donor) availability by adjusting the H_2 pressure and the effect of surface loading by changing the influent flow rate, which resulted in changes to the HRT. I applied five H_2 pressures and three surface loadings designed to find operational conditions that allowed removal of ClO_4^- to a very low concentration, such as below the Arizona advisory level of 14 μg/L, without incurring significant SO_4^{2-} reduction. I started by increasing stepwise the H_2 pressure in the MBfR for steady states 1 - 4 (SS1-SS4). Then, I decreased simultaneously the H_2 pressure and flow rate in SS5, made another decrease of the flow rate in SS6, and then decreased the H_2 pressure in SS7.

Table 4.1 Operating conditions for the seven steady states tested with the one-stage MBfR

Steady state	Absolute H_2 pressure atm	Hydraulic Retention Time, HRT hours	Total electron acceptor loading g H_2/m^2 day	O_2 surface loading		NO_3^- surface loading		ClO_4^- surface loading		SO_4^{2-} surface loading	
				g O_2/m^2 day	g H_2/m^2 day	g N/ m^2 day	g H_2/m^2 day	g ClO_4^-/m^2 day	g H_2/m^2 day	g SO_4^{2-} $/m^2$ day	g H_2/m^2 day
1	1.3	2.7	0.49	0.46	0.07	0.05	0.02	0.57	0.06	3.8	0.34
2	1.4	2.7	0.49	0.46	0.07	0.05	0.02	0.57	0.06	3.8	0.34
3	1.5	2.7	0.49	0.46	0.07	0.05	0.02	0.57	0.06	3.8	0.34
4	1.7	2.7	0.49	0.46	0.07	0.05	0.02	0.57	0.06	3.8	0.34
5	1.3	5.9	0.21	0.21	0.03	0.05	0.02	0.27	0.03	1.5	0.13
6	1.3	17.2	0.07	0.07	0.01	0.02	0.007	0.09	0.01	0.48	0.04
7	1.1	17.2	0.07	0.07	0.01	0.02	0.007	0.09	0.01	0.48	0.04

Notes:

(1) Pressure in atm = (psig/14.7) + 1. Pressure in kPa =atm*101.32.

(2) HRT= reactor volume/Q, where the reactor volume was 60 mL.

(3) Loading rates of each acceptor were calculated by following the formula:

$$Loading = \frac{Q \times (S^{\circ})}{A} \qquad (Equation\ 4.1)$$

where Q = volumetric flow rate (L/day), A = membrane surface area (m^2), and S° is the influent concentration (g/L) for an electron acceptor. Each electron acceptor loading value was normalized to g H_2/m^2 day based on stoichiometric relationships (Zhao et al., 2011; Ontiveros-Valencia et al., 2012, and Tang et al., 2012a).

(4) Total electron-acceptor loading was calculated as the sum of the loadings for O_2, NO_3^-, ClO_4^-, and SO_4^{2-}.

Chemical analyses

I took influent and effluent samples with 6-mL syringes and filtered them immediately through 0.2-µm membrane filters (LC+PVDF membrane, Pall Life Sciences Acrodisc Syringe Filters, USA). I assayed for NO_3^-, NO_2^-, and SO_4^{2-} using an IC (Dionex ICS 3000) having an AG18 pre-column, an AS18 column, an eluent of 22 mM potassium hydroxide (KOH), and an eluent flow rate of 1 ml/min. I measured ClO_4^- by using IC (Dionex ICS 2000) with an AG16 pre-column, AS16 column, an eluent concentration of 35mM KOH, and a 1.5 ml/min flow rate. I detected sulfide production by odor and quantified it by loss of SO_4^{2-}. I analyzed the pH of influent and effluent samples with a pH meter (Orion Star, USA).

The influent O_2 concentration was measured with a DO probe (Orion Star, USA); the range of O_2 in the groundwater was 8-9 mg/L. Effluent O_2 concentrations were assumed to be negligible (Lee and Rittmann, 2002; Nerenberg and Rittmann, 2004; Ziv-El and Rittmann, 2009).

ClO_4^-, NO_3^-, SO_4^{2-} and O_2 removal fluxes

Once the reactor reached steady state (SS) conditions (defined by stable removals of ClO_4^- and SO_4^{2-}, a situation achieved within 10 to 25 days), I calculated the ClO_4^-, NO_3^-, SO_4^{2-}, and O_2 removal fluxes based on equation 1:

$$J = \frac{Q \times (S^{\circ} - S)}{A} \qquad (Equation\ 4.2)$$

where Q = volumetric flow rate (L/day), A = membrane surface area (m^2), and S° and S are the influent and effluent concentrations (g/L) for an electron acceptor. To establish if the delivery rate of the electron donor was limiting or sufficient, I calculated the

experimental H_2 flux from the stoichiometry equations explained previously for ClO_4^- reduction (Zhao et al., 2011), NO_3^- reduction (Tang et al., 2012a), and SO_4^{2-} reduction (Tang et al., 2012a; Ontiveros-Valencia et al., 2012). I computed the total experimental flux by summing the H_2 flux for each acceptor and compared it with the theoretical maximum H_2 flux through the Mitsubishi-Rayon fibers for the given H_2 pressure (Tang et al., 2012d).

DNA extraction and qPCR

I took fiber samples for two SS in which ClO_4^- reduction was successful, but SO_4^{2-} reduction was significant (SS5 and SS7), and extracted DNA as described by Ontiveros-Valencia et al. (2012).

I used plasmids with the desired functional genes (Zhao et al., 2011; Ontiveros-Valencia et al., 2012) to develop calibration curves using serial dilutions from 10^7 to 10^1 gene copies per µL. The gene copy numbers were calculated based on the concentration of the extracted plasmids as described elsewhere (Zhao et al., 2011; Ontiveros-Valencia et al., 2012). I used specific primers to target fragments of the functional genes *pcrA* to quantify PRB (Nozawa-Inoue et al., 2008), *dsrA* to quantify SRB (Kondo et al., 2008), and copper-containing and cytochrome cd1 nitrite reductases *nirK* (Braker et al., 1998) and *nirS* (Throbäck et al., 2004) to assess DB.

I used the SYBR Premix Ex Taq Kit (Takara Bio, Inc, Japan) and performed the qPCR reaction in a 20-µl volume: 10 µl SYBR, 8.6 µl H_2O, 0.2 µl of each forward and reverse primer (10 pmol/µl), and 1 µl of DNA template. Negative controls had water instead of DNA templates, and qPCR reactions were carried out in triplicate. The qPCR protocols are those described in Zhao et al. (2011) and Ontiveros-Valencia et al. (2012).

I quantified the area of the membrane occupied by the biofilm at each sampled SS and then converted the qPCR data from gene copies to cells by assuming one *pcrA* gene per PRB cell (Coates et al., 2001), one *dsrA* gene per SRB (Kondo et al., 2004*)*, one *nirK* gene per DB (Phillipot, 2006), and two *nirS* genes per cell of DB based on the genome of *Dechloromonas aromatica* (Coates et al., 2001). Lastly, the biofilm samples represented an area of 1.2-1.7 cm^2, which is large enough that localized heterogeneities did not bias the microbial distributions (Ziv-El et al., 2012).

4.3 Results and Discussion

MBfR performance

The practical objective of this work was to test if a H_2-fed biofilm could remove ClO_4^- to very low concentrations while minimizing SO_4^{2-} reduction from a groundwater containing significant SO_4^{2-} and a very high concentration of ClO_4^-. Figure 4.1 shows that the single-stage MBfR reduced the influent ClO_4^- by at least 94%, and the lowest effluent ClO_4^- concentration was 41 µg/L (achieved in SS6), or 99.6% removal (Figure 4.1 Insert a). All 7 steady states achieved complete denitrification (effluent NO_3^- below the detection limit, 0.01 mg/L, data not shown). Table 4.1 shows that the decreases in total electron-acceptor surface loading (calculated as the sum of the individual electron-acceptor surface loadings for NO_3^-, O_2, ClO_4^-, and SO_4^{2-}) in SS5-SS7 resulted in major SO_4^{2-} reduction (Insert a). While SS6 achieved the lowest effluent ClO_4^- concentration (41 µg/L, Insert b), SO_4^{2-} reduction was ~ 85% (Insert a) as the result of the combination of a relatively high H_2 pressure (1.3 atm) and the lowest total electron-acceptor surface loading tested (0.07 g H_2/m^2 day). A decrease of H_2 pressure in SS7 at the same low

surface loading offered some control of SO_4^{2-} reduction, which decreased to ~37% (Insert a), but the effluent ClO_4^- concentration increased slightly (Insert b). Even though the effluent ClO_4^- concentration never decreased below the Arizona advisory level of 14 μg/L (Insert b), Figure 4.1 shows that very high percentage reduction of ClO_4^- was achieved in all cases (Insert a). It also shows a trade-off between achieving the lowest ClO_4^- effluent concentrations and allowing SO_4^{2-} reduction.

To quantify how much H_2 was consumed to reduce each electron acceptor, I compare acceptor-removal rates expressed as H_2 fluxes. Figure 4.2a summarizes the total H_2 consumption fluxes and the break down by electron acceptor. During SS1-SS4, the highest fraction of H_2 consumption was for O_2 respiration (34-36% of the total H_2 consumption), followed by ClO_4^- reduction (29-33%), SO_4^{2-} reduction (20-26%), and denitrification (~10%) (Figure 4.2b). This distribution is quite different from what is typical for groundwater treatment, for which denitrification is >80% of the H_2 demand and ClO_4^- reduction is minor (Nerenberg and Rittmann, 2004; Van Ginkel et al., 2008; Ziv-El and Rittmann, 2009; Zhao et al, 2011). When I decreased the acceptor surface loading (SS5-SS7), SO_4^{2-} reduction became the largest electron sink (36-44% of the total H_2 consumption); ClO_4^- reduction (20-22% H_2 consumption) and O_2 respiration (22-24% H_2 consumption) were similar, with denitrification being 14-16%.

Based on the comparison between the experimental and maximum H_2 fluxes (data not shown), I conclude that the single-stage MBfR was never limited by H_2 delivery. This means that the inherent kinetics of the microbial community in the biofilm controlled the reduction rates for each electron acceptor (Ziv-El and Rittmann, 2009).

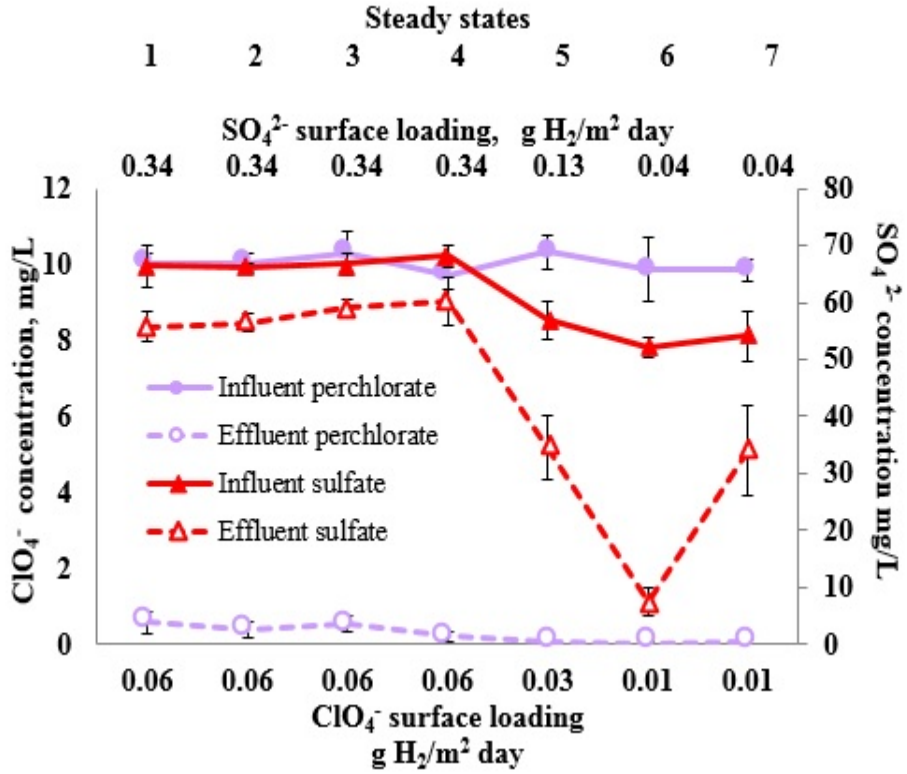

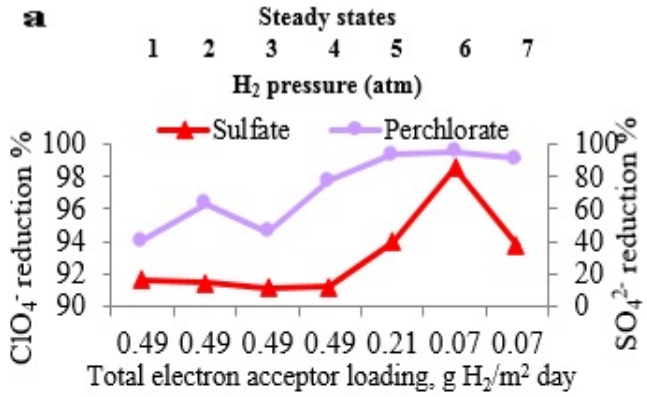

Insert b Experimental MBfR effluent concentrations

Steady state	Effluent ClO_4^-, µg/L
1	590
2	370
3	558
4	215
5	63
6	41
7	85

Figure 4.1 Influent and effluent ClO_4^- and SO_4^{2-} concentrations for seven steady states for the single-stage MBfR. Insert a shows the % removal of ClO_4^- and SO_4^{2-}. Insert b shows the actual effluent ClO_4^- concentrations. While performing the experiments, I received several shipments of groundwater from the same contaminated well. However, the influent SO_4^{2-} concentrations varied slightly for the last three steady states.

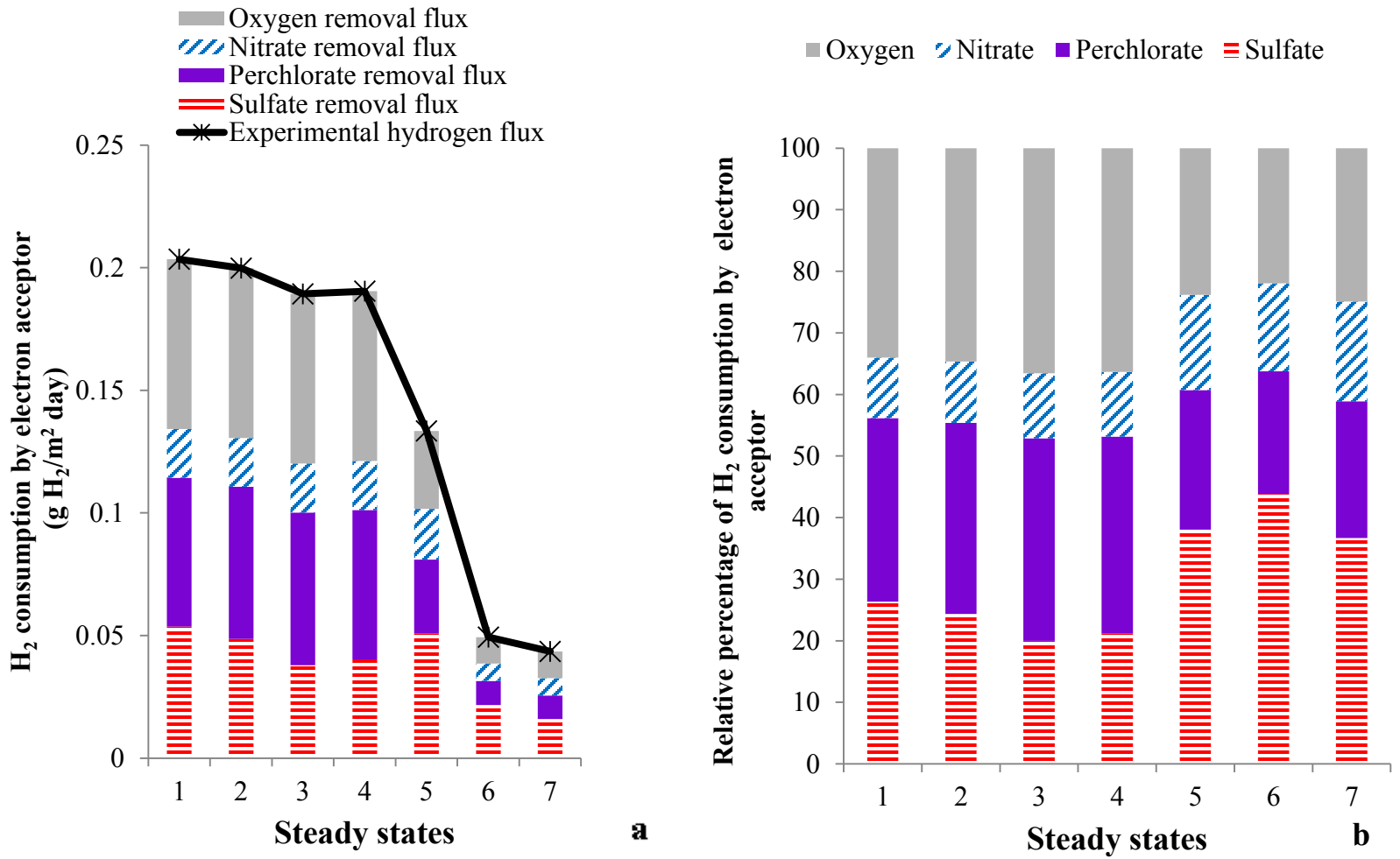

Figure 4.2 a) H_2 consumption by electron acceptor and total experimental H_2 flux. b) Relative amounts of H_2 consumption for the seven steady states for the single-stage MBfR.

Analysis of the structure of the microbial community

Figure 4.3 compares the qPCR data in cells/cm^2 for the two sampled steady states with their H_2 consumption fluxes. The only large change in the microbial community structure from SS5 to SS7 was the approximately 10-fold increase is *dsrA*. Although SS7 had a lower rate of SO_4^{2-} reduction (Figure 4.1, Insert a), the large decrease in NO_3^- surface loading in SS6 and SS7 (Table 4.1) allowed SRB to become greater in number than PRB in SS7.

Despite the relatively low NO_3^- concentration in the groundwater and low H_2 demand for denitrification (Figure 4.2b), denitrifying genes were significant. Since most PRB also respire NO_3^- and O_2, I summed the H_2 consumption fluxes from NO_3^-, O_2, and ClO_4^- and compared them to the H_2 consumption flux from SO_4^{2-} reduction for SS4-SS7.

The abundance of PRB roughly corresponded to the H_2 consumption for ClO_4^-, NO_3^-, and O_2 reductions. In SS5, the biofilm community showed about 2-fold higher PRB/cm^2 than in SS7, while the sum of ClO_4^-, NO_3^-, and O_2 flux was about 3-fold greater in SS5 than in SS7. The number of DB cells also correlated with the changes on NO_3^-, ClO_4^-, and O_2 fluxes: DB/cm^2 and sum of NO_3^-, ClO_4^-, and O_2 fluxes decreased about 2- and 3-fold, respectively, from SS5 to SS7. While qPCR values are not absolute and a 2-fold change may or may not be significant, the PRB and DB consistently responded to the surface loading. This trend also supports that DB were driving the microbial reduction of ClO_4^-, as shown previously (Van Ginkel, et al., 2010; Zhao et al., 2011).

The trend for SRB was substantially different than with PRB and DB: SRB did not correlate with the SO_4^{2-} reduction fluxes for SS5 and SS7. As the one-stage MBfR was not limited by H_2-delivery, SRB appeared to be controlled by other factors,

particularly the lower NO_3^- + ClO_4^- + O_2 surface loading in SS6 and SS7, which should favor SRB (Tang et al., 2012a; Ontiveros-Valencia et al., 2012). Having relatively slow kinetics, SRB benefit when the NO_3^- + ClO_4^- + O_2 surface loading is smaller, because they are able to compete better for space in the biofilm near the membrane substratum. In the case studied here, the smallest NO_3^- + ClO_4^- + O_2 surface loadings, also with a relatively high H_2 pressure (SS6) (Table 4.1), corresponded to the highest SO_4^{2-} reduction percentage (~85%) (Figure 4.1 insert a). The effect of NO_3^- + ClO_4^- + O_2 surface loading explains how SRB could become more important in the biofilm despite a lower absolute value of the H_2 flux for SO_4^{2-} reduction in SS7 (Figure 4.2a). Besides, lower fluxes do not necessarily correspond to lower reduction percentages if the acceptor loading also declines. In fact, the SO_4^{2-} reduction percentage was higher for SS5-7 than for SS1-4 (Figure 4.1 insert a) due to the larger HRT (Table 4.1), which caused lower surface loadings for all acceptors. The lower loadings of O_2 + NO_3^- + ClO_4^- made it possible for SRB to outnumber the normally faster growing DB and PRB, as the qPCR results show, and the decrease in SO_4^{2-} surface loading made it possible for the SRB to achieve a higher percentage reduction of SO_4^{2-}, as the effluent concentrations show.

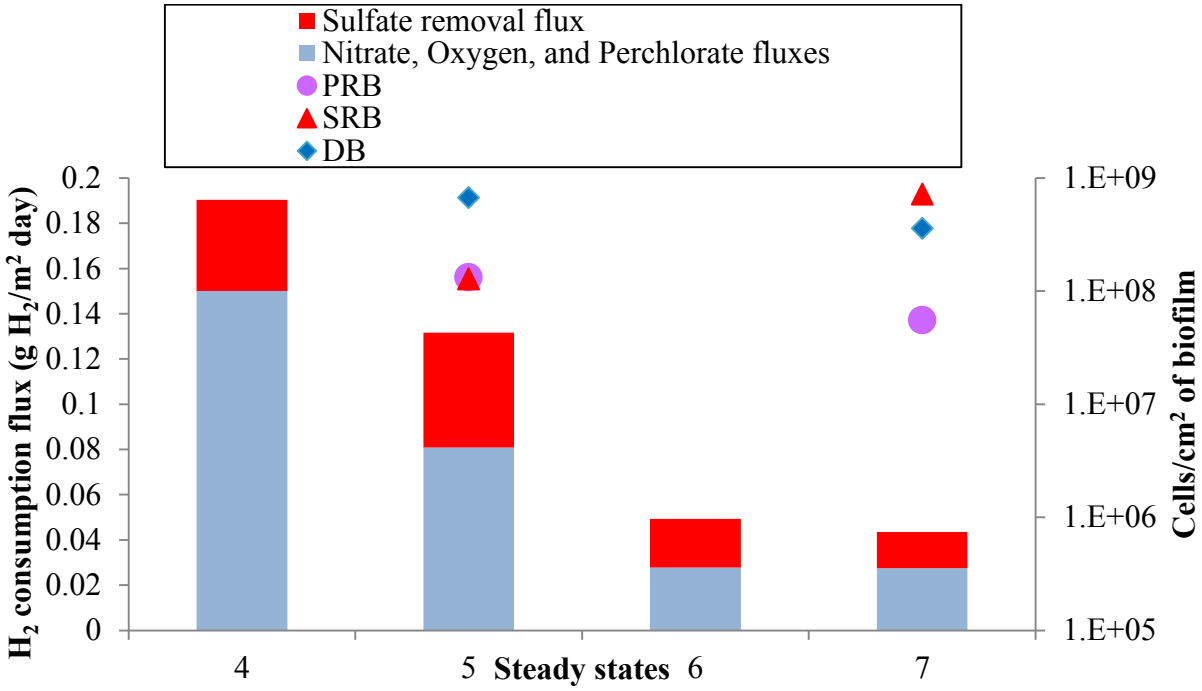

Insert a Standard deviation for qPCR results.

SS Microbial group	5	7
PRB	8.7E6	1.5E6
SRB	1.2E7	8.3E6
DB	5E7	1.6E7

Figure 4.3 qPCR results (converted to cells/cm^{2}of biofilm) and removal fluxes for the electron acceptors for critical steady states. Insert a table shows the standard deviation for the qPCR results.

Factors controlling the perchlorate concentration in the effluent

The inherent kinetics of the PRB and competition with SRB and/or DB appeared to govern the degree of ClO_4^- reduction, because the MBfR did not experience H_2 limitation. Since SO_4^{2-} had by far the largest surface loading among all acceptors in the groundwater (Table 4.1), significant SO_4^{2-} reduction in SS5-SS7 may have allowed SRB to be the strongest competitors to PRB for the most favorable space in the biofilm. According to Tang et al. (2012a, b), competition for space between microbial types in a H_2-based biofilm depends on their relative specific growth rates, which are inherently related to kinetic parameters such as the maximum specific growth rate (μ_{max}, d^{-1}) and half-maximum-rate concentration (K_s, mg/L). For co-existing SRB and DB, Tang et al. (2012a) indicated that SRB must grow in the proximity to the fiber surface, which allows them to compete for H_2 against faster-growing DB. Tang et al. (2012a) concluded that significant accumulation of SRB at the fiber surface only occurs when the specific growth rate of DB inside the biofilm is slowed by depletion of NO_3^- due to nearly complete denitrification. In this study, denitrification was complete for each steady state, and DB consumed much less H_2 than did SRB (Table 4.1); thus, the situation was favorable for SRB in its competition for favorable space in the biofilm.

With SRB growing preferentially in proximity to the fiber surface (Tang et al., 2012a), a high abundance of SRB (as shown by the qPCR results) may have pushed PRB away from the most favorable location within the biofilm. Forcing the PRB to accumulate more in the outer layers of the biofilm put them at higher risk of detachment losses (Furumai and Rittmann, 1994; Wanner et al. 2006), which requires a higher bulk-liquid ClO_4^- concentration to maintain the PRB in the biofilm. Microorganisms growing

at the inner layers of the biofilm have a higher protection from detachment than those microorganisms growing at the surface of the biofilm.

To interpret quantitatively why the effluent ClO_4^- concentration could not be driven to less than 41 µg/L in the MBfR, I applied a key concept from steady-state-biofilm modeling (Rittmann and McCarty, 2001). The concept is the minimum substrate concentration to support a steady-state biofilm, or S_{min} (mg/l). For a biofilm, S_{min} is computed as

$$S_{min} = K_s[b + b_{det}]/[\mu_{max} - b - b_{det}] \qquad (Equation\ 4.3)$$

in which b is the endogenous decay rate (d^{-1}) and b_{det} is the specific detachment rate (d^{-1}). Biomass near the outer surface of the biofilm experiences a higher b_{det} value, while biomass deep inside the biofilm may have a b_{det} value approaching zero (Furumai and Rittmann, 1994; Wanner et al., 2006). Any ClO_4^- concentration lower than S_{min} will lead to washout of PRB from the biofilm; thus, the ClO_4^- concentration can never go below S_{min} for sustained ClO_4^- reduction.

I computed S_{min} values for PRB with a range of scenarios in which competition from SRB imposes a higher PRB b_{det} by pushing the PRB closer to the biofilm's outer surface. The left side of Table 4.2 lists the kinetic and stoichiometric parameter for PRB. The right side of Table 4.2 summarizes the ClO_4^- S_{min} values for b_{det} from 0 to 0.5 d^{-1}. S_{min} was as low as 8 µg/L when b_{det} was zero, because the PRB were very well protected deep inside the biofilm. However, S_{min} was greater than 41 µg/L when b_{det} was ~0.25 d^{-1} or higher. This simple modeling exercise illustrates how competition from SRB likely contributed to the reason that PRB were not able to reduce ClO_4^- to less than 41 µg/L.

Table 4.2 Parameters used in the steady-state-biofilm model and S_{min} results

Modeling inputs			**Modeling outputs for different b_{det} values**	
Parameter	Value	Reference	b_{det} day^{-1}	S_{min} ClO_4^- µg ClO_4^-/L
Endogenous respiration, b_{resp} (day^{-1})	0.075	Rittmann and McCarty (2001)	0	8
Maximum growth rate, μ_{max} (day^{-1})	1.5	Tang et al. (2012b, c)	0.01	10
Half-maximum-rate concentration, K_s (mg ClO_4^-/L)	0.2	Nerenberg et al. (2006)	0.05	15
			0.1	21
			0.25	44
			0.5	100

4.4 Conclusions

I demonstrated that the H_2-based biofilm could reduce up to 99.6% of the 10 000 µg/L ClO_4^- in a groundwater that also contained dissolved O_2, SO_4^{2-}, and NO_3^-. In this unique case of a high ClO_4^- concentration coupled with a relatively low NO_3^- concentration and substantial SO_4^{2-}, strategies to promote more complete ClO_4^- reduction (lower acceptor surface loading and increased H_2 pressure) were beneficial for SRB, which then competed with PRB for space in the biofilm, contributing to incomplete ClO_4^- reduction. SRB appeared to force PRB away from the membrane substratum and, therefore, to areas within the biofilm where biomass detachment was more important.

Chapter 5

MANAGING THE INTERACTIONS BETWEEN SULFATE AND PERCHLORATE-REDUCING BACTERIA WHEN USING HYDROGEN-FED BIOFILMS TO TREAT A GROUNDWATER WITH A HIGH PERCHLORATE CONCENTRATION

This chapter was accepted for publication in an altered format by *Water Research* (Ontiveros-Valencia et al., 2014a).

5.1 Introduction

My research in Chapter 4 suggested that strong competition between SRB and PRB was the most important factor for not achieving complete ClO_4^- reduction in one-stage MBfR, although the MBfR attained 99.6% ClO_4^- removal from groundwater with exceptionally high ClO_4^- contamination. In this chapter, I further investigated the ecological interactions between SRB and PRB as I sought to achieve complete ClO_4^- reduction in a two-stage MBfR.

ClO_4^- is mostly found in low concentration (μg/L range) due to dilution of plumes from contamination sources located at facilities that manufacture and use rocket fuels (Gingras and Batista, 2002). However, groundwater close to the source can have higher concentrations, such as in the mg/L range.

ClO_4^- can be transformed into innocuous Cl^- and H_2O by microbial respiration that requires 8 electron equivalents per mole of ClO_4^- (Nerenberg et al., 2002). PRB are microorganisms capable of respiring ClO_4^-, and are phylogenetically diverse, mostly found in the α, β, γ, and ε-Proteobacteria (Coates and Achenbach, 2004). The MBfR is a technology capable of reclaiming ClO_4^--contaminated groundwater (Nerenberg et al.,

2002). Biofilms fed with H_2 are the core of the MBfR: H_2 is the electron donor and the oxidized compounds are the electron acceptors for bacteria growing as a biofilm on the membranes' wall. Because several electron acceptors can be co-reduced (Rittmann, 2007), competition occurs for common resources, such as H_2 and space in the biofilm (Ontiveros-Valencia et al., 2012; Tang et al., 2012a, b, c). For example, the groundwater tested in the current study had four electron acceptors: ClO_4^-, SO_4^{2-}, NO_3^-, and O_2. The unusually high concentration of ClO_4^- along with substantial SO_4^{2-} made treating this groundwater an unusual challenge. In particular, this combination of ClO_4^- and SO_4^{2-} required a well management of the microbial ecology to achieve complete ClO_4^- reduction without also incurring major SO_4^{2-} reduction.

In Chapter 4 with similarly high ClO_4^- concentrations, I documented undesirable competition for space between PRB and SRB in a single-stage MBfR. The effluent concentration of ClO_4^- could not be reduced to below the detection limit of 4 μg/L. In an attempt to reach non-detectable ClO_4^- concentrations in the single-stage MBfR, I lowered the total electron-acceptor loading from 0.49 to 0.07 g H_2/m^2 day, but this promoted higher SO_4^{2-} reduction rates. SRB then outcompeted PRB (both assayed by qPCR), and complete ClO_4^- removal was not achieved.

To overcome the ecological limitations of the one-stage MBfR so that the ClO_4^- could be driven to below the detection limit, I set up a two-stage MBfR in which the lead MBfR treated the raw groundwater and the lag MBfR treated the effluent from the lead MBfR. The two-stage MBfR setup had a unique characteristic: the combination of two types of membranes (Mitsubishi-Rayon composite fibers in the lead-MBfR, and polypropylene fibers in the lag-MBfR) as a means to control H_2 delivery and, as a

consequence, minimize the amount of SO_4^{2-} reduction in the lag-MBfR. Because of the lower permeation coefficient of the polypropylene fiber (Tang et al., 2012d), I hypothesized that the bulk of ClO_4^- reduction would occur in the lead MBfR. Then, the less permeable membrane in the lag MBfR would allow me complete ClO_4^- reduction, but without an excessive rate of SO_4^{2-} reduction.

The practical objective of this work was to test if ClO_4^- could be reduced to non-detectable levels in a two-stage MBfR setup while I minimized SO_4^{2-} reduction by controlling the H_2-delivery capacity. Achieving this practical objective also allowed me to understand the ecological relationships between PRB and SRB for the different conditions. To my knowledge, these ecological interactions have not been explored in other bioremediation approaches (Hatzinger, 2005). Engineered efforts for perchlorate bioremediation have been done with either a single strain of PRB (e.g., Zhang et al., 2002; Evans et al., 2002, 2003; Min et al., 2004) or with mixed cultures in which the microbial community structure of PRB and SRB was not assessed (e.g., Wallace et al., 1998; Kim and Logan, 2000). To achieve this ecological aim, I used qPCR to target characteristic microbial reductase genes: *dsrA* for SRB, *pcrA* for PRB, and *nirS* and *nirK* for DB. Additionally, by employing high-throughput sequencing (454 pyrosequencing), I identified specific SRB-phylotypes that affect the performance of PRB when treating high concentrations of ClO_4^- in groundwater, and the relationships between SRB with other members in the microbial community.

5.2 Materials and Methods

Two-stage MBfR configuration

Figure 5.1 shows a schematic of the two-stage MBfR, in which the lag MBfR treated the effluent from the lead MBfR. Each MBfR was composed of two cylindrical glass tubes connected with Norprene tubing, plastic fittings, and three-way polycarbonate valves for inlet and outlet sampling ports. One glass cylindrical tube had a set of 49 25-cm length fibers (main bundle) glued at both ends and connected to a H_2 gas supply. The other glass tube had a set of 10 25-cm length fibers (a "coupon" bundle for biofilm sampling), which was also connected to a H_2 gas supply on one extreme and knotted at the other. The total surface area per each MBfR was 94.5 cm^2. Each MBfR had a total volume of 60 mL and a HRT of 6 hours at the constant feed flow rate of 0.17 ml/min.

As stated earlier, I used two different membranes: the lead MBfR had composite Mitsubishi-Rayon (MR) membranes (Model MHF200TL), which have highly efficient H_2 permeation (Tang et al., 2012d), while the lag MBfR used polypropylene (Pol) membranes (Teijin, LTD, Japan), which have lower H_2-permeability (Tang et al., 2012d). The lower H_2 permeability of the Pol membranes was part of the strategy to minimize SO_4^{2-} reduction in the lag MBfR.

I inoculated each reactor with 1 ml activated sludge from the Mesa Wastewater Treatment Plant, which was diluted with 59 ml of the groundwater to be treated. The sludge inoculum has been analyzed elsewhere (Li et al., 2011). After inoculation, I operated the reactors in batch mode for 24 h and then switched to continuous mode at a flow rate of 0.17 mL/min. Each MBfR was operated at room temperature (25°C) and recirculated at 150 ml/min to guarantee complete mixing of the bulk liquid. The effluent

from the lead MBfR was collected over time and exposed to the atmosphere, which re-oxygenated the water before its feeding into the lag MBfR.

Influent groundwater characterization

I collected a ClO_4^--contaminated groundwater from a local industrial site, brought the groundwater to the Swette Center for Environmental Biotechnology in ice containers, and immediately stored the water at 4°C. I analyzed the groundwater for alkalinity by titration (Hach alkalinity kit test model AL-AP MG/L, 25-400 mg/L), hardness by titration (Hach total hardness kit model HA-71A 1-20 mg/L), pH with a pH meter (Orion Star, USA), and dissolved oxygen (DO) with a DO probe (Orion Star, USA).

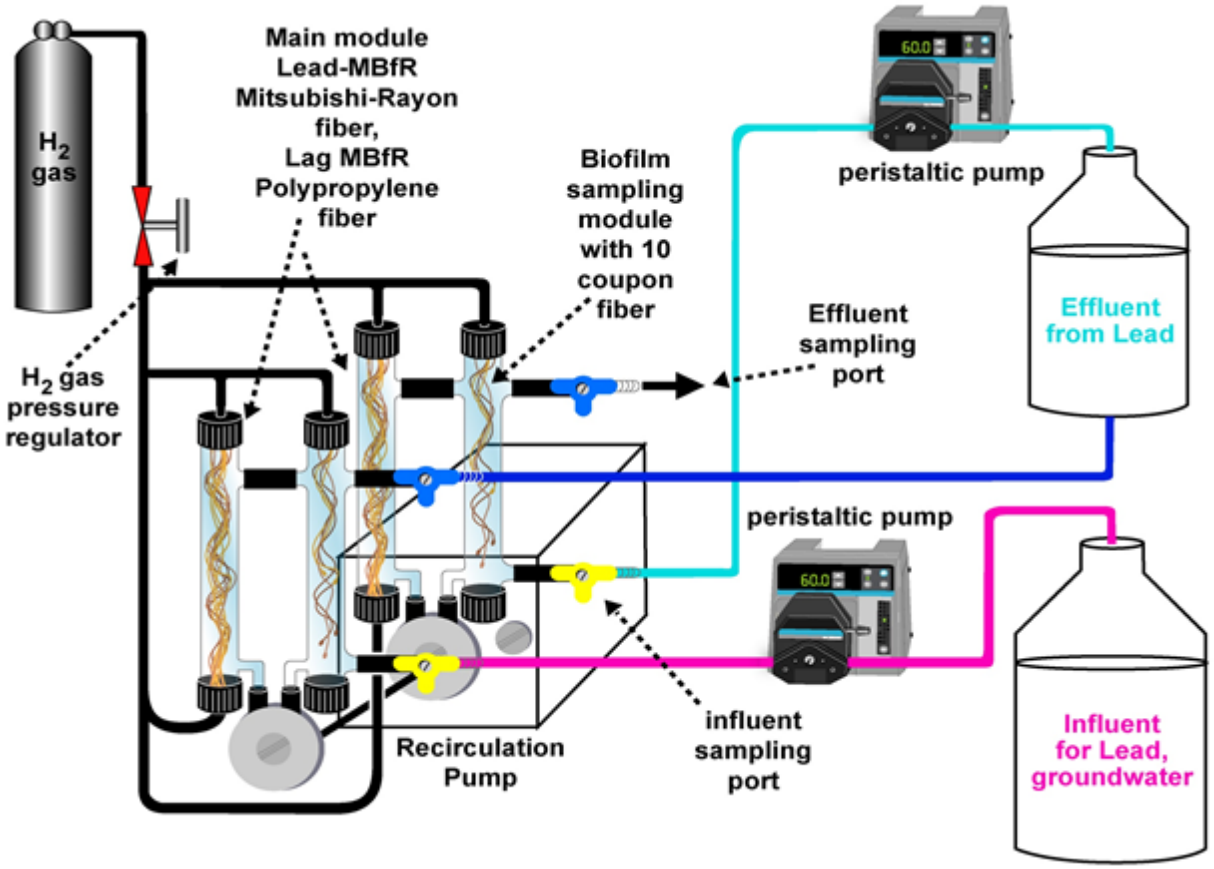

Figure 5.1 Schematic of the two-stage MBfR. The lead MBfR is at the front and receives the influent groundwater. The lag MBfR is behind and receives the effluent from the lead MBfR after it is temporarily stored in a reservoir, which exposes it to atmospheric O_2.

Analyses for ClO_4^-, SO_4^{2-}, NO_3^- and O_2

I took influent and effluent samples with 6-mL plastic syringes and filtered them immediately through 0.2-µm membrane filters (LC+PVDF membrane, Pall Life Sciences Acrodisc Syringe Filters, USA). I assayed for NO_3^-, NO_2^-, ClO_3^-, ClO_2^-, and SO_4^{2-} using IC (Dionex ICS 3000). The IC had an AG18 pre-column, an AS18 column, an eluent of 22 mM potassium hydroxide (KOH), and an eluent flow rate of 1 ml/min. I measured ClO_4^- by using IC (Dionex ICS 2000) with an AS16 column and AG16 pre-column, an eluent concentration of 35 mM KOH, and an eluent flow rate of 1.5 ml/min.

The influent O_2 concentration to both MBfRs was measured with the DO probe. Effluent O_2 concentrations were assumed to be negligible (Ontiveros-Valencia et al., 2012).

Electron acceptor and donor fluxes

I calculated the ClO_4^-, SO_4^{2-}, NO_3^-, and O_2 removal fluxes based on equation 5.1:

$$J = \frac{Q \times (S^\circ - S)}{A} \qquad (Equation\ 5.1)$$

where Q = volumetric flow rate (L/day), A = membrane surface area (m^2), and S° and S are the influent and effluent concentrations (g/L) for an electron acceptor. I calculated the experimental H_2 flux from the stoichiometry equations explained previously for ClO_4^- reduction (Tang et al., b, c), NO_3^- reduction (Tang et al., 2012a), and SO_4^{2-} reduction (Tang et al., 2012a; Ontiveros-Valencia et al., 2012). Then, I compared the total experimental H_2 flux with the theoretical maximum H_2 flux through the MR and Pol fibers for the given H_2 pressure (Tang et al., 2012d).

Steady state conditions and operational parameters

The two-stage MBfR followed the operating conditions summarized in Table 5.1. Each steady state, defined by stable concentrations of NO_3^-, ClO_4^-, and SO_4^{2-}, lasted 16 to 22 days. The lead and lag MBfRs were operated with different H_2 pressures. I used lower values of H_2 pressure to minimize SO_4^{2-} reduction for steady states identified as MR2 and Pol1. In contrast, I enhanced SO_4^{2-} reduction using higher H_2 pressures for steady states identified as MR1 and Pol2. Those changes in H_2 pressure made it possible for me to discern changes in the microbial ecology of the biofilm for operational conditions aimed at remediation goals.

Table 5.1 Operational conditions for the two-stage MBfR

Lead MBfR (MR membrane)			***Lag MBfR (Pol membrane)***		
Steady state	H_2 pressure atm	Maximum H_2 flux g H_2 m^2/d	***Steady State***	H_2 pressure atm	Maximum H_2 flux g H_2 m^2/d
MR1	1.52	2.5	***Pol1***	1.37	0.29
MR2	1.2	2.0	***Pol2***	1.88	0.39

MR: Mitsubishi-Rayon composite fibers, Pol: polypropylene fibers

On a similar way as described earlier in the fluxes section of this Chapter, I calculated the individual and total electron acceptor loadings along the H_2 availability per each steady state and per MBfR. I report those values in Table 5.2.

Table 5.2 Maximum rates of electron donor (H_2) availability and electron acceptor surface loadings for lead and lag MBfRs for the two steady states

Steady State	***Maximum H_2 flux***	***NO_3^- loading***	***O_2 loading***	***SO_4^{2-} loading***	***ClO_4^- loading***	***Total electron acceptor loading***
	g H_2/m^2 day	*g H_2/m^2 day*	*g H_2/m^2 day*	*g H_2/m^2 day*	*g H_2/m^2 day*	*g H_2/m^2 day*
MR1	2.5	0.025	0.039	0.131	0.012	0.207
POL1	0.29	0	0.035	0.115	0.0004	0.1504
MR2	2.0	0.025	0.039	0.125	0.012	0.201
POL2	0.39	0	0.035	0.117	0.00007	0.1521

I calculated the electron acceptor loading rates according to:

$$Loading = \frac{Q \times (S^{\circ})}{A} \qquad (Equation\ 5.2)$$

where Q = volumetric flow rate (L/day), A = membrane surface area (m^2), and S° is the influent concentration (g/L) for an electron acceptor. I normalized each electron acceptor loading value to g H_2/m^2 day based on stoichiometric relationships described elsewhere (Ontiveros-Valencia et al., 2012; Tang et al., 2012a, b, c).
The sum of loadings for O_2, NO_3^-, ClO_4^-, and SO_4^{2-} made the total electron acceptor loading. The maximum H_2 flux was obtained as explained by Tang et al. (2012d).

Biofilm microbial ecology

At the end of each steady state, I took a coupon-fiber sample to analyze the microbial community of the biofilm. The biofilm was detached from the fiber as described by Ontiveros-Valencia et al. (2012). I extracted the biofilm's DNA by following the directions of the manufacturer (Qiagen, USA). DNA samples were stored at -20°C until qPCR and shipping for 454 pyrosequencing. I used plasmids with the desired functional or 16S rRNA genes (Ontiveros-Valencia et al., 2012, 2013b) to develop calibration curves using serial dilutions from 10^7 to 10^1 gene copies per µL. I used the SYBR Premix Ex Taq Kit (Takara Bio, Inc, Japan) and performed the qPCR reaction in a 20-µl volume: 10 µl SYBR, 8.6 µl H_2O, 0.2 µl of each forward and reverse

primer (10 pmol/µl), and 1 µl of DNA template. Negative controls had water instead of DNA templates, and qPCR reactions were carried out in triplicate. Normalization to cells/cm^2 was as described in Ontiveros-Valencia et al. (2013b).

I sent all DNA samples for 454 pyrosequencing at the Molecular Research DNA lab (Texas, USA), which performed amplicon pyrosequencing using a standard Roche 454/GS-FLX Titanium (Sun et al., 2011). The Bacteria domain was targeted by selecting the V6 and V7 regions of the 16S rRNA gene with primers 939F (5'-TTGACGGGGGCCCGCAC-3') and 1492R (5'TACCTTGTTACGACTT-3') (Ontiveros-Valencia et al., 2013a). The potential presence of Archaea was not determined. I processed the raw data using QIIME 1.6.0 suite (Caporaso et al., 2010a) and removed sequences having fewer than 250 bps, homopolymers of more than 6 bps, primer mismatches, or an average quality score lower than 25. I picked the OTUs using the Greengenes 16S rDNA database with *uclust* (Edgar, 2010) based on ≥ 97% identity, removed OTUs that contain less than two sequences (singletons) from the analysis, and aligned the representative sequence of each OTU to the Greengenes Database using *PyNast* (DeSantis et al., 2006; Caporaso et al., 2010b). The potentially chimeric sequences were identified by using ChimeraSlayer (Haas et al., 2011), and a python script in QIIME was employed to remove the chimeric sequences. To assign taxonomy to OTUs, I used the RDP classifier with a 80% confidence threshold (Wang et al., 2007). I constructed Newick-formatted phylogenetic trees using FastTree (Price et al., 2009).

For the purpose of eliminating heterogeneity related to having different numbers of sequences among the samples, I sub-sampled the OTU table by randomly selecting ten different times 7500 sequences per sample, which was the lowest number of sequences

found in one sample. I generated PCoA plots and UPGMA plots (Lozupone et al., 2006) using jack-knifed beta diversity that subsampled each sample at a depth of 7500 sequences. Sequence data sets are available at NCBI/ SRA under study with accession number SRP032957.

5.3 Results and Discussion

Groundwater properties and reduction kinetics in the two-stage MBfR

Table 5.3 summarizes the physicochemical properties of the groundwater, which contained significant SO_4^{2-} and an atypically high concentration of ClO_4^-: an average of 4000 μg/L. The DO value was ~8 mg/L after bailing and transport. The largest electron acceptor influent concentration in e^-meq/L was SO_4^{2-}, followed by O_2, ClO_4^-, and NO_3^-. The values for alkalinity and hardness are characteristic for hard water (USGS, 2012).

Table 5.4 presents the average influent and effluent concentrations of ClO_4^- and SO_4^{2-} for both MBfRs. NO_3^- and O_2 were fully reduced in the lead MBfRs for both steady states and are not listed. The average ClO_4^- removal was 96.5%+3.3% for MR1 and 99.3%+1.7% for MR2, but the ClO_4^- effluent concentration was higher than 25 μg/L in the effluent from both lead MBfRs (MR1 and MR2). ClO_3^- was produced (~210 μg/L) in the lead MBfR on four days of steady state MR1, when SO_4^{2-} reduction was significant. However, complete ClO_4^- removal (below the detection limit of 4 μg/L) was achieved in both lag MBfRs (Pol1 and Pol2).

Table 5.3 Contaminated groundwater's water-quality properties

Parameter	*Value*	*Units*
pH	7.5-8.5	--
Alkalinity	140-200	mg as $CaCO_3$/L
Hardness	137-205	mg as $CaCO_3$/L
SO_4^{2-}	60*, 5	mg/L , e^-meq/L
Dissolved O_2	8 , 1	mg/L , e^-meq/L
ClO_4^-	4000* , 0.32	µg/L , e^-meqL
NO_3^--N	2 , 0.16	mg/L , e^-meq/L

* Influent concentrations varied slightly over the course of the experiments and were measured. The average concentrations for each steady state are reported in Table 3.

Table 5.4 Average influent and effluent concentrations (along with standard deviations) of ClO_4^- and SO_4^{2-} for the lead and lag MBfRs for the two steady states. Influent ClO_4^- concentrations for the lag MBfR are the same as the effluent ClO_4^- concentrations for the lead MBfR; however, the SO_4^{2-} concentrations increased for the influent to the lag MBfR due to O_2 exposure in the feed reservoir for the lag MBfR. ND = Non detectable, or <4 µg/L ClO_4^-.

Steady State	Influent ClO_4^- µg/L	Effluent ClO_4^- µg/L	Influent SO_4^{2-} mg/L	Effluent SO_4^{2-} mg/L	*Steady State*	Effluent ClO_4^- µg/L	Influent SO_4^{2-} mg/L	Effluent SO_4^{2-} mg/L
MR1	4090± 180	140± 134	57.4± 2.6	23± 9.1	***Pol1***	ND	50.6± 3.2	46.2± 3.8
MR2	3800± 337	25± 7	54.7± 2.2	39.1± 1.4	***Pol2***	ND	51.6± 3	41.5± 3

According to Table 5.3, SO_4^{2-} was by far the largest potential electron sink in the groundwater (e^- meq/L); however, SO_4^{2-} was only partially reduced in both stages, although the characteristic odor of H_2S could be detected. Re-oxygenation of the effluent from the lead to the lag MBfR led to re-oxidation of H_2S to SO_4^{2-}, a situation that I discuss further in the microbial ecology section.

Figure 5.2 presents the calculated relative percentages of H_2 consumed for each electron acceptor for the two-stage MBfRs. In the lead MBfRs, the reduction of NO_3^- plus O_2 consumed an average of 41%±8.7% of the H_2 flux in MR1 and 58%±3% in MR2. By lowering the H_2 pressure, SO_4^{2-} reduction decreased from an average of 51%±10% of the H_2 flux in MR1 to an average of 32%±3% in MR2. With SO_4^{2-} reduction lessened in the lead MBfR (MR2), the H_2 uptake from ClO_4^- reduction increased from an average of 7%±1.5% for MR1 to 10%±0.03% for MR2, and the ClO_4^- concentration was lower in the lead MBfR effluent MR2 than MR1. This improvement to ClO_4^- reduction supports previous evidence that significant SO_4^{2-} reduction rates are detrimental for achieving complete ClO_4^- reduction (Ontiveros-Valencia et al., 2013b). Despite the unusually high ClO_4^- concentration in the groundwater, H_2 consumption for ClO_4^- reduction was the smallest electron sink in MR1 and MR2, since the water contained three other acceptors.

In the lag MBfRs, O_2 respiration was the largest sink for electrons (an average of 77%±9.7% of the total H_2 flux in Pol1 and 60%±9.4% in Pol2), and it was followed by SO_4^{2-} reduction (an average of 22%±9.8% and 40%±9.4% of the total H_2 flux in Pol1 and Pol2, respectively). The low-permeability fibers used in the lag MBfR helped reduce SO_4^{2-} reduction; however, increasing the H_2 pressure in Pol2 led to greater H_2 consumption by SO_4^- reduction. ClO_4^- reduction in the lag MBfR used <1% of the total H_2 flux, but the ClO_4^- concentration was driven to below the detection limit because SO_4^{2-} reduction was controlled in the lag MBfR by the combination of re-oxygenation between the two MBfRs and the low-permeability fibers.

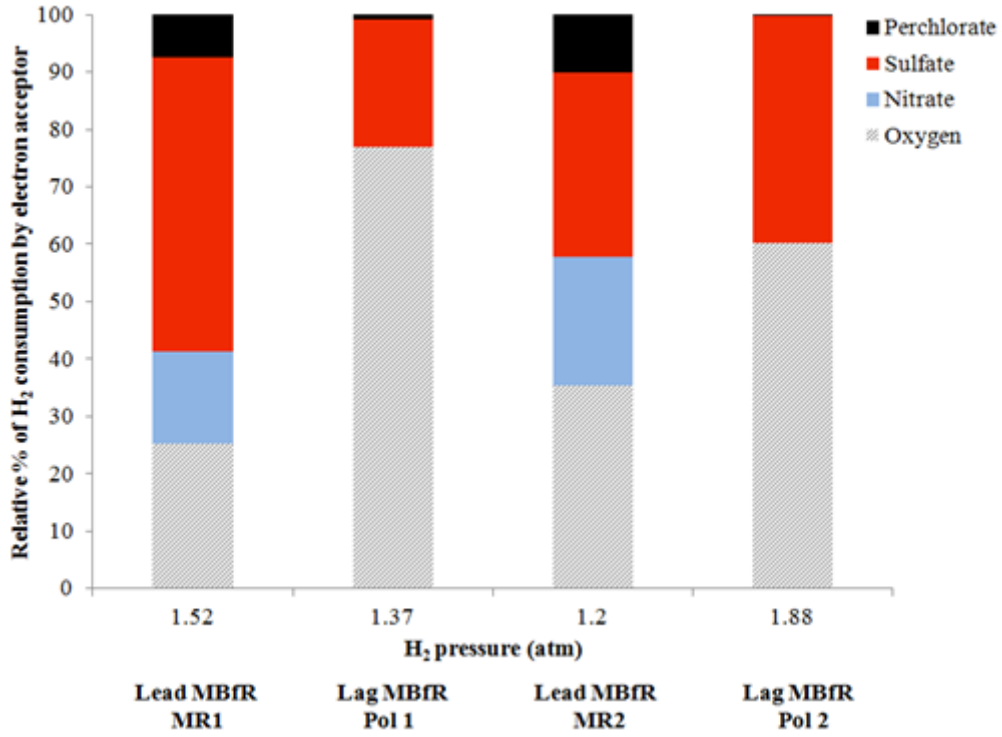

Figure 5.2 Relative amounts of H_2 consumption for the two-stage MBfR. NO_3^- reduction occurred only in the lead MBfRs (MR1 and MR2). The relative amounts were calculated by accounting the H_2 uptake by each microbial respiration process from the total experimental H_2 flux, which was obtained as described elsewhere (Ontiveros-Valencia et al., 2012).

Abundances of microbial groups by functional gene analysis

Figure 5.3 shows the electron fluxes as g H_2/m^2 day for all acceptors, along with the qPCR results in cells/cm^2 for both steady states and MBfRs. In both MBfRs, the biomass distribution followed DB > SRB > PRB, and it corresponded to the trend of the electron-acceptor flux: $O_2 + NO_3^- > SO_4^{2-} > ClO_4^-$. Despite the relatively low NO_3^- concentration in the groundwater (Table 5.3) and low H_2 demand for denitrification (Figure 5.2), DB had the largest biomass fraction according to qPCR results. DB roughly corresponded with the $NO_3^- + O_2$ fluxes in the lead-MBfR and with the O_2 flux in the lag-MBfR. This confirms that DB was reducing NO_3^- and O_2, a normal situation (Ontiveros-

Valencia et al., 2013b). In the lag MBfR, PRB were significantly lower than DB and SRB, and low abundances of PRB matched the low ratio ClO_4^- flux to O_2 and SO_4^{2-} fluxes.

The H_2 pressure (an operational parameter) and the reactor design (i.e., membrane type) showed direct connection to the microbial community structure. Regarding the operational parameter, the lower H_2 pressure in the lead MBfR steady state MR2, compared to in steady state MR1, reduced the total bacteria; however, the fraction of PRB for the steady state with lower H_2 pressure (MR2) was higher than for the steady state with higher H_2 pressure (MR1) (Figure 5.3). A similar trend is observed in the lag MBfRs: The total biomass was lower for steady state Pol1 (reduced H_2 pressure) than for Pol2 (increased H_2 pressure). Also, the lower H_2 pressure in lead MR2 (versus MR1) led to a higher ClO_4^- removal percentage and a lower SO_4^{2-} conversion. Hence, managing H_2 availability was critical for improving the reactor's performance in terms of ClO_4^- reductions, and it corresponded to lessened competition from SRB.

Considering the membrane type and due to the high H_2 delivery capacity by the MR fiber, the lead MBfRs showed significantly higher abundances of SRB than the lag MBfRs. The SO_4^{2-} reduction flux in the lag MBfRs was not larger than 0.02 g H_2/m^2-day, and this correlated with complete ClO_4^- reduction and fewer SRB than in the lead MBfRs, which had higher SO_4^{2-} reduction fluxes. This verified that the strategy of using the less-permeable fiber in the lag MBfR was successful to complete ClO_4^- reduction while minimizing SO_4^{2-} reduction.

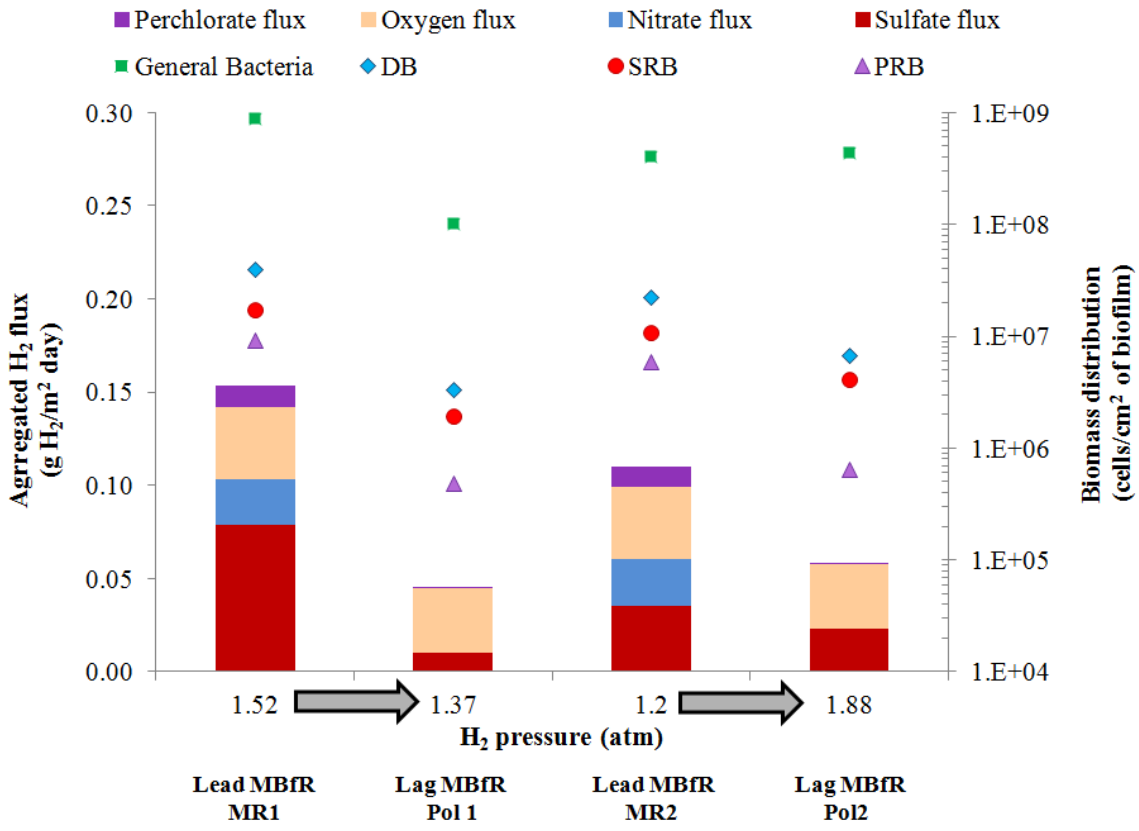

Figure 5.3 Abundances of DB, SRB, and PRB in lead and lag MBfRs, along with the experimental H_2 fluxes by electron acceptor. The results are shown for the two tested SSs and both MBfRs. The lead MBfRs had MR = Mitsubishi-Rayon fibers, and the lag MBfRs had Pol = polypropylene fibers.

As seen in Table 5.2 the SO_4^{2-} electron acceptor loadings were similar between the lead and lag MBfRs, the ClO_4^- electron-acceptor loadings were significantly lower for the lag MBfRs than for the lead MBfRs. Nevertheless, the biofilm composition of the lag MBfRs showed that PRB, although at lower abundances, remained in the biofilm. Re-oxygenation between the stages likely supported PRB in the lag MBfRs (Nerenberg and Rittmann, 2004). Thus, using the lower-permeability polypropylene fibers and re-oxygenation between stages were good strategies to control the growth of SRB without

compromising ClO_4^- reduction when SO_4^{2-} was potentially a much larger electron sink than ClO_4^-.

Framing the microbial community structure in the biofilm of the lead and lag MBfRs

Figure 5.4 shows the results of the unweighted (i.e., based on the presence or absence of microbial phylotypes) UniFrac analysis for an overall community comparison. All biofilm samples from the lead-MBfR formed a cluster (marked in black), while all biofilm samples from the lag-MBfR formed another cluster (marked in gray). Hence, the overall community was dramatically affected by the electron-acceptor surface loadings and donor availability in each MBfR. Ontiveros-Valencia et al. (2013a) demonstrated how H_2 availability and electron-acceptor surface loadings acted as driving forces in denitrifying and SO_4^{2-}-reducing biofilms. The results in Figure 5.4 verify that the microbial community structure in the biofilm was defined by these driving forces.

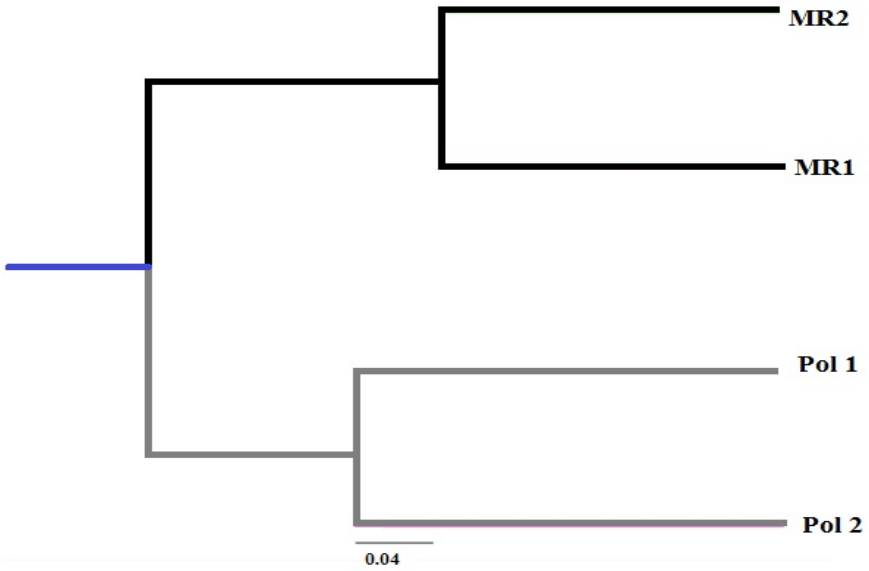

Figure 5.4 Clustering based on the unweighted UniFrac analyses for the two-stage MBfR. The branch length represents the distance between biofilm samples in UniFrac units, as indicated by the scale bar. H_2 pressures: MR1= 1.52 atm, MR2= 1.2 atm, Pol1= 1.37 atm, and Pol2= 1.88 atm.

I performed PCoA with the sequences obtained for all biofilm samples. Figure 5.5 shows the unweighted PCoA. All the samples from the lead MBfR (MR1 and MR2) grouped together, having relatively low values of PC1. This highlights how the microbial community structure of the biofilm is framed according to the electron acceptor loading and H_2 delivery capacity.

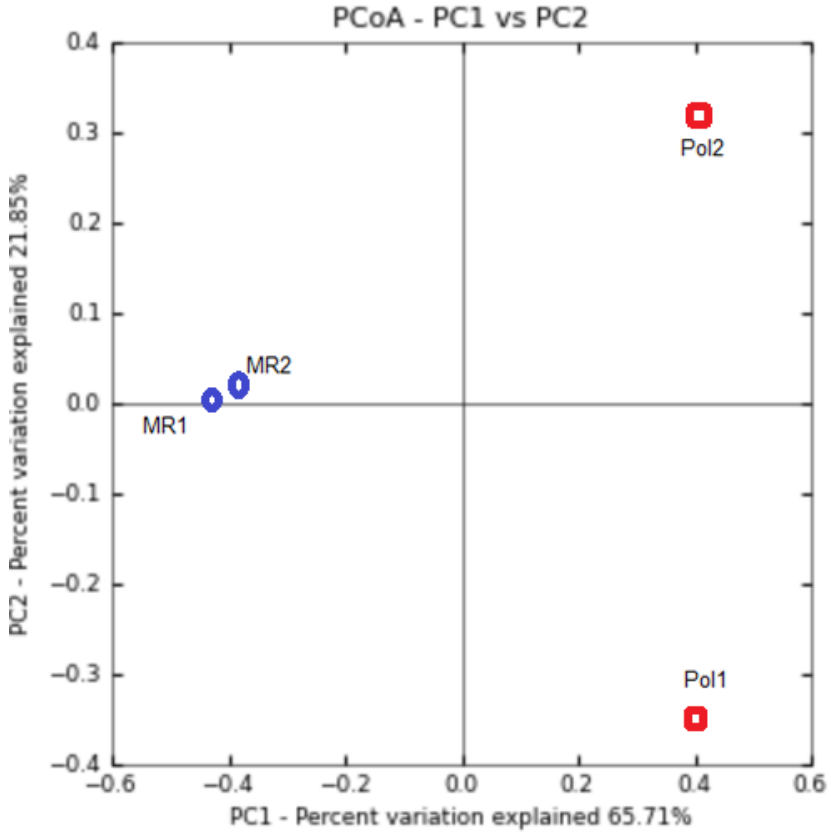

Figure 5.5 PCoA based on the unweighted UniFrac analyses for the two-stage MBfR. PC1 and PC2 axes represent ~66% and 22% of the variance within the microbial community. H_2 pressures: MR1= 1.52 atm, MR2= 1.2 atm, Pol1= 1.37 atm, and Pol2= 1.88 atm.

Microbial phylotypes relevant to community function and structure in the lead and lag-MBfR

Figure 5.6 shows the taxonomy of the biofilm communities in the lead and lag MBfRs classified at the order level. SRB-related phylotypes were represented by members of *Desulfovibrionales* and *Desulfobacterales* orders. *Desulfovibrionales* were important in the lead MBfR biofilms, while *Desulfobacterales* were present in the lag MBfR biofilms. The abundance of different SRB phylotypes in the microbial communities of the lead and lag MBfRs might be related to the kinetics of each SRB, as shown by Sorokin et al. (2003) with sulfur-oxidizing microbes. In particular, *Desulfovibrionales* may be r-strategists, ecotypes capable of growing rapidly when supplied ample electron donor, condition provided with the MR membranes. In contrast, *Desulfobacterales* may be K-strategists, ecotypes capable of thriving despite low availability of electron donor, more the case with the Pol membranes. These trends need to be verified by future studies.

Of special interest is the presence of *Thiobacteriales*, which are sulfur-oxidizing bacteria capable of coupling oxidation of H_2S or S^0 to SO_4^{2-} with reduction of NO_3^- to N_2 (Shao et al., 2010) or ClO_4^- to Cl^- and O_2 (Boles et al., 2012). *Thiobacteriales* were notably more abundant in the lead MBfRs than in the lag MBfRs. This trend correlates well with the rates of SO_4^{2-} reduction (Figure 5.3), a situation that ought to have provided more H_2S for *Thiobacteriales* and led to sulfur cycling inside the biofilm. *Ignavibacteriales*, green sulfur-oxidizing bacteria capable of using H_2S as an electron donor to produce S^0 or SO_4^{2-}, showed a similar trend to *Thiobacteriales*.

PRB were represented by phylotypes most closely related to *Rhodocyclales,* which were largely dominant in the lead and lag MBfRs. *Rhodocyclales* also likely reduced NO_3^- and O_2, since they are highly versatile chemolithoautotrophic bacteria (Ontiveros-Valencia et al., 2013a). Some representative examples are *Dechloromonas*, *Zooglea,* and *Methyloversatilis*; the latter two were found previously in H_2-fed biofilms (Ontiveros-Valencia et al., 2013a). Another phylotype containing microorganisms able to respire NO_3^-, O_2, and ClO_4^- was *Burkholderiales,* which was present at relatively low abundances in both MBfRs.

The relative abundance of *Bacteroidales* was significant, especially under favorable SO_4^{2-}-reducing conditions (MR1 and MR2) (Ontiveros-Valencia et al., 2013a). Another significant microbial phylotype found in the biofilm samples of the lead MBfR was *Spirochaetales*, a known acetogen that can use either fermentable substrates such as mono and di-saccharides (likely available in SMP) or H_2/CO_2 (Breznak, 2002; Pester and Brune, 2006) to produce acetate (Graber and Breznak, 2004). Hence, synergistic relationships among SRB (especially *Desulfovibrionales* in the lead MBfR), *Spirochaetales*, and *Bacteroidales* seem to have been important for SO_4^{2-} reduction in the H_2-fed biofilms.

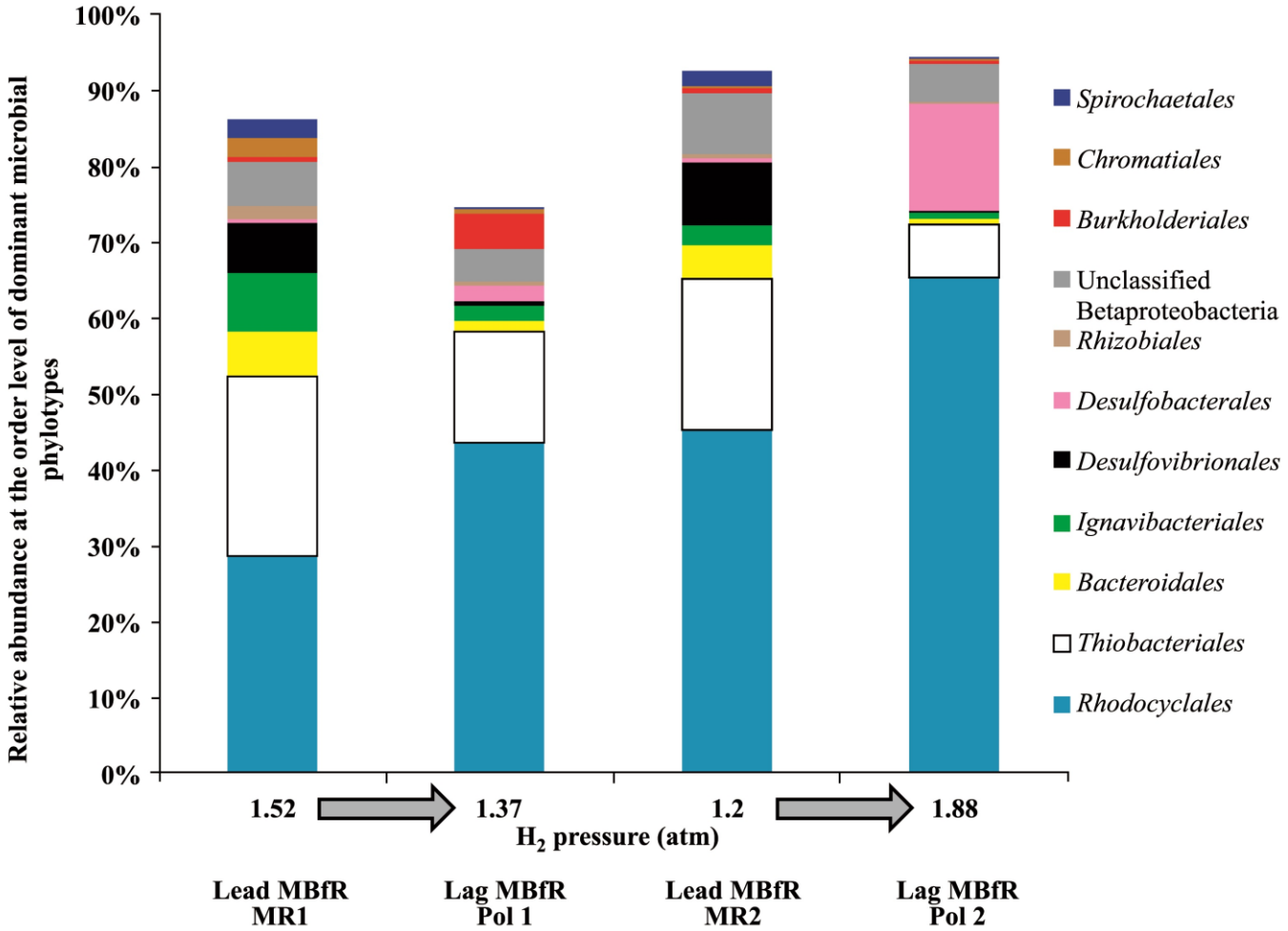

Figure 5.6 Microbial community structure in lead and lag MBfRs as a function of the electron donor availability (H_2 pressure tested). The sum does not add up to 100% in all cases because minor phylotypes (< 1%) are not shown.

5.4 Conclusions

I demonstrated that it was possible to reduce ClO_4^- to below the detection limit in a two-stage MBfR setup, even though the influent ClO_4^- concentration was exceptionally high and the onset of SO_4^{2-} reduction was a high risk. Due to the high concentration of SO_4^{2-} in the groundwater (~60 mg/L), SO_4^{2-} reduction could not be prevented, and, in fact, SRB were more abundant than PRB. Nevertheless, SO_4^{2-} reduction could be minimized sufficiently by lowering the H_2 pressure, using a membrane with lower H_2 permeability in the lag MBfR, and maintaining significant H_2 uptake for O_2 respiration in the lag MBfR by re-oxygenating the influent to the lag MBfR.

The practical strategies to achieve complete ClO_4^- reduction managed the microbial communities in ways that led to achieving the water-reclamation goal. For example, the biofilm communities of the lead and lag MBfRs were significantly different due to the distinct acceptor loadings. A clear differentiation was the lower abundance of SRB in the lag MBfRs than in the lead MBfRs, showing that the competition between SRB and PRB lessened by using a less-H_2 permeable membrane in the lag MBfRs. Because the ClO_4^- and NO_3^- acceptor loadings were small for the lag MBfRs, re-oxygenation between the stages was beneficial to enrich for DB, which ultimately can respire ClO_4^-, and to favor PRB in their competitive relationship with SRB.

Pyrosequencing revealed that the SRB phylotypes in the lag MBfRs (i.e., *Desulfobacterales*) differed from those in the lead MBfRs (i.e., *Desulfovibrionales*). Furthermore, this deeper analysis of the community structure revealed the presence of *Thiobacteriales* and *Ignavibacteriales*; H_2S or S^0 oxidizers, implying that sulfur cycling was taking place in the lead reactors. PRB-phylotypes were represented by

Rhodocyclales, which were enriched when SO_4^{2-} reduction was controlled. I exemplified successful ClO_4^- bioremediation as long as the ecological interactions between SRB and PRB were effectively managed.

Chapter 6

PYROSEQUENCING ANALYSIS YIELDS COMPREHENSIVE ASSESSMENT OF MICROBIAL COMMUNITIES IN PILOT TWO-STAGE MEMBRANE BIOFILM REACTORS

This chapter has been submitted in an altered format for publication (Ontiveros-Valencia et al., 2014b).

6.1 Introduction

Thorough Chapters 2-5, I researched ecological interactions among DB, SRB, and PRB in bench scale MBfRs. In this chapter, I deeply examined the microbial community structure and function of pilot two-stage MBfRs by high throughput pyrosequencing. The practical implications of this work constitute effective means to operate the pilot and full scale MBfRs to achieve the NO_3^- and ClO_4^- remediation goals.

Recently, Evans et al. (2013) documented NO_3^- and ClO_4^- reductions in pilot MBfRs. Contrary to the pollution levels of the groundwater remediated in Chapters 4 and 5, the groundwater remediated by the pilot MBfRs had the typical water contamination scenario in which NO_3^- is most abundant than ClO_4^-. The ratio of these oxidized contaminants was ~76 g N: 1 g ClO_4^-. Hence, the researchers set up a two-stage MBfR: the lead MBfR treated the raw groundwater and performed the bulk of denitrification, while the lag MBfR received the effluent from the lead MBfR and completed the treatment for NO_3^- and ClO_4^-. Even though H_2 availability was not limiting and ClO_4^- removal was typically > 94%, the two-stage pilot MBfR could not consistently drive the ClO_4^- concentrations to below the detection limit of 4 μg/L (Evans et al., 2013).

In an effort to understand the pilot MBfR's performance, Zhao et al. (2014) assessed the microbial community structure of the pilot reactors using qPCR targeting characteristic reductases. DB (determined by the *nirK* and *nirS* genes) were the most abundant microbial group; however, SRB (quantified by the *dsrA* gene) became dominant and may have outnumbered DB in the pilot MBfRs when the NO_3^- + O_2 loading was low, below 0.3 g H_2/m^2 day (Zhao et al., 2014). PRB (quantified by the *pcrA* gene) were the smallest microbial fraction and were affected when SRB became important, a finding consistent with my previous bench-scale study in Chapter 4.

In Chapter 5 and contrasting the pilot results, I was able to achieve complete ClO_4^- reduction in a two-stage bench-scale MBfR, even though the ClO_4^- concentration was unusually high (~4000 μg/L) and SO_4^{2-} was amply present (55 mg/L). I attributed the successful ClO_4^- remediation to an effective management of the microbial ecology of the reactors so that SO_4^{2-} reduction was minimized, especially in the lag MBfR. I effectively suppressed SRB in the lag MBfR by two strategies: 1) re-oxygenating the influent to the lag MBfR to increase the total-acceptor loading, and 2) lowering the H_2 availability by either decreasing the H_2 pressure or by using a less-H_2 permeable membrane. Neither strategy was followed with the pilot two-stage MBfR system: Re-oxygenation of the effluent from the lead MBfRs was not possible with the pilot configuration, and the pilot-MBfRs were mostly run with excess H_2 availability to encourage ClO_4^- reduction (Evans et al., 2013).

Zhao et al. (2014) provided a broad view of the "primary" respiratory groups (i.e., DB, PRB, and SRB) in the pilot MBfRs corresponding to the supplied electron acceptors. In this work, I employ high-throughput pyrosequencing to gain a deeper understanding of

the microbial community structure, including more insight into the phylotypes that constitute the primary respiratory groups present when NO_3^-, ClO_4^-, and SO_4^{2-} are the electron acceptors and a view of other members within the biofilm. In particular, I use UniFrac and PCoA (Lozupone and Knight, 2005; Lozupone et al., 2006) to demonstrate that distinctly different communities developed in the biofilm when the acceptor-loading rate was decreased significantly. Furthermore, I explore how decreased acceptor loading led to shifts within the primary members and the development of important other members (e.g., heterotrophs and sulfur-oxidizing bacteria) in the community. While Zhao et al. (2014), using qPCR, provided an analysis of community structure according to the primary respiratory groups, my findings discriminate which conditions significantly altered the community structure, making the biofilm more diverse and causing shifts within and outside the primary groups.

6.2 Materials and Methods

MBfR configuration and performance

Detailed information about the pilot-MBfRs configuration is given by Evans et al. (2013) and Zhao et al. (2014). In short, the two-stage MBfR was composed of two 500-gallon (1890-L) vessels containing 4 MBfR modules with membrane surface area of 144 m^2 per module. The pilots were set up to treat a site historically used for munitions and explosives manufacture and surroundings agricultural fields. Hence, the oxidized contaminants in the groundwater were NO_3^- at 8-9 mg N/L and ClO_4^{2-} at 160-200 μg/L. The influent also contained O_2 at ~8 mg/L and SO_4^{2-} at ~22 mg/L. The MBfR positions were switched every 3 days to make the biofilm development similar in both MBfRs.

The H_2 pressure and influent flow rate were adjusted according to the conditions in Table 6.1. Adjustment of the influent flow rate led to a proportional change in the total electron-acceptor surface loading: Conditions 3 and 4 had significantly lower total electron acceptor loadings than did Conditions 1 and 2. The measurements of NO_3^- and SO_4^{2-} (US EPA method 300) and ClO_4^- (US EPA 314) were done on a regular basis for lead and lag MBfR according to Evans et al. (2013). O_2 was measured by a dissolved-oxygen field kit (Evans et al., 2013). The lead and lag MBfRs also were equipped with a set of side reactors for taking biofilm samples without disturbing the biofilm in the modules (Evans et al., 2013; Zhao et al., 2014).

The lead MBfRs were responsible for ~99% of the O_2 respiration, 70-90% denitrification, and a small loss of ClO_4^- (Evans et al., 2013; Zhao et al., 2014). In the lead MBfRs, the $NO_3^- + O_2$ flux was greater than ~ 0.3 g H_2/m^2-day (Zhao et al., 2014), which completely suppressed SO_4^{2-} reduction and is consistent with the bench-scale results of Ontiveros-Valencia et al. (2012). Therefore, NO_3^- and SO_4^{2-} were the dominant electron acceptors entering the lag MBfR, and the total acceptor surface loading to the lag MBfR was much lower than for the lead MBfR (Table 6.1). Although the objective of reducing the flow rate and total acceptor loading for Conditions 3 and 4 was to enhance ClO_4^- removal in the lag MBfR, its major impact was to favor SO_4^{2-} reduction, an undesired outcome that led to lower ClO_4^- removal fluxes in the lag MBfR (Zhao et al., 2014).

Biofilm microbial ecology by pyrosequencing analysis

At the end of each Condition (Table 6.1), side reactors were sent in ice containers to the Swette Center for Environmental Biotechnology for microbial community analysis. The samples arrived within 24 hours and were processed according to Zhao et al. (2014) for DNA extraction. DNA samples were stored at -80°C until shipping for 454 pyrosequencing. DNA samples for 454 pyrosequencing were sent to the Molecular Research DNA lab (Austin, Texas, USA), which performed amplicon pyrosequencing using a standard Roche 454/GS-FLX Titanium (Sun et al., 2011). The Bacteria domain was targeted by selecting the V6 and V7 regions of the 16S rRNA gene with primers 939F (5'-TTGACGGGGGCCCGCAC-3') and 1492R (5'TACCTTGTTACGACTT-3') (Ontiveros-Valencia et al., 2013a). I processed the raw data using QIIME 1.7.0 suite (Caporaso et al., 2010a) and removed sequences having fewer than 250 bps, homopolymers of more than 6 bps, primer mismatches, or an average quality score lower than 25. I picked the OTUs using the Greengenes 16S rDNA database with *uclust* (Edgar, 2010) based on ≥ 97% identity, removed OTUs that contain less than two sequences (singletons) from the analysis, and aligned the representative sequence of each OTU to the Greengenes Database using *PyNast* (DeSantis et al., 2006; Caporaso et al., 2010b). Potentially chimeric sequences were identified by using ChimeraSlayer (Haas et al., 2011), and a python script in QIIME was employed to remove the chimeric sequences. I assigned taxonomy to OTUs with BLAST using the SILVA database (Pruesse et al., 2007) and constructed Newick-formatted phylogenetic trees using FastTree (Price et al., 2009).

Table 6.1 Four Conditions identified H_2 availability (controlled by H_2 pressure) and electron-acceptor surface loadings (adjusted by influent flow rate) for pilot lead and lag MBfRs.

Condition	Flow rate m^3/d	H_2 pressure atm		NO_3^--N surface loading g H_2/m^2-d		O_2 surface loading g H_2/m^2-d		SO_4^{2-} surface loading g H_2/m^2-d		ClO_4^- surface loading g H_2/m^2-d		Total electron acceptor surface loading g H_2/m^2 day	
		lead	lag	lead	lag	lead	Lag	lead	lag	lead	lag	lead	lag
1	65	2.2	1.8	0.41	0.13	0.15	0.002	0.22	0.22	0.002	0.002	0.78	0.36
2	98	2.8	2.3	0.66	0.17	0.23	0.006	0.33	0.33	0.003	0.002	1.22	0.51
3	44	2.2	2	0.37	0.03	0.10	0.002	0.18	0.18	0.002	0.0004	0.65	0.22
4	33	2.1	1.6	0.23	0.02	0.08	0.0004	0.11	0.11	0.001	0.0002	0.41	0.13

I calculated the electron acceptor loading rates according to:

$$Loading = \frac{Q \times (S^{\circ})}{A} \qquad (eq. 6.1)$$

where Q = volumetric flow rate (L/day), A = membrane surface area (m^2), and S° is the influent concentration (g/L) for an electron acceptor. Each electron acceptor loading value was normalized to g H_2/m^2 day based on stoichiometric relationships described elsewhere (Ontiveros-Valencia et al., 2012; Tang et al., 2012a; Zhao et al., 2013). Total electron-acceptor loading was calculated as the sum of the loadings for O_2, NO_3^-, ClO_4^-, and SO_4^{2-}. The oversupply of H_2 was computed as the maximum delivery capacity of the polypropylene fibers at a given pressure (Tang et al., 2012d) minus the experimental total H_2 flux (Zhao et al., 2014).

For the purpose of eliminating heterogeneity related to having different numbers of sequences among the samples, I sub-sampled the OTU table by randomly selecting ten different times the lowest number of sequences (6800) found among the samples. I then generated PCoA plots and UPGMAplots (Lozupone et al., 2006) using jack-knifed beta diversity that subsampled each sample at a depth of the lowest number of sequences found among the samples.

I estimated the OTU richness by calculating Chao1 (Hughes et al., 2001), which determines the asymptote on an accumulative curve, predicting how many OTUs would be present if a high number of sequences had been collected, and the phylogenetic relationships by using PD (Faith, 1992), which estimates the cumulative branch lengths from random OTUs. To evaluate the microbial species diversity and evenness, I computed the Shannon (1948) and Simpson (1949) indices. A higher value for the Shannon index indicates greater microbial diversity, while a value for the Simpson metric near one shows an even distribution of bacterial groups within the sample. Sequence data sets are available at NCBI/ SRA under study with accession number SRP038958.

6.3 Results and Discussion

Microbial diversity and structure affected by operational conditions

Table 6.2 reports the Chao1, Shannon, Simpson, and PD metrics for the four conditions listed in Table 6.1. Chao1, Shannon, and PD values show that the microbial diversity of biofilm samples from Conditions 3 and 4, which had an ample H_2 supply and low acceptor loading (Table 6.1), was greater than from Conditions 1 and 2, which had a lower H_2 supply compared to the higher acceptor loading. Thus, higher diversity

correlated with an ample supply of electron donor and a significantly decreased total acceptor loading (Table 6.1). This situation allowed the growth of SRB at the expense of DB and PRB (Zhao et al., 2014). Consistent with the Chao1 results and based on the Simpson index, biofilm samples from Conditions 3 and 4 were more evenly distributed than those in Conditions 1 and 2.

Table 6.2 Alpha diversity metrics for the biofilm samples of the pilot lead and lag MBfRs for the four conditions

	1 Lead	**1 Lag**	**2 Lead**	**2 Lag**	**3 Lead**	**3 Lag**	**4 Lead**	**4 Lag**
Chao1	769± 1.5	780± 2.4	992± 2.2	1271± 1.9	1327± 3.3	1387± 5	1259± 5.3	1776± 6.3
Shannon	5.44± 0.002	5.17± 0.002	6.48± 0.002	6.77± 0.002	6.75± 0.001	7.84± 0.002	6.62± 0.002	6.85± 0.001
Simpson	0.92± 0.0001	0.88± 0.0001	0.94± 0.0001	0.94± 0.0001	0.94± 0.0001	0.98	0.95± 0.0001	0.95
PD	11.7	13.5	17.4	22.9	20.2	26.9	23.1	21.3

Figure 6.1 shows the unweighted UniFrac analysis of the biofilm samples, which is based on the presence or absence of all the phylotypes within a sample. The biofilm samples with high acceptor loading (Conditions 1 and 2) clearly formed a cluster (blue branch) distinct from the cluster of Conditions 3 and 4 (red branch). Particularly for Conditions 1 and 2, the lead and lag biofilms were not significantly different due to the

regular switching of positions, as pointed by Zhao et al. (2014). Thus, the large changes in acceptor loading between Conditions 2 and 3 led to very different microbial communities.

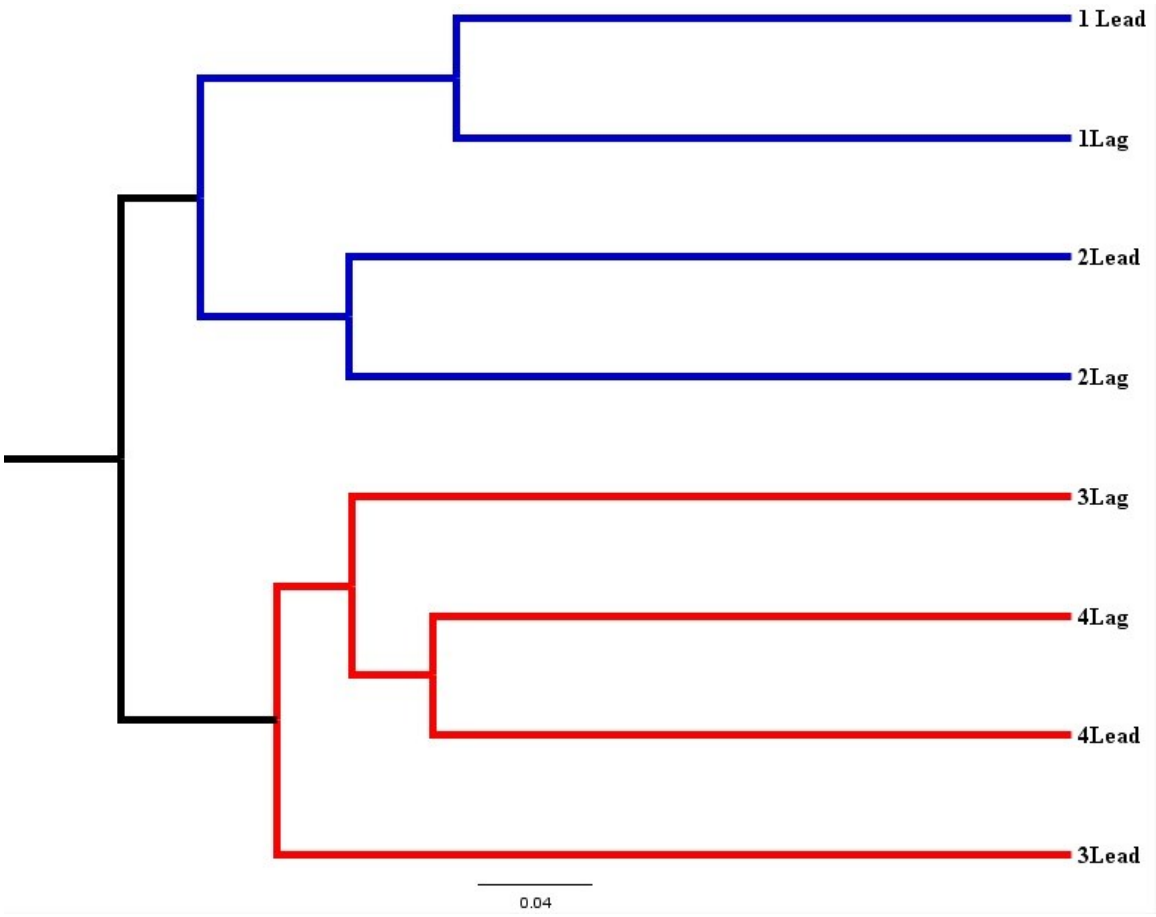

Figure 6.1 Clustering based on the unweighted UniFrac analyses for the pilot two-stage MBfR. The branch length represents the distance between biofilm samples in UniFrac units, as indicated by the scale bar. The labels on each branch indicate the biofilm sample of either lead or lag MBfR at the four conditions applied to the reactors. The blue branch correspond to the reactors operated at high electron acceptor surface loadings (Conditions 1 and 2), while the red branch reflect the microbial community performing under low total electron acceptor surface loading (Conditions 3 and 4).

Figure 6.2 presents the unweighted PCoA plot, which reinforces the clustering found with the UniFrac analysis. The biofilm communities of Conditions 1 and 2 were close to each other along the PC1 vector, while those biofilm samples of Conditions 3 and 4 were distant. In an attempt to differentiate the driving force for the PC1 vector, I prepared the accompanying table summarizing selected operational parameters for each condition. The accompanying table shows that Conditions 3 and 4 had severely decreased acceptor loadings and that SO_4^{2-} reduction became more important. SO_4^{2-} reduction resulted from a combination of the ample oversupply of H_2 (Table 6.1) and the longer HRTs, which lowered loading rates of all acceptors. The PC1 vector correlates with increased SO_4^{2-} reduction, particularly from Condition 2 to Condition 3. Hence, the microbial community structure was substantially modified when SO_4^{2-} reduction became a more important electron sink, a trend also noted by Ontiveros-Valencia et al. (2013a). Condition 2 was different from Conditions 1, 3, and 4 along the PC2 vector. This trend is most likely explained by the substantially higher ClO_4^- flux for Condition 2, which is illustrated in the accompanying table in Figure 6.2.

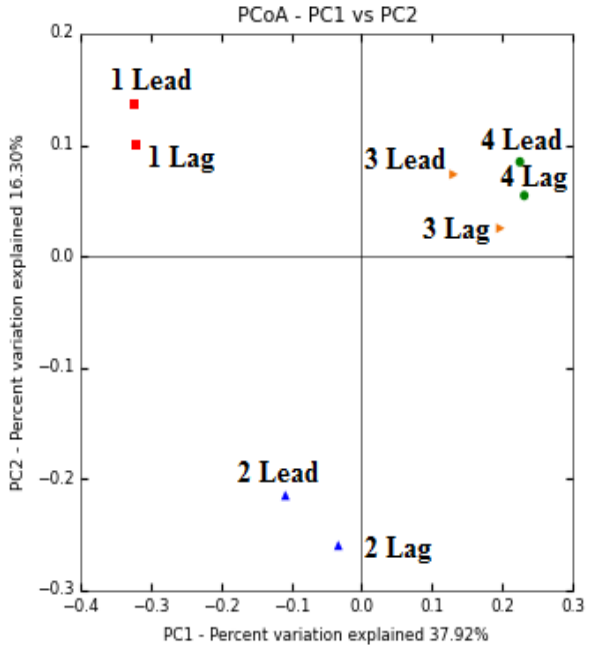

Condition	Biofilm development	HRT	Average electron acceptor loading	Sulfate flux g H_2/m^2 day		Perchlorate flux g H_2/m^2 day	
	days	hour	g H_2/m^2 day	Lead	Lag	Lead	Lag
1	60	0.7	0.6	0	0.0006	0	0.0008
2	116	0.5	0.9	0	0.0010	0.0013	0.0018
3	221	1	0.4	0	0.0026	0.0008	0.0006
4	263	1.4	0.3	0	0.0030	0.0007	0.0004

Figure 6.2 PCoA based on the unweighted UniFrac for the pilot two-stage MBfR. The accompanying table shows the parameters driving the microbial community. The average electron acceptor loading was calculated from the lead and lag electron acceptor loadings at each condition (Table 6.1). The lead and lag positions were switched every three days; therefore, an average estimate of the acceptor loading is valuable. The HRT was the same for each reactor regardless of the position.

Taxonomic breakdown and shifts in the microbial community structure

Figure 6.3 synthesizes the taxonomical break down at the order level of the most abundant phylotypes. Consistent with UniFrac and PCoA, the biofilm communities of the lead and lag MBfR were similar for each Condition. The brackets in the legend of Fig. 3 identify the known DB, PRB, SRB, and other types. The groupings show four important trends. First, ~86% of the total taxonomic breakdown was constituted by DB and PRB for Condition 1, but these primary groups decreased for subsequent conditions, being only ~60% by Condition 4. Connecting this community trend to community function, DB and PRB phylotypes (reported by pyrosequencing in Figure 6.3) follow the same trend as the NO_3^-, O_2, and ClO_4^- fluxes (Zhao et al., 2014).

Second, the decrease of DB and PRB was accompanied by the significant increase in SRB, which were augmented from <1% in Condition 1 to ~13% in Condition 4. The SRB trend by pyrosequencing is similar to the SRB trend noted by Zhao et al. (2014) using qPCR; however, the qPCR study found that SRB had become the largest primary group in Condition 4, followed by DB and PRB. It is possible that qPCR overestimated SRB, because some DB harbor *dsrA* gene (Wu et al., 2005). Regardless of the method employed, the key trend is that SRB became important with lower acceptor loading. As noted by Ontiveros-Valencia et al. (2013b), SRB become detrimental to PRB when they are able to occupy the most favorable zones in the biofilm (near the H_2-delivering substratum) (Tang et al., 2012a). Therefore, incomplete ClO_4^- reduction in the lag MBfR can be at least partially attributed to increased competition from SRB.

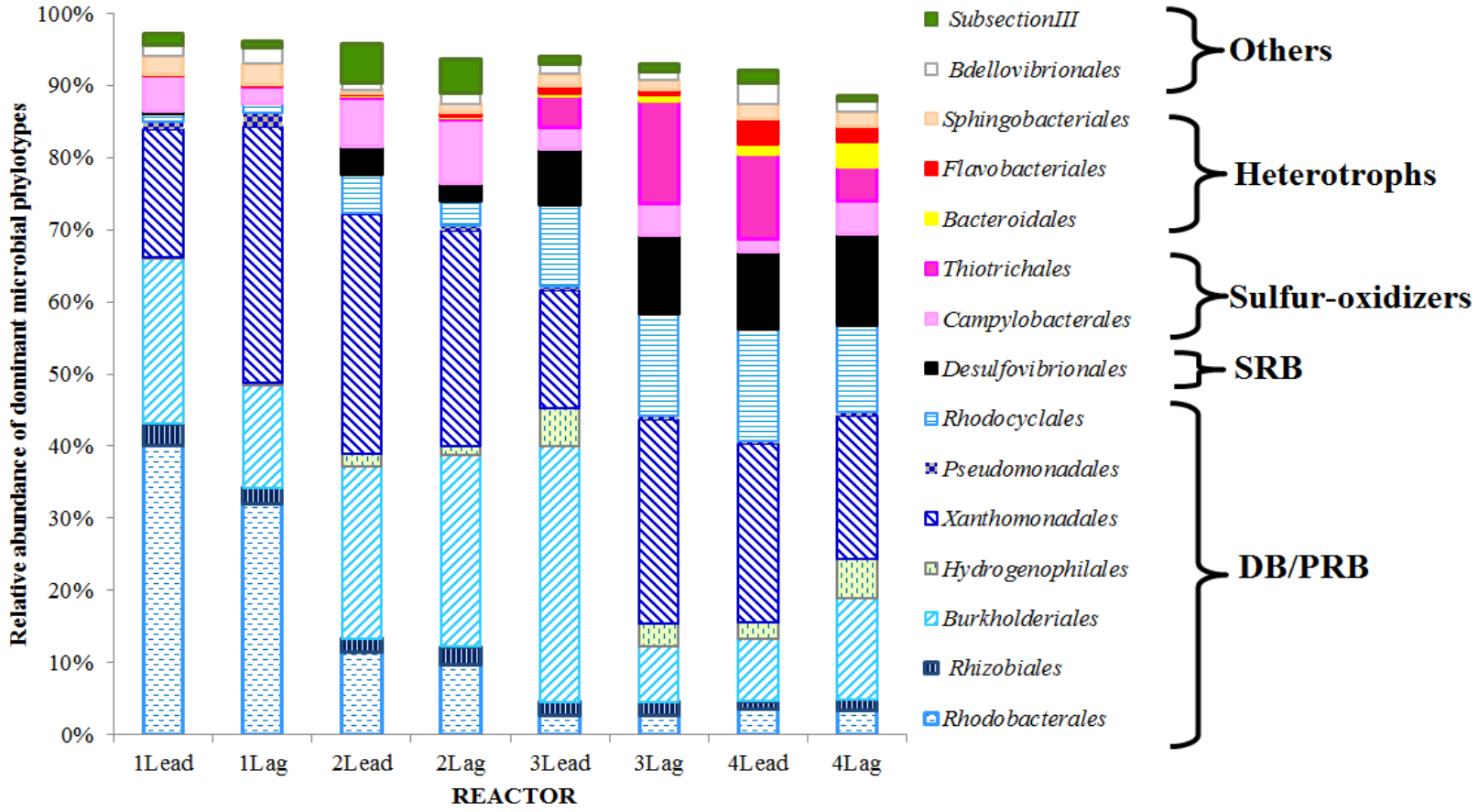

Figure 6.3 Microbial community structure in pilot lead and lag MBfRs at the order level. The sum does not add up to 100% in all cases because phylotypes < 1% are not shown. The brackets in the legend group the orders according to known members of the noted metabolic groups. DB/PRB phylotypes are shown which hatched fills that clearly show a decline from Condition 1 to Condition 4. Some members of the "heterotrophic microorganisms," are capable of denitrification under specific circumnstances, such as when using acetate as electron donor and carbon source (Adav et al., 2010).

Third, with augmented SO_4^{2-} reduction (Conditions 3 and 4), sulfur-oxidizing *Thiotrichales* and the SRB *Desulfovibrionales* were boosted. This combination points towards a cooperative relationship based on active S cycling in which *Thiotrichales* oxidize H_2S produced by SRB while respiring NO_3^- to NH_4^+. Sulfide oxidation by *Thiotrichales* provides additional SO_4^{2-} for SRBs and allow them to grow at higher concentrations than predictable from the one time SO_4^{2-} reduction. Sulfide-oxidizers also were reported in MBfR biofilms by Zhao et al. (2013), who observed abundant *Campylobacteriales* (sulfur-oxidizing bacteria), and by Ontiveros-Valencia et al. (2014), who reported significant presence of *Ignavibacteriales* (green sulfur-oxidizing bacteria) and *Thiobacteriales* (sulfur-oxidizing bacteria) when SO_4^{2-} reduction was favored in bench-scale MBfRs. The differences in the phylotypes of the sulfur-oxidizers observed in the bench- versus pilot-scale MBfRs probably can be attributed to the different inocula in each study. Despite the different inocula, the cooperative relationship between SRB and sulfur-oxidizing bacteria seems to be common once SO_4^{2-} reduction becomes important and seems to have accentuated an ecological advantage for SRB.

Besides sulfur-oxidizers, heterotrophic microorganisms such as *Bacteroidales* and *Flavobacteriales* increased in Conditions 3 and 4. The heterotrophs likely consumed SMPs, whose rate of release increased with high rates of SO_4^{2-} reduction. (Tang et al., 2012a; Ontiveros-Valencia et al., 2013a). Likewise, the relative abundance of "unclassified" bacteria and minor phylotypes (microbial groups at <1% abundance) (not shown in Figure 3) went from an average ~3% in Condition 1 to ~8% in Condition 4. The upswing of heterotrophs, unclassified bacteria, and minor phylotypes was the foundation for the increase in the microbial diversity with decreased acceptor loading

(Table 6.2). The greater abundance of other groups and SRB certainly imposed more competition for space in the biofilm, forcing PRB to less favorable positions in the biofilm (Tang et al., 2012a; Ontiveros Valencia et al., 2013b). Recently, Martin et al. (2013a) employed modeling to explain how increased detachment hindered the MBfR performance. Thus, increasing diversity in the biofilm was correlated to poorer performance for ClO_4^- reduction.

Fourth, the DB and PRB groups showed important shifts with acceptor loading. In Conditions 1 and 2, *Rhodobacterales* were dominant; however, the most abundant DB and PRB phylotypes shifted to *Xanthomonadales* and *Rhodocyclales* in Conditions 3 and 4. Also, while the DB and PRB phylotype *Rhizobiales* remained relatively constant across conditions, the phylotype *Hydrogenophilales* increased in Conditions 3 and 4. Lastly, phylotype *Burkholderiales* decreased abruptly while phylotype *Pseudomonadales* decreased slightly. These substantial shifts in the DB and PRB support that the biofilm communities were functionally redundant, which allowed different phylotypes to gain or lose prominence as acceptor loading changed without affecting denitrification performance .

Figure 6.4 identifies the most abundant microbial phylotypes at the genus level. *Aquimonas*, microbes capable of respiring NO_3^- and ClO_4^-, was common to all biofilm samples and showed the greatest resilience by remaining in the biofilm regardless of competition. In contrast, *Rhodobacter,* a photoautotrophic microorganism capable of reducing NO_3^- by a periplasmic NO_3^- reductase (Reyes et al., 1998), was most specific to Condition 1 and declined dramatically in Conditions 3 and 4. Species *Rhodobacter capsulatus* and *Rhodobacter sphaeroides* can reduce ClO_3^- to ClO_2^-; however, no growth

was associated with this metabolism (Roldan et al., 1994). It seems that its photoautotrophic nature and inability to grow when reducing ClO_3- to ClO_2^- may have made *Rhodobacter* susceptible to replacement by more resilient DB/PRB phylotypes.

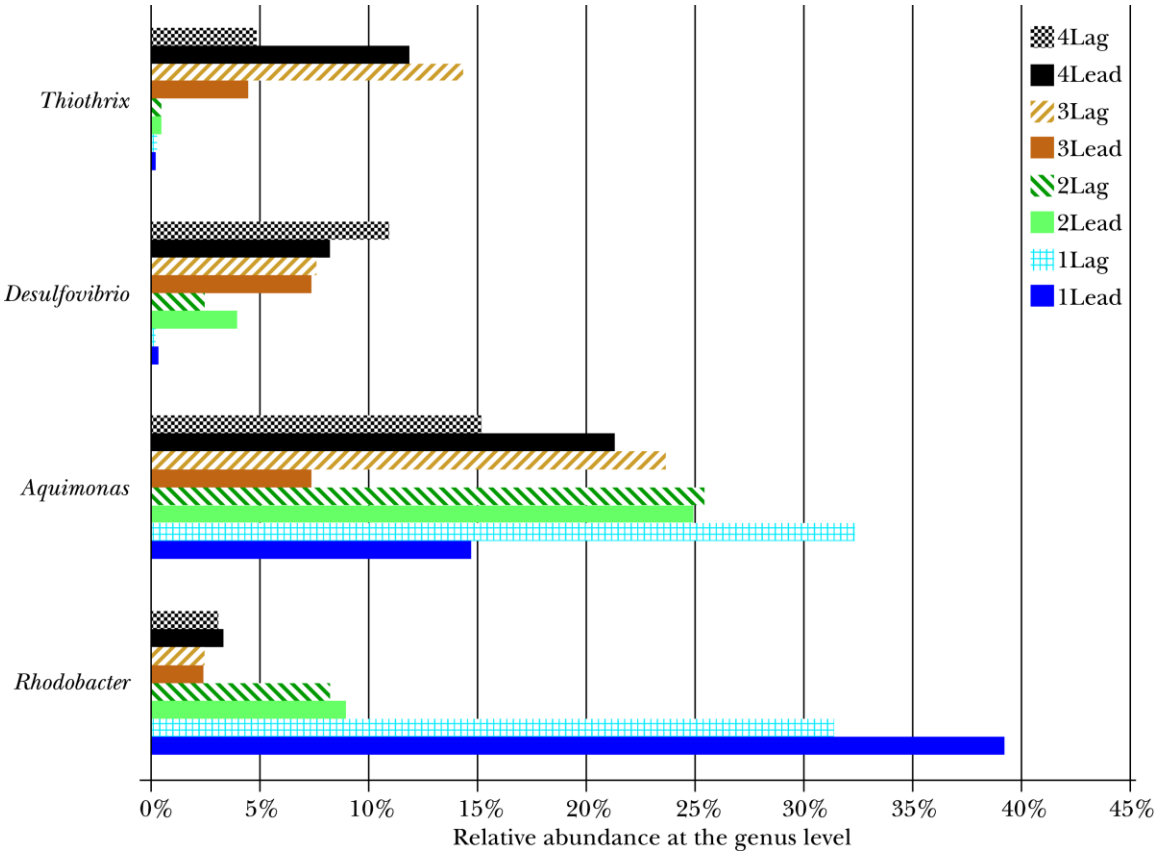

Figure 6.4 Evolution of the 5 most abundant genera in pilot lead and lag MBfRs for the four condition tested.

Desulfovibrio and *Thiothrix,* which appeared in Conditions 3 and 4, seemed to be drivers of the large change in community structure between Conditions 1 and 2 versus 3 and 4. Of practical relevance, *Thiothix* imposes a risk for fouling the membranes due to its filamentous growth (Madigan et al., 2009). *Thiothrix* can accumulate S granules in their interior from the oxidation of H_2S and form rosettes, which are arrangements of

filaments (Williams and Unz, 1985; Williams et al., 1987). Staff operating the pilot MBfRs reported filaments in some biofilms.

6.4 Conclusions

Pyrosequencing allowed me to comprehensively assess the microbial community diversity and structure of pilot two-stage MBfR. UniFrac, PCoA, and microbial diversity metrics helped me understand the main drivers for the shifts in microbial structures. Biofilm communities developed with low total acceptor loading were more diverse and phylogenetic distant from communities with a higher acceptor loading. Primary members (i.e., DB, PRB, and SRB) overall tracked the reduction of the electron acceptors, but showed important shifts with acceptor loading. The DB/PRB phylotype *Rhodobacter* was significantly abundant at high acceptor loading; however, the *Aquimonas* genus was overall the most dominant DB/PRB phylotype in all biofilm samples. *Desulfovibrio* and *Thiothrix* appeared together when SO_4^{2-} reduction was strong, and this corresponded to a slowing of the ClO_4^--reduction rate. Likewise, heterotrophic bacteria became more important with lower acceptor loading. The abundance of SRB and sulfur-oxidizing partners, as well as heterotrophs, likely accentuated competition for space and forced PRB to less favorable positions in the biofilm. Thus, the increase in diversity with low acceptor loading was due to the increases in SRB, sulfur-oxidizers, and heterotrophs, and it correlated with poorer performance in terms of ClO_4^- reduction.

Chapter 7

SUMMARY, CONCLUSIONS, AND RECOMMENDATIONS FOR FUTURE WORK

7.1 Summary

In Chapter 1, I explained how the MBfR can be used to reduce two important oxidized contaminants in water -- NO_3^- and ClO_4^- -- to harmless products. I also pointed out that SO_4^{2-} often is present at the same time. Normally, SO_4^{2-} reduction is an undesired outcome, while NO_3^- and ClO_4^- are the targets for water remediation. Thus, I needed to gain deep understanding on how controllable parameters in the MBfR (i.e., H_2 availability and electron acceptor loading) affect the competitive interactions among the DB, PRB, and SRB so that only the desired bacteria and reactions would be promoted. This was the goal of my research, and Chapters 2 – 6 present a set of experimental studies that allowed me to gain and apply the scientific knowledge I needed to achieve my practical goal.

In Chapters 2 and 3, I systematically studied the ecological interactions between DB and SRB in H_2-fed biofilms. In brief, I operated two MBfRs with either electron-donor limitation (EDvSS) or electron-acceptor variation (EAvSS). When the electron donor (H_2) was limited (EDvSS), DB responded to the H_2 pressure, outnumbered SRB, and prevented SO_4^{2-} reduction activity, even though SRB remained as part of the biofilm due to their metabolic diversity. Without H_2 restriction (EAvSS), NO_3^- was the preferred electron acceptor, and SO_4^{2-} reduction only occurred at a NO_3^- surface loading <0.13 g N/m^2 day. Pyrosequencing results revealed that *Burkholderiales* (heterotrophic DB) were abundant with H_2 limitation, while *Holophagales* (acetogenic bacteria) and *Bacteroidales*

(bacteria that break down complex organic molecules such as SMPs) were diminished and increased, respectively, with onset of SO_4^{2-} reduction. UniFrac and PCoA analyses also showed that the onset of SO_4^{2-} reduction profoundly affected the structure of the biofilm communities, making them more diverse. In these two Chapters, I documented the ways in which SO_4^{2-} reduction altered the microbial community, and I provided practical means to control SO_4^{2-} reduction in the MBfR: either by limiting H_2 availability by decreasing the H_2 gas pressure or by increasing the NO_3^- loading.

In Chapter 4, I researched the ecological interactions between SRB and PRB when using the MBfR to treat a groundwater highly contaminated with ClO_4^-, at 10000 μg/L, but with low NO_3^- and high SO_4^{2-}. In order to achieve high ClO_4^--removal efficiency, I either increased the H_2 pressure (from 1.3 to 1.7 atm) or decreased the total electron acceptor surface loading (from 0.49 to 0.07 g H_2/m^2 day) by reducing the influent flow rate. While the MBfR attained 99.6% ClO_4^- reduction, SO_4^{2-} reduction was enhanced when the electron acceptor loading was low (0.07 g H_2/m^2 day). Because the MBfR was not H_2-limited, the onset of SO_4^{2-} reduction slowed ClO_4^- reduction, and SRB became more abundant than PRB. The high abundance of SRB likely pushed the PBR to outer layers within the biofilm, which led to higher detachment rates that prevented enough PRB accumulation in the biofilm to drive the effluent ClO_4^- concentration below 41 μg/L (lowest achieved effluent concentration during the experiments).

In Chapter 5, I solved the performance obstacle of Chapter 4 by using a two-stage MBfR (lead and lag MBfRs), in which the lag MBfR received the effluent from the lead MBfR. The groundwater had high ClO_4^- concentration (~4000 μg/L) and significant SO_4^{2-} concentration (~60 mg/L). Besides monitoring performance, I combined qPCR and

pyrosequencing to better understand the ecological interactions between PRB and SRB. I achieved the practical treatment target with the two-stage MBfR: The lead MBfR achieved between 96-99% ClO_4^- reduction, while the lag MBfR reduced ClO_4^- to non-detectable levels (<4 μg/L). Consistent with the results in Chapter 4, key to successful ClO_4^- removal was minimizing SO_4^{2-} reduction by lowering the H_2 pressure, by using a lower-H_2-permeation capacity fiber in the lag MBfR, and by re-oxygenating between stages. According to qPCR and pyrosequencing analyses, the biofilm communities of the lead and lag MBfR were distinct from each other. For example, SRB were less abundant in the lag MBfRs because of the successful strategies to minimize SO_4^{2-} reduction. In particular, re-oxygenation enriched PRB and DB (microorganisms that also can respire ClO_4^-) in the lag MBfRs. Pyrosequencing showed which SRB phylotypes competed well for space in the lead MBfRs (i.e., D*esulfovibrionales*) and for H_2 in the lag MBfRs (i.e., *Desulfobacterales*). Sulfur cycling was evidenced by the presence of sulfur-oxidizers *Thiobacteriales* and *Ignavibacteriales* whenever the SO_4^{2-} reduction rate was enhanced.

In Chapter 6, I applied pyrosequencing analysis to study the microbial community structure of two-stage pilot MBfR that had similarities and differences from the configuration described in Chapter 5. The pilot treated contaminated groundwater with ~ 9 mg/L NO_3^- and 160 – 200 μg/L ClO_4^-, while O_2 and SO_4^{2-} also were present at ~9 mg/L and 20-22 mg/L, respectively. The removal efficiencies were ~99% for NO_3^- and ~94 % for ClO_4^-, but the effluent ClO_4^- concentration could not be driven consistently to below the detection level. Different from the setup described in Chapter 5, the pilot MBfRs did not expose the effluent from the lead MBfR to re-oxygenation, and this led to the decreased electron acceptor loading and then higher chances for onset of SO_4^{2-} reduction

in the lag MBfR. Also, H_2 was not limiting in the lag MBfR, which facilitated SO_4^{2-} reduction and boosted the opportunistic growth of secondary members, such as sulfur-oxidizers and heterotrophs. In parallel to Chapter 4, strong SO_4^{2-} reduction appeared to be the reason for incomplete ClO_4^- reduction. SO_4^{2-} reduction was greatly favored after lowering the total electron acceptor loading in the pilots: SRB *Desulfovibrionales* along sulfur-oxidizers *Thiotrichales* took over a big portion within the biofilm community structure. Moreover, the pilots were unique because the MBfR positions were switched every three days, which means similar microbial communities developed for the lead and lag MBfRs, quite different from the findings of Chapter 5.

My research advances knowledge on managing microbial communities toward NO_3^- and ClO_4^- water bioremediation in H_2-fed biofilms while suppressing unwelcome microbial SO_4^{2-} reduction. I achieved the first-ever successful MBfR capable of handling highly ClO_4^--contaminated groundwater even when the risk for SO_4^{2-} reduction was significant. The comprehensive understanding between the community structure and function in the microbial community was a key factor for the success I report here. As observed in the results from Chapters 2-6 and with the help of molecular biology tools (i.e., qPCR and pyrosequencing), the biofilm community responded promptly to stimuli such as the H_2 availability and electron acceptor loadings. Armed with this knowledge, pilot- and full-scale MBfR applications now can be managed to avoid electron sinks that harm remediation results by promoting the growth of unwanted guests such as SRB. SO_4^{2-} reduction not only is undesirable for the extra expenditure of electrons and deleterious water aesthetics, but also because promotes the growth of heterotrophic (e.g.

Bacteroidales, *Flavobacteriales*) and sulfur-oxidizing microorganisms, as observed in Chapters 3, 5, and 6.

7.2 Conclusions

My research showed how the onset of SO_4^{2-} reduction in the H_2-fed biofilms changed the microbial community structure: The microbial diversity was augmented, and the abundance of several DB and PRB microbial phylotypes was affected. Significant SO_4^{2-} reduction led to increments on SRB abundance, as expected, but the biofilm community also became populated by sulfur-oxidizers and heterotrophs. Particularly important, sulfur-oxidizing bacteria appear to have enhanced the ecological advantage for SRB by allowing S cycling in the bench and pilot MBfRs regardless of the inoculum source. Heterotrophic bacteria also appeared whenever SO_4^{2-} reduction was important, and, as a result, the microbial diversity of the biofilm communities increased. The overall increase on diversity under SO_4^{2-} reducing conditions did not lead to better MBfR performance; in fact, the bench- and pilot-scale results showed that SO_4^{2-} reduction was detrimental to ClO_4^- reduction.

Managing electron acceptor loadings and H_2 availability is crucial to enhance DB and PRB. An unrestricted H_2 supply should be avoided, because it enhances SRB and sulfur cycling. Only electron-donor limitation allowed DB to outcompete SRB. Once donor limitation was relieved and when the NO_3- and O_2 loadings were low, SRB responded favorably to excess of H_2 and outnumbered PRB. Hence, careful balancing of H_2 availability and total electron acceptor loading must be achieved to achieve remediation standards, especially for ClO_4^-.

7.3 Recommendations for future work

In this section, I describe several follow up studies that will lead to deeper understanding of the microbial ecology in H_2-fed biofilms treating NO_3^- and ClO_4^- in the presence of SO_4^{2-}. I propose these research topics based on my interests in microbial ecology of mixed communities towards water bioremediation, especially when SO_4^{2-} reduction is a high risk. Lastly, I offer insights on how to look at the sustainability of the MBfR as a full-scale water-remediation technology. The order in which I present the suggested future works is important, as each study builds from the previous studies.

Study 1: Reduction kinetics of SRB phylotypes *Desulfovibrionale*s and *Desulfobacterales*

In Chapter 5, I was able to control the onset of SO_4^{2-} reduction in a two-stage MBfR setup. I used two different membranes, which allowed me to completely remove a high ClO_4^- influent concentration and still control SO_4^{2-} reduction. Pyrosequencing analysis of biofilm samples of the lead and lag MBfRs clearly showed different SRB phylotypes: *Desulfovibrionales* were significant in the lead MBfRs, while *Desulfobacterales* were in the lag MBfRs. Because the membranes I used in the lead and lag MBfRs deliver H_2 in significantly different permeation capacities (Tang et al., 2012d), H_2-utilization kinetics appear to relate with the different SRB phylotypes above mentioned.

To understand under which conditions some SRB phylotypes are favored over others, and to verify if *Desulfovibrionales* are r-strategists (microorganisms capable to grow quickly under abundant resources) while *Desulfobacterales* are K-strategists

(microbes able to compete for scarce resources, even though the offspring do not multiply rapidly when resources are ample), I propose to set up 160-ml batch serum bottles, which should be run in triplicates. I would inoculate the batch bottles with either *Desulfovibrionales* or *Desulfobacterales* pure cultures, using aseptic techniques to avoid contamination. H_2 at variable concentrations (i.e., limiting range to oversupply based on stoichiometric calculations) would be injected in the headspace to reduce the only electron acceptor: SO_4^{2-}. Biomass growth (tracked by optical density) and respiration rates of SO_4^{2-} (tracked by IC) would determine the kinetic parameters of each strain. H_2 consumption should be monitored by gas chromatography.

This study would help to understand why under high H_2 delivery capacities (lead MBfRs in Chapter 5) *Desulfovibrionales* were the most abundant SRB phylotype and why under low H_2 delivery capacities *Desulfobacterales* were the most significant SRB phylotype. While fundamental in nature, this study would shed light on ecological interactions in H_2-fed biofilms in which SRB are able to co-exist with DB and PRB.

Study 2: Role of sulfur-oxidizing microorganisms in H_2-fed biofilms.

In Chapters 5 and 6, the presence of sulfur-oxidizing microorganisms *Thiobacteriales*, *Ignavibacteriales*, and *Thiotrichales* gave evidence of active sulfur cycling when SO_4^{2-} reduction was significant. This also was reported in other bench-scale MBfRs (Zhao et al., 2013) by the abundance of *Campylobacteriales*. The presence of sulfur-oxidizers overall incremented the microbial diversity in the MBfR biofilm in Chapter 6; however, a more diverse microbial community was not correlated with better MBfR performance, but with poorer performance for ClO_4^- reduction. From my

experiments, sulfur-oxidizers came along whenever NO_3^- was mostly depleted and SO_4^{2-} had a greater electron equivalence than ClO_4^- as electron acceptors. Interestingly, some sulfur-oxidizers can use NO_3^- as an electron acceptor, while they use either H_2S or S as the electron donor. From the results in Chapter 5, it is hard to distinguish if sulfur-oxidizers performed sulfur-driven denitrification in which the final product is N_2 (Shao et al., 2010) or even ClO_4^- reduction (Boles et al., 2012). In Chapter 6, the findings shed light on NH_4^+ production, as genus *Thiotrix* is well known to oxidize H_2S and S while reducing NO_3^- (Williams, 1985; Williams et al., 1987), but further evidence on how this affects ClO_4^- reduction is necessary.

I would set up fiber-containing bottles such as those described in Tang et al. (2012d) to study the activity of SRB and sulfur-oxidizers growing in H_2-fed biofilms. I would not use the typical MBfR setup, as in Chapters 2-5, because the bottles can be run easily in duplicates while still allowing a biofilm to develop. I would start by inoculating the bottles with activated sludge, which guarantees SRB in the inoculum, and I would feed a synthetic medium with variable amount of either NO_3^- or ClO_4^- and constant SO_4^{2-} concentration, as indicated in Table 7.1. The synthetic medium should be aerobic, have a good buffer system, and include trace mineral components (Chapters 2 and 3). I would pressurize the fibers at a constant H_2 pressure and operate the bottles in semi-batch mode (i.e., regular replacement of some of the medium). The electron donor (H_2) would be supplied with relative excess to allow some degree of SO_4^{2-} reduction, which would also depend on the electron acceptor loading controlled by the acceptor concentrations. Based on my findings reported in Chapters 2 and 4-6, I expect high SO_4^{2-} reduction fluxes and SRB when the influent NO_3^- concentration is <1 mg N/L or the ClO_4^- concentration is

<~200 µg/L. Higher SO_4^{2-} reduction activity ought to start enhancing sulfur-oxidizers in the biofilm.

Careful monitoring of the anions NO_3^-, ClO_4^-, and SO_4^{2-} by IC analysis and H_2S measurements of liquid samples (Hach, USA) would be implemented on a daily basis. Samples should also be monitored for NH_4^+ by IC, as some sulfur-oxidizers reduce NO_3^- to NH_4^+.

Table 7.1 Proposed experimental setup for studying the role of sulfur-oxidizers

Batch run	*NO_3^- mg N/L*	*ClO_4^- µg/L*	*SO_4^{2-} mg/L*
1	0	-	46
2	1	-	46
3	10	-	46
4	-	200	46
5	-	1000	46
6	-	10000	46

New media would be added every time the acceptors are depleted, and after repeating this for at least 3 times, I would take biofilm samples when the results look steady from one medium replacement to the next. I would extract DNA for qPCR analysis of reductases in DB, PRB, and SRB, but I would also analyze for sulfite oxidase (*sox*). DNA samples should be analyzed as well by pyrosequencing.

The diversity of sulfur-oxidizers found in Chapters 5 and 6, as well as those mentioned in Zhao et al. (2013), could be potentially explained by the systematic work suggested here. Contrary to Chapters 5 and 6 and Zhao et al. (2013), who used several inocula, the same inoculum would be used for all the studies, and it must be characterized at the startup and follow up by qPCR and pyrosequencing. To pair the results of the

proposed study, fluorescence *in situ* hybridization (FISH) probes can be implemented to target DB, PRB, SRB, and sulfur-oxidizers to visualize trends on competition for space in the biofilm.

Study 3: SO_4^{2-} reduction and the growth of heterotrophs.

The findings about the microbial community structure in Chapters 3, 5, and 6 very consistently showed that high rates of SO_4^{2-} reduction incremented the relative abundance of heterotrophic bacteria (i.e., *Bacteroidales* and *Flavobacteriales*). Modeling work by Tang et al. (2012a) showed a larger production of utilization associated products (UAP) when SO_4^{2-} reduction occurred in a denitrifying biofilm. UAP are SMP, and, according to the unified theory by Laspidou and Rittmann (2002), hydrolyzed extracellular polymeric substances (EPS) also are SMP. Therefore, assessing qualitatively and quantitatively the EPS in the MBfR biofilm during active SO_4^{2-} reduction can be a proxy to prospect the "blooming" of heterotrophic microorganisms.

The composition of EPS is of interest and would be a novel study of H_2-fed biofilms. EPS can be observed by confocal laser scanning microscopy (CLSM), because several probes to visualize individual components of EPS (e.g., glycoconjugates, amino sugars, lipids) are reported (e.g., Staud et al., 2004; Zippel and Neu, 2011). I would start by setting SO_4^{2-}-reducing MBfRs and then proceed by taking biomass samples for CLSM. Biofilm samples should also be analyzed by pyrosequencing to demonstrate the presence of heterotrophs as those found in Chapters 3, 5, and 6. Control MBfRs could be NO_3^-- or ClO_4^--reducing MBfRs to compare how rates of SO_4^{2-} reduction enhanced the amount of EPS within the biofilm.

Lastly, the proposed work in this section is also of value for assessing sequestration of metals and solids within the EPS matrix in the MBfR, as well as for determining the potential risk for membrane fouling if too much EPS is produced in the MBfR biofilms.

Study 4: Modeling competition for space between SRB and PRB

My research in Chapter 4 suggests that SRB are capable of outcompeting fast-growing PRB when the MBfR has an ample supply of H_2 and also has low total electron acceptor loading. In fact, my qPCR analysis of characteristic reductases for SRB and PRB showed greater biomass fractions of SRB than PRB under these conditions. With this scenario, SRB are likely forcing PRB to the outer layers in the biofilm, where they are more susceptible to biofilm detachment. A model focused on competition for space between these two microbial groups ought to better elucidate the findings of Chapter 4.

Modeling studies in the MBfR by Tang et al. (2012a, b, c) built a strong foundation for competitive behaviors between either DB and SRB or DB and PRB. However, a model to represent the competition between PRB and SRB has not been developed and is worth pursuing as pointed out by the findings of Chapters 4-6, which suggests competition for common sources. Moreover, the work done by Tang et al. (2012a, b, c) has limited capacity to demonstrate the impact of biomass detachment. As noted in Chapter 4, if PRB are growing in outer layers, they are more exposed to detachment and could potentially been unable to complete microbial ClO_4^- reduction.

Recently, Martin et al. (2013b) reported modeling efforts to track sloughing and biomass detachment by erosion. Given the counter-diffusional nature of the biofilm in

the MBfR (the electron donor diffuses from the fiber through the biofilm to the bulk liquid, while the electron acceptor travels from the bulk liquid through the biofilm in the opposite direction), the biofilm thickness is a particular parameter to probe. For instance, a thick biofilm might prevent the diffusion of the electron donor across the biofilm, and a very thin biofilm might not support enough microbial growth to reduce the electron acceptor loading. Moreover, Martin et al. (2013b) reported competitive behaviors between DB, SRB, and methanogens in MBfR in a 2D model by combining MATLAB and COMSOL platforms. The geometry of the substratum, which was a fiber sheet in Martin's et al. (2013b) work, allowed the formation of niches in the biofilm. Specifically, methanogens grew between two continuous membranes in the fiber sheet. This placement allowed methanogens to be protected from detachment and to be close to the H_2 source. In Martin's et al. (2013b) 2D model, SRB were spread vertically (i.e., away from the membrane sheet) and horizontally (forming micro-colonies), but more towards the inner layers. DB were distributed on the outer portions of the biofilm and were the first to detach in major sloughing events. However, DB recovered faster than SRB and methanogens from biomass detachment. Only at very low NO_3^- concentrations and high H_2 supply (e.g., inner zones of the biofilm, niches) were methanogens and SRB good competitors against DB. This agrees with the findings of Chapter 2 about the competitive and coexistence behaviors between DB and SRB. Specially, if the biofilm was thick enough, it allowed more SRB and methanogens to accumulate, and potentially lead to fouling the membranes (Martin et al., 2013b).

As pointed by Martin et al. (2013a, b), considering the geometry of the biofilm's substratum holds great promise to better capture the competitive behaviors for space

between microorganisms. The formation of niches in the biofilm might be a reason of the incomplete ClO_4^- removal observed in the pilot study reported in Chapter 6. The pilot reactors were set up in fiber sheets held apart by plastic spacers. Martin et al. (2013a) developed a 2D model work for the spiral-wound MBfR used in the pilots. This geometry was particularly complex, with alternated layers of plastic spacers and membrane fabric with a top and bottom wall of membranes. In their 2D model, Martin et al. (2013a) found that the spacer configuration increased the shear forces on the top membranes and prevented biofilm accumulation than on the bottom membranes. The authors attributed hindered MBfR performance to the high shear forces and poor biomass accumulation on the top membranes. Therefore, modeling the spatial distribution of microbial groups with the aid of 2D models is significant for gaining a holistic understanding of the community structure and function.

I propose to utilize a combination of MATLAB and COMSOL, as explained in detail in Martin et al. (2013a, b), to demonstrate competitive behaviors between PRB and SRB. The models would focus on biofilm detachment and formation of niches in typical bench scale MBfR's geometry, which, contrary to the pilot MBfR's configuration, has a fiber bundle and lacks any kind of spacers. The findings of this PRB-SRB 2D model could potentially be translated to study the unique pilot MBfR's geometry (i.e., spacers and membrane fabric). The trade off with 2D models is the computational efforts to run the study. However, the output is worth pursuing and could be coupled with FISH targeting PRB and SRB in a biofilm sample. This would advance the microbial-ecology based findings of Chapters 4-6.

Study 5: The sustainability of the MBfR, insights from life-cycle assessment (LCA) and policy analysis

Biologically based water treatment technologies are gaining popularity and are claimed to be more sustainable based on their biological nature (e.g., biomimic principles, intrinsic capacity of living organisms to clean up pollution). Among these technologies, the MBfR is widely applicable for the remediation of an ample spectrum of water contaminants. My research through Chapters 2-6 focused on discerning how to manage the microbial community to facilitate NO_3^- and ClO_4^- water remediation goals while avoiding SO_4^{2-} reduction. The findings of my research establish key lessons "inside of the box"; however, the full scale application of this technology (APTwater, Inc., Long Beach, CA, USA) would be greatly favored by a careful analysis "outside of the box" such as determining its environmental footprint, social impacts, and policy-making implications.

Overall, the MBfR appears to be relatively sustainable because it makes use of biological players (microorganisms) to drive the decontamination of water. Several studies have attempted to consolidate the sustainability of the MBfR by different approaches: weighting criteria by stakeholder engagement (Meyer et al., 2010), economic assessment (Adham et al., 2003; Meyer et al., 2010; Evans et al., 2013), and greenhouse gas (GHG) emissions quantification (Meyer et al., 2010). Nevertheless, those studies did not systematically consider the environmental footprint of the technology, the benefits for treatment, and the roadblocks for full-scale application related to permits and policies for water treatment (Day, 1993; Lin et al., 1996).

To overcome this gap, I propose to develop an LCA for establishing how sustainable the MBfR is. An LCA is an important tool for systematic thinking to determine the environmental implications of a new technology. An LCA is able to capture the environmental footprint of a product, service, or technology from either a "cradle to grave" approach (i.e., from raw material extraction to end of life) or a "cradle to gate" approach (i.e., from raw material extraction to delivery of product or service). LCAs can be broadly classified as attributional-LCA (aLCA) if the output is the associated environmental impact with a product versus consequential-LCA (cLCA) if the outcome reports the directly and the indirectly induced consequences of a product (e.g., generation of co-products). In other words, the cLCA attempts to address the "system-wide change" on the environment and material flows, and it is more holistic than the aLCA (Rebitzer et al., 2004; Pennington et al., 2004).

To comprehensively assess the sustainability of the MBfR, I suggest a "cradle to grave" cLCA to elucidate the implications of changing a mature technology such as ion exchange (IX) by the MBfR and to monitor the related co-products at full scale operation for water drinking processes. Moreover, with a cLCA is possible to determine required changes on policies, permits, and regulations for the application of new technologies. A cLCA gives support for strategic policy making based on the "change-oriented" driven assessment. Therefore, the cLCA approach is more advantageous than the aLCA and holds greater power with new technologies (Chen et al., 2012).

In Table 7.2, I broadly define the unique and common aspects of IX and MBfR to be considered while developing the LCA framework and inventory steps. For the inventory part in the LCA process, data for full-scale MBfR application can be obtained

from APTwater, Inc. (Long Beach, CA, USA; Rancho Cucamonga's case study), while data for IX systems is widely available through several manufacturers and field practitioners (e.g., Evans et al., 2013).

Table 7.2 Unique and common aspects of MBfRs and IX to be considered during development of LCA

Factors	MBfR	IX
Destroy pollutant?	Mostly YES	Absolutely NO
Generates waste stream	Yes, detached biomass	Yes, brines
Required further waste disposal?	Yes, management of solids. (e.g., filtration)	Yes, brine disposal
Typical by-products	Intermediate products if microbial reduction is stalled	Exhausted resins
Chemicals needed to operate?	H_2, CO_2, phosphate (if deficient), N_2 or compressed air	Salts
Highest operational cost	Energy input	Brine disposal
Weakness	Clogging, fouling	Exhausted resins go to incineration or regeneration with brines
Full scale operation?	Rancho Cucamonga, CA	YES

The advantages and disadvantages involved in each technology are particularly important information within Table 7.2. On one hand, the MBfR requires several chemicals, particularly H_2, that might be important drivers of the sustainability of this technology. H_2 consumption by microorganisms is the principle of the MBfR, as H_2 acts as electron donor for microorganisms and becomes oxidized while the pollutant is reduced and transformed into innocuous substances, which means pollutant destruction in

most cases. However, the source of H_2 might not be environmentally sustainable. Currently, H_2 is produced by steam reforming from hydrocarbons, and some alternative methods for its generation are electrolysis and thermolysis. These alternatives are quite energy-intensive. Besides H_2, carbon dioxide (CO_2) is supplied through gas manifolds to manage the pH of the system, and phosphate is supplemented as needed to provide a phosphorus source for microbial growth. Lastly, sodium hypochlorite is added to disinfect the product water to attain drinking water quality standards. In addition, to avoid fouling of the MBfR membranes due to excessive biomass growth, air scouring (either with nitrogen gas or with compressed air) aids on detaching excessive biomass, and this generates a wastewater. Therefore, the LCA should consider this wastewater production, although this wastewater is expected to be minimal (Evans et al., 2013) and can be disposed into the sewer system with proper removal of solids.

While the addition of chemicals for the MBfR appears at first to work against sustainability, it is worth mentioning that IX does not destroy the pollutant. Instead, IX concentrates the pollutant and produces brines. To be more efficient, the IX system requires a specific type of resin with enough capacity to remain functional without repetitive regeneration processes. A good IX design and configuration would decrease the production of brines, and therefore the operational costs. Resin regeneration extends the life-span of the process and guarantees an optimal performance of the IX column. However, this regeneration process produces a significant amount of brines or wastewater with extreme salt concentrations. Improper handling of the brines might result in an even worse environmental problem than the original need for treatment. Furthermore, the

disposal of brines has to be customized based on the facility's location, logistics (Meyer et al., 2010), and land and electrical costs (Evans et al., 2013).

Finally, I propose to establish a fair comparison between the two technologies by using a functional unit (as required in any LCA), such as energy usage (e.g., kilowatts per hour (kWH)) per rate of pollutant removal. Another metric can relate to the environmental footprint, such as GHG per volume of treated water.

REFERENCES

Adav SS, Lee DJ, Lai JY. 2010. Microbial community of acetate utilizing denitrifiers in aerobic granules. Appl Microbiol Biotechnol 85(3): 753-762.

Adham S, Gillogly T, Lehman G, Rittmann BE, Nerenberg R. 2003. Application of bioreactor systems to low-concentration perchlorate-contaminated water. Denver, Colorado: AWWA Research Foundation and American Water Works Association.

APTWater ®. 2013. An environmentally-friendly approach to nitrate removal. Retrieved on February 19, 2014 from: http://www.aptwater.com/our-technologies/specialist-membrane-systems/nitrate-removal/

Attaway H, Smith M. 1993. Reduction of perchlorate by an anaerobic enrichment culture. J Ind Microbiol 12(6): 408-412.

Bardiya N, Bae JH. 2005. Bioremediation potential of a perchlorate-enriched sewage sludge consortium. Chemosphere 58(1): 83-90.

Bárta J, Melichová T, Vaněk D, Picek T, Šantrůčková H. 2010. Effect of pH and dissolved organic matter on the abundance of nirK and nirS denitrifiers in spruce forest soil. Biogeochemistry 101(1-3): 123-132.

Beller HR, Chain PSG, Letain TE, Chakicherla A, Larimer FW, Richardson PM, Coleman MA, Wood AP, Kelly DP. 2006. The genome sequence of the obligately chemolithoautotrophic, facultative anaerobic bacterium *Thiobacillus denitrificans.* J Bacteriol 188(4): 1473-1488.

Ben-Dov E, Brenner A, Kushmaro A. 2007. Quantification of sulfate-reducing bacteria in industrial wastewater, by real-time polymerase chain reaction (PCR) using *dsrA* and *apsA* genes. Microb Ecol 54 (3): 439-451.

Bentzen G, Smith AT, Benett D, Webster NJ, Reinholt F, Sletholt E, Hobson J. 1995. Controlled dosing of nitrate for prevention of H_2S in a sewer network and the effects of the subsequent treatment processes. Water Sci Technol 31(7): 293-302.

Boles AR, Conneely T, McKeever R, Nixon P, Nüsslein KR, Ergas SJ. 2012. Performance of a pilot-scale packed bed reactor for perchlorate reduction using a sulfur oxidizing bacterial consortium. Biotechnol Bioeng 109(3): 637–646.

Braker G, Fesefeldt A, Witzel KP. 1998. Development of PCR primer systems for amplification of nitrite reductase genes (*nirK* and *nirS*) to detect denitrifying bacteria in environmental samples. Appl Environ Microbiol 64(10): 3769-3775.

Braker G, Zhou J, Wu L, Devol AH, Tiedje JM. 2000. Nitrite reductase genes (*nirK* and *nirS*) as functional markers to investigate diversity of denitrifying bacteria in Pacific Northwest marine sediment communities. Appl Environ Microbiol 66(5): 2096-2104.

Breznak JA. 2002. Phylogenetic diversity and physiology of termite gut spirochetes. Integr Comp Biol 42(2): 313-318.

Caporaso JG, Kuczynski J, Stombaugh J, Bittinger K, Bushman FD, Costello EK, Fierer N, Pena AG, Goodrich JK, Gordon JI, Huttley GA, Kelley ST, Knight D, Koenig JE, Ley RE, Lozupone CA, McDonald D, Muegge BD, Pirrung M, Reeder J, Sevinsky JR, Tumbaugh PJ, Walters WA, Widmann J, Yatsunenko T, Zaneveld J, Knight R. 2010a. Qiime allows analysis of high-throughput community sequencing data. Nat Methods 7(5): 335-336.

Caporaso JG, Bittinger K, Bushman FD, DeSantis TZ, Andersen GL, Knight R. 2010b. PyNAST: a flexible tool for aligning sequences to a template alignment. Bioinformatics 26(2): 266-267.

Cha DK, Chiu PC, Kim SD, Chang JS. 1999. Treatment technologies. Water Environ Res 71: 870-885.

Chaudhuri SK, O'Connor SM, Gustavson RL, Achenbach LA, Coates JD. 2002. Environmental factors that control microbial perchlorate reduction. Appl Environ Microbiol 68(9): 4425-4430.

Chen C, Wang AJ, Ren NQ, Den XL, Lee DJ. 2009a. Optimal process pattern for simultaneous sulfur, nitrogen and carbon removal. Water Sci Technol 59: 833‑837.

Chen C, Wang AJ, Ren NQ, Lee DJ, Lai JY. 2009b. High-rate denitrifying sulfide removal process in expanded granular sludge bed reactor. Bioresour Technol 100: 2316‑2319.

Chen C, Ren NQ, Wang AJ, Liu LH, Lee DJ. 2010. Functional consortium for denitriying sulfide removal process. Appl Microbiol Biotechnol 86(1): 353-358.

Chen IC, Fukushima Y, Kikuchi Y, Hirao M. 2012. A graphical representation for consequential life cycle assessment of future technologies. Part 1: methodological framework. Int J Life Cycle Ass 17(2): 119-125.

Chin K-J, Sharma ML, Russell LA, O'Neill KR, Lovley DR. 2008. Quantifying expression of a dissimilatory (bi) sulfite reductase gene in petroleum-contaminated marine harbor sediments. Microb Ecol 55(3): 489-499.

Choi H, Silverstein J. 2008. Inhibition of perchlorate reduction by nitrate in a fixed biofilm reactor. J Hazard Mater 159: 440–445.

Chung J, Li X, Rittmann BE. 2006a. Bio-reduction of arsenate using a hydrogen-based membrane biofilm reactor. Chemosphere 65(1): 24-34.

Chung J, Nerenberg R, Rittmann BE. 2006b. Bio-reduction of selenate using a hydrogen-based membrane biofilm reactor. Environ Sci Technol 40: 1664-1671.

Chung J, Nerenberg R, Rittmann BE. 2006c. Bio-reduction of soluble chromate using a hydrogen-based membrane biofilm reactor. Water Res 40(8): 1634-1642.

Chung J, Ryu H, Abbaszadegan M, Rittmann BE. 2006d. Community structure and function in an H2-based membrane biofilm reactor capable of bio-reduction of selenate and chromate. Appl Microb Biotechnol 72(6): 1330-1339.

Chung J, Rittmann BE. 2007. Bio-reductive dechlorination of 1,1,1-trichloroethane and chloroform using a hydrogen-based membrane biofilm reactor. Biotechnol Bioeng 97(1): 52-60.

Chung J, Nerenberg R, Rittmann BE. 2007a. Simultaneous biological reduction of nitrate and perchlorate in brine water using the hydrogen-based membrane biofilm reactor. J Environ Eng 130: 157-164.

Chung J, Rittmann BE, Wright WF, Bowman RH. 2007b. Simultaneous bio-reduction of nitrate, perchlorate, selenate, chromate, arsenate, and dibromochloropropane using a hydrogen-based membrane biofilm reactor. Biodegradation 18(2): 199-209.

Chung J, Krajmalnik-Brown R, Rittmann BE. 2008. Bioreduction of trichloroethene using a hydrogen-based membrane biofilm reactor. Environ Sci Technol 42(2)**:** 477-483.

Chung J, Rittmann BE. 2008. Simultaneous bio-reduction of trichloroethene, trichloroethane, and chloroform using a hydrogen-based membrane biofilm reactor. Water Sci Technol 58(3): 495-501.

Church MJ. 2008. Resource control of bacterial dynamics in the sea. In Microbial Ecology in the Oceans, 2nd ed. Ed. DL Kirchman (Hoboken, NJ: Wiley & Sons), 335-382.

Coates JD, Ellis DJ, Gaw CV, Lovley DR. 1999a. Geothrix fermentans gen. nov., sp. nov., a novel Fe(III)-reducing bacterium from a hydrocarbon-contaminated aquifer. Int J Sys Bacteriol 49(4): 1615-1622.

Coates JD, Michaelidou U, Bruce RA, O'Connor SM, Crepsi JN, Achenbach LA. 1999b. Ubiquity and diversity of dissimilatory (per)chlorate-reducing bacteria. Appl Environ Microbiol 65(12): 5234–5241.

Coates JD, Anderson RT. 2000. Emerging techniques for anaerobic bioremediation of contaminated environments. Trends Biotechnol 18(10): 408-412.

Coates JD, Chakraborty R, Lack JG, O'Connor SM, Cole KA, Bender KS, Achenbach LA. 2001. Anaerobic benzene oxidation coupled to nitrate reduction in pure culture by two strains of *Dechloromonas*. Nature 411(6841): 1039-1043.

Coates JD, Achenbach LA. 2004. Microbial perchlorate reduction: rocket fuelled metabolism. Nature Rev Microbiol 2(7): 569-580.

Dalsgaard T, Bak F. 1994. Nitrate reduction in a sulfate-reducing bacterium, *Desulfovibrio desulfuricans*, isolated from rice paddy soil: sulfide inhibition, kinetics, and regulation. Appl Environ Microbiol 60(1): 291-297.

Day SM. 1993. US environmental regulations and policies -their impact on the commercial development of bioremediation. Trends Biotechnol 11: 324-328.

DeLong EF. 2002. Microbial population genomics and ecology. Curr Opin Microbiol 5: 520-524.

DeSantis TZ, Hugenholtz P, Larsen N, Rojas M, Brodie EL, Keller K, Huber T, Dalevi D, Hu P, Andersen GL. 2006. Greengenes, a chimera-checked 16s rrna gene database and workbench compatible with ARB. Appl Environ Microbiol 72(7): 5069-5072.

Dilling W, Cypionka H. 1990. Aerobic respiration in sulfate-reducing bacteria. FEMS Microbiol Lett 71: 123-128.

Drake HL, Kusel K, Matthies C. 2002. Ecological consequences of the phylogenetic and physiological diversities of acetogens. A Van Leeuw J Microb 81: 203-213.

Edgar RC. 2010. Search and clustering orders of magnitude faster than blast. Bioinformatics 26(19): 2460-2461.

Evans PJ, Chu A, Liao S, Price S, Moody M, Headrick D, Min B, Logan BE. 2002. Pilot testing of a bioreactor for perchlorate-contaminated groundwater treatment. Proceedings of the Third International Conference on Remediation of Chlorinated and Recalcitrant Compounds (Monterey, CA). May 20-23.

Evans PJ, Price S, Min B, Logan BE. 2003. Biotreatment and downstream processing of perchlorate contaminated groundwater. In Situ and On-Site bioremediation−The Seventh International Symposium. June 2-5.

Evans PJ, Smith J, Singh T, Hyung H, Arucan C, Berokoff D, Friese D, Overstreet R, Vigo R, Rittmann BE, Ontiveros-Valencia A, Zhao H-P, Tang Y, Kim B-O, van Ginkel SW, Krajmalnik-Brown R. 2013. Final Report: Nitrate and Perchlorate Destruction and Potable Water Production Using Membrane Biofilm Reduction. ESTCP Project ER-200541.

Faith DP. 1992. Conservation evaluation and phylogenetic diversity. Biol Conserv 61: 1-10.

Fields MW, Bagwell CE, Carroll SL, Yan T, Liu X,Watson DB, Jardine PM, Criddle CS, Hazen TC, Zhou J. 2006. Phylogenetic and functional biomakers as indicators of bacterial community responses to mixed-waste contamination. Environ Sci Technol 40: 2601–2607.

Foti M, Sorokin DY, Lomans B, Mussman M, Zacharova EE, Pimenov NV, Kuenen JG, Muyzer G. 2007. Diversity, activity, and abundance of sulfate-reducing bacteria in saline and hypersaline soda lakes. Appl Environ Microbiol 73(7): 2093-2100.

Furumai H, Rittmann BE. 1994. Evaluation of multiple-species biofilm and floc processes under a simplified aggregate model. Water Sci Technol 29(10-11): 439-446.

Garcia de Lomas J, Corzo A, Gonzalez JM, Andrades JA, Iglesias E, Montero MJ. 2005. Nitrate promotes biological oxidation of sulfide in wastewaters: Experiment at plant scale. Biotechnol Bioeng 4: 801-811.

Gingras T, Batista JR. 2002. Biological reduction of perchlorate in ion exchange regenerant solutions containing high salinity and ammonium levels. J Environ Monitor 4(1): 96-101.

Graber JR, Breznak JA. 2004. Physiology and nutrition of *Treponema primitia*, an H_2/CO_2-acetogenic spirochete from termite hindguts. Appl Environ Microbiol 70(3): 1307-1314.

Graham JR, Cannon FS, Parette R, Headrick D, Yamamato G. 2004. Commercial demonstration of the use of tailored carbon for the removal of perchlorate ions from potable water. Presented at National Groundwater Association Conference on MTBE and Perchlorate, Costa Mesa, California. June 3 –4.

Gu BH, Brown GM, Alexandratos SD, Ober R, Dale JA, Plant S. 2000. Efficient treatment of perchlorate-contaminated groundwater with bifunctional anion exchange resins. In E.T. Urbansky, Ed., Perchlorate in the Environment. New York: Kluwer Academic/Plenum Publishers, pp. 165–176.

Gu BH, Brown GM, Maya L, Lance MJ, Moyer BA. 2001. Regeneration of perchlorate (ClO_4^-)-loaded anion exchange resins by a novel tetrachloroferrate ($FeCl_4^-$) displacement technique. Environ Sci Technol 35(16): 3363–3368.

Gu B, Wu W-M, Ginder-Vogel MA, Yan H, Fields MW, Zhou J, Fendorf S, Criddle CS, Jardine P. 2005. Bioreduction of uranium in a contaminated soil column. Environ Sci Technol 39: 4841-4847.

Gullick RQ, Lechvallier MW, Barhorst TAS. 2001. Occurrence of perchlorate in drinking water sources. J Am Water Work Assoc 93(1): 66–77.

Haas BJ, Gevers D, Earl AM, Feldgarden M, Ward DV, Giannoukos G, Ciulla D, Tabaa D, Highlander SK, Sordergren E, Methé B, DeSantis TZ, The Human Microbiome Consortium, Petrosino JF, Knight R, Birren BW. 2011. Chimeric 16s rrna sequence formation and detection in sanger and 454-pyrosequenced pcr amplicons. Genome Res 21(3): 494-504.

Hao OJ, Chen JM, Huang L, Buglass RL. 1996. Sulfate-reducing bacteria. Crit Rev Env Sci Tec 26-2: 155-187.

Hatzinger PB. 2005. Perchlorate biodegradation for water treatment. Environ Sci Technol 39(11): 239A-247A.

Herman DC, Frankenberger WT. 1999. Bacterial reduction of perchlorate and nitrate in water. J Environ Qual 28(3): 1018–1024.

Hughes JB, Hellmann JJ, Ricketts TH, Bohannan BJ. 2001. Counting the uncountable: statistical approaches to estimating microbial diversity. Appl Environ Microbiol 67(10): 4399-4406.

Iwamoto T, Nasu M. 2001. Current bioremediation practice and perspective. J Biosci Bioeng 92(1): 1-8.

Jackson WA, Anderson T, Harvey G, Orris G, Rajagopalan S, Kang N. 2006. Occurrence and formation of non-anthropogenic perchlorate. In Perchlorate: Environmental occurrence, interactions, and treatment. Ed. Gu B, Coates JD. Springer

Jenneman GE, McInerney MJ, Knapp RM. 1986. Effect of nitrate on biogenic sulfide production. Appl Environ Microbiol 51(6): 1205-1211.

Kandeler E, Deiglmayr K, Tscherko D, Bru D, Philippot L. 2006. Abundance of *narG*, *nirS*, *nirK*, and *nosZ* genes of denitrifying bacteria during primary successions of a glacier foreland. Appl Environ Microbiol 72(9): 5957-5962.

Kapplenbach JA, Saxman PR, Cole JR, Schmidt TM. 2001. rrndb: The ribosomal RNA operon copy number database. Nucleic Acids Res 29: 181-184.

Kim K, Logan BE. 2000. Fixed-Bed bioreactor treating perchlorate-contaminated waters. Environ Eng Sci 17(5): 257-265.

Kindaichi T, Ito T, Okabe S. 2004. Ecophysiological interaction between nitrifying bacteria and heterotrophic bacteria in autotrophic nitrifying biofilms as determined by microautoradiography-fluorescence in situ hybridization. Appl Environ Microbiol 70(3): 1641-1650.

Knowles R. 1982. Denitrification. Microbiol Rev 46: 43-70.

Kondo R, Nedwell DB, Purdy KJ Quiroz Silva S. 2004. Detection and enumeration of sulphate-reducing bacteria in estuarine sediments by competitive PCR. J Geomicrobiology 21: 145-157.

Kondo R, Shigematsu K, Butani J. 2008. Rapid enumeration of sulphate-reducing bacteria from aquatic environments using real-time PCR. Plankton Benthos Res 3(3): 180-183.

Lee HS, Parameswaran P, Marcus AK, Torres CL, Rittmann BE. 2008. Evaluation of energy-conversion efficiencies in microbial fuel cells (MFCs) utilizing fermentable and non-fermentable substrates. Water Res 42 (6-7): 1501-1510.

Lee KC, Rittmann BE. 2000. A novel hollow-fiber membrane biofilm reactor for autohydrogenotrophic denitrification of drinking water. Water Sci Technol 41: 219-226.

Lee KC, Rittmann BE. 2002. Applying a novel autohydrogenotrophic hollow-fiber membrane biofilm reactor for denitrification of drinking water. Water Res 36: 2040-2052.

Lee ZM-P, Bussema III C, Schmidt TM. 2008. rrnDB: documenting the number of rRNA and tRNA genes in bacteria and archaea. Nucleic Acids Res 37: D489-D493.

Li G, Park S, Kang D, Krajmalnik-Brown R, Rittmann BE. 2011. 2-4-5 Trichlorophenol degradation using a novel TiO_2-coated biofilm carrier: Roles of adsorption, photocatalysis, and biodegradation. Environ Sci Technol 45(19): 8359-8367.

Lin G-H, Sauer NE, Cutright TJ. 1996. Environmental regulations: A brief overview of their applications to bioremediation. Int Biodeter Biodegr 1-8.

Liu S, Suflita JM. 1993. Ecology and evolution of microbial populations for bioremediation. Trends Biotechnol 11: 344-352.

Logan BE, Lapoint D. 2002. Treatment of perchlorate-and nitrate-contaminated groundwater in an autotrophic, gas phase, packed-bed bioreactor. Water Res 36(14): 3647–3653.

Londry KL, Suflita JM. 1999. Use of nitrate to control sulfide generation by sulfate-reducing bacteria associated with oily waste. J Ind Microbiol Biotechnol 22(6): 582-589.

Losi ME, Giblin T, Hosangadi V, Frankenberger WT. 2002. Bioremediation of perchlorate-contaminated groundwater using a packed bed biological reactor. Bioremediation J 6(2): 97-103.

Lovett GM. 1994. Atmospheric deposition of nutrients and pollutants in North America: An ecological perspective. Ecol Appl 4(4): 629-650.

Lozupone C, Knight R. 2005. UniFrac: a new phylogenetic method for comparing microbial communities. App Environ Microbiol 71: 8228-8235.

Lozupone C, Hamady M, Knight R. 2006. Unifrac - an online tool for comparing microbial community diversity in a phylogenetic context. Bmc Bioinformatics 7(1): 371.

Madigan M, Markinko J, Stahl D, Clark D. 2009. Brock Biology of microorganisms; 12th ed.; Pearson: San Francisco California.

Maeda H, Fujimoto C, Haruki Y, Maeda T, Kokeguchi S, Petelin M, Arai H, Tanimoto I, Nishimura F, Takashiba S. 2003. Quantitative real-time PCR using TaqMan and SYBR green for *Actinobacillus actinomycetemcomitans*, *Porphyromonas gingivalis*, *Prevotella intermedia*, *teqQ* gene and total bacteria. FEMS Immnunol Med Microbiol 39(1): 81-86.

Maillacheruvu KY, Parkin GF, Peng CY, Kuo WC, Oonge ZL, Lebduschka V. 1993. Sulfide toxicity in anaerobic systems fed sulfate and various organics. Water Environ Res 65: 100.

Marschall C, Frenzel P, Cypionka H. 1993. Influence of oxygen on sulfate-reduction and growth of sulfate-reducing bacteria. Arch Microbiol 159(2): 168-173.

Marsili E, Beyenal H, Palma L, Merli C, Dohnalkova A, Amonette JE, Lewandowski Z. 2005. Uranium removal by sulfate reducing biofilms in the presence of carbonates. Water Sci Technol 52(7): 49-55.

Martin KJ, Picioreanu C, Nerenberg R. 2013a. Multidimensional modeling of biofilm development and fluid dynamics in a hydrogen-based, membrane biofilm reactor (MBfR). Water Res 47(13): 4739-4751.

Martin KJ, Picioreanu C, Nerenberg R. 2013b. Modeling Competition of Denitrification, Sulfate-Reduction, and Methanogenesis in a Hydrogen-Based Membrane Biofilm Reactor (MBfR), WEFTEC 2013, Chicago, IL.

Mateju V, Cizinska S, Krejci J, Janoch T. 1992. Biological water denitrification−a review. Enzyme Microb Technol 14(3): 170-183.

Matsuzaka E, Nomura N, Maseda H, Otagaki H, Nakajima-Kambe T, Nakahara T, Uchiyama H. 2003. Participation of nitrite reductase in conversion of NO_2^- to NO_3^- in a heterotrophic nitrifier, *Burkholderia cepacia* NH-17, with denitrification activity. Microbes Environ 18: 203-209.

McInerney MJ, Wofford NQ, Sublette KL. 1996. Microbial control of hydrogen sulfide by sulfate-reducing bacteria. Appl Biochem Biotechnol 57: 933-944.

Merkey BV, Rittmann BE, Chopp DL. 2009. Modeling how soluble microbial products (SMP) support heterotrophs in autotroph-based biofilms. J Theor Biol 259: 670-683.

Meyer KJ, Swaim PD, Bellamy WD, Rittmann BE, Tang Y, Scott R. 2010. Biological and ion exchange nitrate removal evaluation. Water Research Foundation. Subject Area: Water quality.

Min B, Evans PJ, Chu AK, Logan BE. 2004. Perchlorate removal in sand and plastic media bioreactors. Water Res 38(1): 47-60.

Mohanakrishnan J, Kofoed MVW, Barr J, Yuan Z, Schramm A, Meyer RL. 2011. Dynamic microbial response of sulfidogenic wastewater biofilm to nitrate. Appl Microbiol Biotechnol 91: 1647-1657.

Moura JG, Gonzalez P, Moura I, Fauque G. 2007. Dissimilatory nitrate and nitrite ammonification by sulphate-reducing eubacteria. In Sulphate-reducing bacteria. Environmental and Engineered systems; Barton LL, Hamilton WA. Eds; Cambridge. University press: New York pp 241-264.

Muyzer G, Stams AJM. 2008. The ecology and biotechnology of sulphate-reducing bacteria. Nat Rev Microbiol 6(6): 441-454.

Nagata T. 2008. Organic matter bacteria interactions in seawater. In Microbial Ecology in the Oceans, 2nd ed. Ed. DL Kirchman (Hoboken, NJ: Wiley & Sons), 207-242.

Nakamura N, Leigh SR, Mackie RI, Gaskins HR. 2009. Microbial community analysis of rectal methanogens and sulfate reducing bacteria in two non-human primate species. J Med Primatol 38(5): 360-370.

Nerenberg R, Rittmann BE. 2002. Perchlorate as a secondary substrate in a denitrifying hollow-fiber membrane biofilm reactor. Water Sci Technol 2(2): 259-265.

Nerenberg R, Rittmann BE, Najm I. 2002. Perchlorate reduction in a hydrogen-based membrane biofilm reactor. J Am Water Works Assoc 94(11): 103-114.

Nerenberg R, Rittmann BE. 2004. Hydrogen-based, hollow fiber membrane biofilm reactor for reduction of perchlorate and other oxidized contaminants. Water Sci Technol 49 (11-21): 223-230.

Nerenberg R, Kawagoshi Y, Rittmann BE. 2006. Kinetics of a hydrogen-oxidizing, perchlorate-reducing bacterium. Water Res 40 (17): 3290−3296.

Nerenberg R, Kawagoshi Y, Rittmann BE. 2008. Microbial ecology of a perchlorate-reducing, hydrogen-based membrane biofilm reactor. Water Res 42(4): 1151-1159.

Ni B-J, Rittmann BE, Yu H-Q. 2011. Soluble microbial products and their implications in mixed culture biotechnology. Trends Biotechnol 29: 254-263.

Nozawa-Inoue M, Jien M, Hamilton NS, Stewart V, Scow KM, Hristova KR. 2008. Quantitative detection of perchlorate reducing bacteria by real-time PCR targeting the perchlorate reductase gene. Appl Environ Microbiol 74(6): 1941–1944.

Odom JM. 1990. Industrial and environmental concerns with sulfate-reducing bacteria. ASM News 56: 473–476.

Okabe S, Nielsen PH, Characklis WG. 1992. Factors affecting microbial sulfate reduction by *Desulfovibrio desulfuricans* in continuous culture: limiting nutrients and sulfide concentration. Biotechnol Bioeng 40(6): 725-734.

Ontiveros-Valencia A, Ziv-El M, Zhao H-P, Feng L, Rittmann BE, Krajmalnik-Brown R. 2012. Interactions between nitrate-reducing and sulfate-reducing bacteria coexisting in a hydrogen-fed biofilm. Environ Sci Technol 46(20): 11289-11298.

Ontiveros-Valencia A, Ilhan ZE, Kang D-W, Rittmann BE, Krajmalnik-Brown R. 2013a. Phylogenetic analysis of nitrate- and sulfate-reducing bacteria in a hydrogen-fed biofilm. FEMS Microbiol Ecol 85(1): 158-167.

Ontiveros-Valencia A, Tang Y, Krajmalnik-Brown R, Rittmann BE. 2013b. Perchlorate reduction from a highly contaminated groundwater in the presence of sulfate-reducing bacteria in a hydrogen-fed biofilm. Biotechnol Bioeng 110(12): 3139-3147.

Ontiveros-Valencia A, Tang Y, Krajmalnik-Brown R, Rittmann BE. 2014a. Managing the interactions between sulfate- and perchlorate-reducing bacteria when using hydrogen-fed biofilms to treat a groundwater with a high perchlorate concentration. Water Res. 55: 215-224.

Ontiveros-Valencia A, Tan Y, Zhao H-P, Friese D, Overstreet R, Smith J, Evans PJ, Rittmann BE, Krajmalnik-Brown R. 2014b. Pyrosequencing analysis yields comprehensive assessment of microbial communities in pilot two-stage membrane biofilm reactors. Submitted for publication.

Payne WJ. 1973. Reduction of nitrogenous oxides by microorganisms. Bacteriol Rev 409-452.

Payne WJ. 1981. Denitrification. Wiley, NY. 214pp.

Peck HD Jr. 1959. The ATP-dependent reduction of sulfate with hydrogen in extracts of *Desulfovibrio desulfuricans*. Proc Natl Acad Sci US 45: 701-708.

Pennington DW, Potting J, Finnveden G, Lindeijer E, Jolliet O, Rydberg T, Rebitzer G. 2004. Life cycle assessment Part 2: Current impact assessment practice. Environ Int 30(5): 721-739.

Pereyra LP, Hiibel SR, Prieto Riquelme MV, Reardon KF, Pruden A. 2010. Detection and quantification of functional genes of cellulose-degrading, fermentative, and sulfate-reducing bacteria and methanogenic archaea. Appl Environ Microbiol 76: 2192-2202.

Pester M, Brune A. 2006. Expression profile of fhs (FTFHS) genes support the hypothesis that *Spirochaetes* dominate reductive acetogenesis in the hindgut of lower termites. Environ Microbiol 8(7): 1261-1270.

Phillippot L. 2006. Use of functional genes to quantify denitrifiers in the environment. Biochem Soc Trans 34: 101-103.

Philippot L, Hallin S, Schloter M. 2007. Ecology of denitrifying prokaryotes in agricultural soils. Adv Agron 96: 249-305.

Price MN, Dehal PS, Arkin AP. 2009. FastTree: Computing large minimum evolution trees with profiles instead of a distance matrix. Mol Biol Evol 26(7): 1641-1650.

Pruesse E, Quast C, Knittel K, Fuchs BM, Ludwig W, Peplies J, Gloeckner FO. 2007. Silva. A comprehensive online resource for quality checked and aligned ribosomal RNA sequence data compatible with ARB. Nucleic Acids Res 35: 7188-7196.

Rebitzer G, Tomas E, Frischknecht R, Hunkeler D, Norris G, Rydberg T, Schmidt W-P, Suh S, Weidema BP, Pennington DW. 2004. Life cycle assessment: Part 1: Framework, goal and scope definition, inventory analysis, and applications. Environ Int 30(5): 701-720.

Reyes-Avila J, Razo-Flores E, Gomez J. 2004. Simultaneous biological removal of nitrogen, carbon and sulfur by denitrification. Water Res 38(14): 3313‑3321.

Reyes F, Gavira M, Castillo F, Moreno-Vivian C. 1998. Periplasmic nitrate-reducing system of the phototrophic bacterium *Rhodobacter sphaeroides* DSM 158: transcriptional and mutational analysis of the napKEFDABC gene cluster. J Biochem 331: 897-904.

Rittmann BE, Manem JA. 1992. Development and experimental evaluation of a steady-state, multispecies biofilm. Biotechnol Bioeng 9: 914-922.

Rittmann BE, McCartyPL. 2001. Environmental Biotechnology. Principles and applications; McGraw-Hill Companies, Inc.; New York.

Rittmann BE. 2006. Microbial ecology to manage processes in environmental biotechnology. Trends Biotechnol 24: 261-266.

Rittmann BE. 2007. The membrane biofilm reactor is a versatile platform for water and wastewater treatment. Environ Eng Res 12(4): 157-175.

Rittmann BE, Tang Y, Meyer K, Bellamy WD, Nerenberg R. 2012. Biological processes, chapter 17. In: Water treatment design. Ed Randtke SJ and Horsley MB. American Water Works Association (AWWA). McGraw Hill.

Roldan MD, Reyes F, Moreno-Vivian C, Castillo F. 1994. Chlorate and nitrate reduction in phototrophic bacteria *Rhodobacter capsulatus* and *Rhodobacter sphaeroides*. Curr Microbiol 29(4): 241-245.

Ronaghi M. 2001. Pyrosequencing sheds light on DNA sequencing. Genome Res 11(1): 3-11.

Santegoeds CM, Ferdelman TG, Muyzer G, de Beer D. 1998. Structural and functional dynamics of sulfate-reducing populations in bacterial biofilms. Appl Environ Microbiol 64(10): 3731-3739.

Saunders NFW, Ferguson SJ, Baker SC. 2000. Transcriptional analysis of the *nirS* gene, encoding cytochrome cd1 nitrite reductase, of *Paracoccus pantotrophus* LMD 92.63. Microbiol 146(2): 509-516.

Scharwz AO, Rittmann BE. 2007a. A biogeochemical framework for metal detoxification in sulfidic systems. Biodegradation 18(6): 675-692.

Scharwz AO, Rittmann BE. 2007b. Modeling bio-protection and the gradient-resistance mechanism. Biodegradation 18(6): 693-701.

Shannon CE. 1948. A mathematical theory of communication. Bell System Technical Journal. 27: 379–423.

Shao M-F, Zhang T, Fang HH. 2010. Sulfur-driven autotrophic denitrification: diversity, biochemistry, and engineering applications. Appl Microbiol Biotechnol 88(5): 1027-1042.

Simpson EH. 1949. Measurement of diversity. Nature 163: 688.

Smith CJ, Osborn AM. 2009. Advantages and limitations of quantitative PCR (Q-PCR)-based approaches in microbial ecology. FEMS Microbiol Ecol 67: 6–20.

Sorokin DY, Banciu H, van Loosdrecht M, Kuenen JG. 2003. Growth physiology and competitive interaction of obligately chemolithoautotrophic, haloalkaliphilic, sulfur-oxidizing bacteria from soda lakes. Extremophiles 7(3): 195-203.

Staudt C, Horn H, Hempel DC, Neu TR. 2004. Volumetric measurements of bacterial cells and extracellular polymeric substance glycoconjugates in biofilms. Biotechnol Bioeng 88(5): 585-592.

Sun Y, Wolcott RD, Dowd SE. 2011. Tag-encoded FLX amplicon pyrosequencing for the elucidation of microbial and functional gene diversity in any environment. High-Throughput Next Generation Sequencing. Meth Mol Biol 733: 129-141.

Tang Y, Ziv-El M, Zhou C, Shin JH, Ahn CH, Meyer K, Candelaria D, Swaim P, Friese D, Overstreet R, Scott R, Rittmann BE. 2010. Bioreduction of nitrate in groundwater using a pilot-scale hydrogen-base membrane biofilm reactor. Frontiers Environ Sci Eng 4: 280-285.

Tang Y, Ontiveros-Valencia A, Liang F, Zhou C, Krajmalnik-Brown R, Rittmann BE. 2012a. A biofilm model to understand the onset of sulfate reduction in denitrifying membrane biofilm reactors. Biotechnol Bioeng 110(3): 763-772.

Tang Y, Zhao H-P, Marcus AK, Krajmalnik-Brown R, Rittmann BE. 2012b. A steady-state biofilm model for simultaneous reduction of nitrate and perchlorate -- Part 1: model development and numerical solution. Environ Sci Technol 46(3): 1598 – 1607.

Tang Y, Zhao H-P, Marcus AK, Krajmalnik-Brown R, Rittmann BE. 2012c. A steady-state-biofilm model for simultaneous reduction of nitrate and perchlorate –Part 2: Parameter optimization and results and discussion. Environ Sci Technol 46(3): 1608-1615.

Tang Y, Zhou C, van Ginkel SW, Ontiveros-Valencia A, Shin J, Rittmann BE. 2012d. Hydrogen-Permeation Coefficients of the Fibers Used in H_2-Based Membrane Biofilm Reactors. J Membrane Sci 407-408: 176-183.

Tang Y, Krajmalnik-Brown R, Rittmann BE. 2013. Modeling trichloroethene reduction in a hydrogen-based biofilm. Water Sci Technol, 68(5).

Throbäck IN, Enwall K, Jarvis Å, Hallin S. 2004. Reassessing PCR primers targeting *nirS*, *nirK*, and *nosZ* genes for community surveys of denitrifying bacteria with DGGE. FEMS Microbiol Ecol 49(3): 401-417.

Tiemann M. 2006. SDWA: Implementation and Issues, CRS Report for Congress.

Tiemann M. 2008. Perchlorate Contamination of Drinking Water: Regulatory Issues and Legislative Actions, CRS Report for Congress.

Urbansky ET, Schock MR. 1999. Issues in managing the risks associated with perchlorate in drinking water. J Environ Manage 56(2): 79–95.

United Nations (UN). 2012. The Millenium Development Goals Report.

United Nations Environment Programme (UNEP). 2010. Clearing the waters: A focus on water quality solutions.

USEPA. 2005. Perchlorate treatment technology update. No.EPA 542-R-05-015.

USEPA. 2012a. Basic Information about Nitrate in Drinking Water. Accessed on February 17, 2014 from http://water.epa.gov/drink/contaminants/basicinformation/nitrate.cfm

USEPA. 2012b. Perchlorate. Accessed on February 17, 2014 from: http://water.epa.gov/drink/contaminants/unregulated/perchlorate.cfm

USEPA. 2012c. Sulfate in drinking water. Accessed on February 23, 2014 from: http://water.epa.gov/drink/contaminants/unregulated/sulfate.cfm

USEPA IRIS. 2005. Perchlorate and perchlorate salts. Accessed on February 25, 2014 from: http://www.epa.gov/iris/subst/1007.htm

USGS. 2012. Water hardness and alkalinity. Accessed on February 24, 2014 from: http://water.usgs.gov/owq/hardness-alkalinity.html

Van Breemen N, Van Dijk HFG. 1988. Ecosystems effects of atmospheric deposition of nitrogen in the Netherlands. Environ Pollut 54(3): 249-274.

Van Ginkel CG, Rikken GB, Kroon AGM, Kengen SWM. 1996. Purification and characterization of chlorite dismutase: a novel oxygen-generating enzyme. Arch Microbiol 166(5): 321–326.

Van Ginkel SW, Ahn CH, Badruzzaman M, Roberts DJ, Lehman G, Adham SS, Rittamnn BE. 2008. Kinetics of nitrate and perchlorate reduction in ion exchange-brine using the membrane biofilm reactor (MBfR). Water Res 42(15): 4197-4205.

Van Ginkel SW, Lamendella R, Kovacik Jr WP, Santo Domingo JW, Rittmann BE. 2010. Microbial community structure during nitrate and perchlorate reduction in ion-exchange brine using the hydrogen-based membrane biofilm reactor (MBfR). Bioresource Technol 101(10): 3747-3750

Vorosmarty CJ, Green P, Salisbury J, Lammers RB. 2000. Global water resources: vulnerability from climate change and population growth. Science 289(5477): 284-288.

Wallace W, Beshear S, Williams D, Hospadar S, Owens M. 1998. Perchlorate reduction by a mixed culture in an up-flow anaerobic fixed bed reactor. J Ind Microbiol Biot 20(2): 126-131.

Waller S. 2002. Bioremediation of perchlorate-contaminated groundwater. Master thesis. University of Toronto.

Wang CL, Maratukulam PD, Lum AM, Clark DS, Keasling JD. 2000. Metabolic engineering of an aerobic sulfate reduction pathway and its application to precipitation of cadmium on the cell surface. Appl Environ Microbiol 66(10): 4497-4502.

Wang Q, Garrity GM, Tiedje JM, Cole JR. 2007. Naive bayesian classifier for rapid assignment of rrna sequences into the new bacterial taxonomy. Appl Environ Microbiol 73(16): 5261-5267.

Wanner O, Eberl H, Morgenroth E, Noguera D, Picioreanu C, Rittmann BE, van Loosdrecht MCM. 2006. Mathematical Modeling of Biofilms. Report of the IWA Biofilm Modeling Task Group, Scientific and Technical Report No. 18, IWA Publishing, London.

Ward OP. 2004. The industrial sustainability of bioremediation processes. J Ind Microbiol Biot 31: 1-4.

Widdel F, Hansen TA. 1991. The dissimilatory sulfate-and sulfur-reducing bacteria. In The prokaryotes, 2nd ed.; Balows A, Trüper HG, Dworking M, Harder W, Schleifer K-H. Eds.; Springer-Verlag: New York, pp 583-616.

Williams TM, Unz RF. 1985. Isolation and characterization of filamentous bacteria present in bulking activated sludge. Appl Microbiol Biotechnol 22(4): 273-282.

Williams TM, Unz RF, Doman JT. 1987. Ultrastructure of *Thiothrix* spp. and "type 021N" bacteria. Appl Environ Microbiol 53(7): 1560-1570.

World Health Organization. 2002. European Commission. Eutrophication and health p 28

Wu W-M, Gu B, Fields MW, Gentile M, Ku Y-K, Yan H, Tiquias S, Yan T, Nyman J, Zhou J, Jardine PM, Craig CS. 2005. Uranium reduction by denitrifying biomass. J Bioremed 9(1): 41-61.

Yoshida M, Ishii S, Otsuka S, Senoo K. 2009. Temporal shifts in diversity and quantity of nirS and nirK in a rice paddy field soil. Soil Biol Biochem 41: 2044-2051.

Yoshida M, Ishii S, Otsuka S, Senoo K. 2010. nirK-Harboring denitrifiers are more responsive to denitrification inducing conditions in rice paddy soil than nirS-Harboring bacteria. Microbes Environ 25: 45-48.

Zhang H, Bruns MA, Logan BE. 2002. Perchlorate reduction by a novel chemolithoautotrophic, hydrogen-oxidizing bacterium. Environ Microbiol 4(10): 570–576.

Zhang H, Ziv-El M, Rittmann BE, Krajmalnik-Brown R. 2010. Effect of dechlorination and sulfate reduction on the microbial community structure in denitrifying membrane-biofilm reactors. Environ Sci Technol 44(13): 5159-5164.

Zhang H, Parameswaran P, Badalamenti J, Rittmann BE, Krajmalnik-Brown R. 2011. Integrating high-throughput pyrosequencing and quantitative real-time PCR to analyze complex microbial communities. In High-Throughput Next Generation Sequencing (pp. 107-128). Humana Press.

Zhang L, De Schryver P, De Gusseme B, De Muynck W, Boon N, Verstraete W. 2008. Chemical and biological technologies for hydrogen sulfide emission control in sewer systems: a review. Water Res 42(1): 1-12.

Zhao H-P, van Ginkel SW, Tang Y, Kang D-W, Rittmann BE, Krajmalnik-Brown R. 2011. Interactions between perchlorate and nitrate reductions in the biofilm of a hydrogen-based membrane biofilm reactor. Environ Sci Technol 45(23): 10155-10162.

Zhao H-P, Ilhan ZE, Ontiveros-Valencia A, Tang Y, Rittmann BE, Krajmalnik-Brown R. 2013. Effects of multiple electron acceptors on microbial interactions in a hydrogen-based biofilm. Environ Sci Technol 47(13): 7396-7403.

Zhao H-P, Ontiveros-Valencia A, Tang Y, Kim B-O, van Ginkel SW, Friese D, Overstreet R, Smith J, Evans PJ, Krajmalnik-Brown R, Rittmann B. 2014. Removal of multiple electron acceptors by pilot-scale, two-stage membrane biofilm reactors. Water Res. 54: 115-122.

Zippel B, Neu TR. 2011. Characterization of glycoconjugates of extracellular polymeric substances in tufa-associated biofilms by using fluorescence lectin-binding analysis. Appl Environ Microbiol 77(2): 505-516.

Ziv-El M, Rittmann BE. 2009. Systematic evaluation of nitrate and perchlorate bioreduction kinetics in groundwater using a hydrogen-based membrane biofilm reactor. Water Res 43(1): 173-181.

Ziv-El M, Delgado A, Yao Y, Kang D-W, Nelson KG, Halden RU, Krajamlnik-Brown R. Development and characterization of DehaloR^2, a novel anaerobic microbial consortium performing rapid dechlorination of TCE to ethene. 2011. Appl Microbiol Biotechnol 92: 1063-1071.

Ziv-El M, Popat SC, Kai C, Halden RU, Krajmalnik-Brown R, Rittmann BE. 2012. Managing methanogens and homoacetogens to promote reductive dechlorination of trichloroethene with direct delivery of H_2 in a membrane biofilm reactor. Biotechnol Bioeng 109: 2200-2210.